



**Aalto University
School of Chemical
Engineering**

Leo Antti Juhani Kukkonen

**DETERMINING THE EFFECT OF WASH WATER PARAMETERS ON THE
POLYCYCLIC AROMATIC HYDROCARBONS MASS BALANCE IN THE OPEN LOOP
EXHAUST GAS CLEANING SYSTEMS**

Master's Programme in Chemical, Biochemical and Materials Engineering
Major in Chemical and Process Engineering

Master's thesis for the degree of Master of Science in Technology submitted for
inspection, Espoo, 01.07.2019.

Supervisor

Professor Ville Alopaeus

Instructor

M.Sc. Toni Chwojka

Author Kukkonen Leo

Title of thesis Determining the Effect of Wash Water Parameters on the Polycyclic Aromatic Hydrocarbons Mass Balance in Open Loop Exhaust Gas Cleaning Systems

Degree Programme Chemical, Biochemical and Materials Engineering

Major Chemical and Process Engineering

Thesis supervisor Professor Ville Alopaeus

Thesis advisor(s) / Thesis examiner(s) M.Sc. Toni Chwojka

Date 01.07.2019

Number of pages 82+32

Language English

Abstract

The main objective is to investigate the influence of wash water parameters in open loop exhaust gas desulphurization systems on the absorption of polycyclic aromatic hydrocarbons (PAH). Selected PAH are listed in the Environment Protection Agency 16 priority pollutants. Secondary objective was to propose a method for PAH mass balance calculation.

The literature part is a literature review, that investigates the PAH formation and possible interaction in aqueous phase with particulate matter. The effect of wash water salinity and temperature on individual PAH pollutants was investigated in depth.

For the applied part, three samples from two ships were collected and sent to the laboratory for detailed gas-chromatography mass-spectrometry (GC-MS) PAH analysis in aqueous phase and in filtered particulate matter. To verify the accuracy of the analysis, quality control and quality assurance analysis were requested. For establishing the mass balance of PAH species, the Henry's law was applied, which relied on the solubilities of PAH species discussed in the literature part. The mass balance was calculated with 1-Stage method, which is based on the equilibrium achieved with Henry's law. In addition, the mass balance was simulated in Aspen Plus with multiple absorption stages.

An extensive sensitivity analysis was carried out with 1-Stage method and with Aspen Plus. Both sensitivity analysis were compared with each other and an error evaluation function was regressed in IBM SPSS 25. The obtained error estimation was used to correct the 1-Stage method towards the Aspen Plus results.

Based on the quality control and quality assurance results, parent PAH concentration was up to 70% lower than the corrected PAH concentration. Up to 22 % of the total PAH were found in in particulate matter. PAH mass balance can be calculated with proposed method with accuracy of 17.25 % with 95% probability.

Keywords PAH, scrubber, absorption, salinity, Henry's law, ship



Tekijä Leo Kukkonen

Työn nimi Pesuveden parametrien vaikutuksen määrittäminen polysyklisen aromaattisten hiilivetyjen massataseeseen avoinkierto merivesirikkipesureissa

Koulutusohjelma Chemical, Biochemical and Materials Engineering

Pääaine Chemical and Process Engineering

Työn valvoja Professor Ville Alopaeus

Työn ohjaaja(t)/Työn tarkastaja(t) M.Sc. Toni Chwojka

Päivämäärä 01.07.2019

Sivumäärä 82+32

Kieli Englanti

Tiivistelmä

Työn päätarkoituksena on tutkia laivojen merivesirikkipesureiden pesuveden parametrien vaikutusta polysyklisen aromaattisten hiilivetyjen (PAH) absorptioon. Valitut PAH-aineet kuuluvat Environment Protection Agency 16 prioriteettisaasteisiin. Toissijaisena tarkoituksena on ehdottaa metodi PAH-aineiden massataseen laskemiseen.

Työn kirjallisuusosa keskittyy PAH muodostumiseen ja mahdollisiin vuorovaikutuksiin PAH ja hiukkaspäästöjen välillä nesteessä. Kirjallisuusosassa perehdytään myös pesuveden saliniteetin ja lämpötilan vaikutuksiin yksittäisiin PAH-molekyyleihin.

Käytännön osaa varten, kolme kenttänäytettä kahdelta laivalta lähetettiin laboratorioon analysoitavaksi. Analyysi sisälsi tarkan kaasukromatografia massa spektrometria analyysin neste- ja hiukkasmafazeista. Lisäksi laboratoriossa suoritettiin analyysin laatu tarkastelun tarkkuutta varten. PAH-aineiden massataseen muodostamista varten työssä käytettiin Henryn lakia. Massatase laskettiin 1-ideaaliaskleen metodilla ja simuloitiin Aspen Plus ohjelmalla usealla ideaaliaskleella.

Laaja herkkyysanalyysi suoritettiin kummallakin metodilla ja tulokset verrattiin keskenään. Virhearviointi suoritettiin IBM SPSS 25 ohjelmalla ja virheet sovitettiin funktioon regressiolla.

Laboratorion analyysin laatutarkastelun perusteella, alkuperäinen PAH konsentraatio on jopa 70 % matalampi kuin korjattu konsentraatio ja jopa 22 % koko PAH konsentraatiosta löytyi hiukkaspäästöistä. PAH massataseen voi laskea ehdotetulla metodilla 17.25% tarkkuudella 95% todennäköisyydellä.

Avainsanat PAH, scrubber, absorption, salinity, Henry's law, ship

Preface

I still tell the story how I ended up into shipping industry. It was in 2012 in January when I walked past a summer job recruitment exhibition in Otaniemi. For an unknown reason, I was most confident that a certain finnish shipping company recruited chemical engineers by default. Therefore, I went to their stand and after somewhat confused discussion I was introduced to the concept of exhaust gas scrubbers. I applied then for the summer trainee position. Later I checked my guild's student overalls and saw the logo of finnish consulting company, that actually recruits chemical engineers. The logos apparently got mixed up in my head. Since that fortunate mix up, I am still passionately viewing the development of shipping industry, especially the emission regulations and will be doing so in the future.

I want to thank Professor Ville Alopaeus for his tenacious guidance during this thesis, especially with the simulation program. Otherwise, this thesis would have ended at the very beginning of the applied part. I want to thank my instructor Mr. Toni Chwojka, who introduced me to this topic and who helped to make this thesis more comprehensible – even to myself.

I want to thank my family. My mother who took care of me, even when I was not at home. Who bought to me healthier snacks and food to the ever-open computer halls. My father, who always listened me face to face and on the phone and never let me submerge into desperation, when something went amiss. To my little sister, with whom I could chat about anything and everything disregarding the time of the day.

Special thanks goes to my friend of the past 21 years Mr. Pekka Rantakallio, who helped me with the admission exams to Helsinki University of Technology – and now he helped me to graduate from Aalto University. Without his expertise in data analysis, the thesis would have been just a bland statement.

I also want to thank Aalto Predators, who introduce me to American football. It has been an honour to play in your jerseys!

Of course a huge thanks goes to Joutomiehet – nuo mainiot veikot, who taught me the most valuable lesson in life – most important thing in life, is not to make any mistakes. With this lesson in mind, I will continue my journey in life.

Espoo 01.07.2019

Leo Kukkonen

Contents

Preface	4
Abbreviations	i
Symbols	ii
Introduction	1
Literature part	4
1. Structure of emission regulating and monitoring organizations.....	4
2. Process.....	6
3. Seawater.....	7
4. Scrubber reaction	9
5. Fuel	10
6. Polycyclic aromatic hydrocarbons and soot	12
7. Fuel treatment process	13
7.1. Settling tank.....	13
7.2. Purifier.....	13
7.3. Service tank.....	14
7.4. Pressure loop	14
8. Combustion	15
9. Soot and PAH formation.....	17
9.1. Flame.....	18
9.2. PAH formation	20
9.2.1. HACA	21
9.2.2. Physical growth	23
9.2.3. Nucleation.....	23
9.2.4. Coagulation and agglomeration.....	24
9.2.5. Oxidation	25
9.2.6. Influence of various parameters.....	25
10. PAH and Soot in Exhaust Gas.....	27
11. PAH and soot solubility in water	33
11.1. Solubility in pure water.....	33
11.2. Solubility in saline water.....	34
12. PAH quenching.....	36

12.1.	Dynamic quenching.....	36
12.2.	Static quenching in fresh water.....	37
12.3.	Static quenching seawater.....	39
	Applied part.....	41
13.	Estimating unknown solubilities.....	42
14.	Henry's law constants calculation	45
15.	Sampling.....	50
15.1.	Annual analysis.....	51
15.2.	Analysis for this thesis.....	51
15.3.	Quality control.....	51
15.4.	Laboratory results evaluation.....	51
16.	Laboratory results.....	54
17.	PAH simulation	56
17.1.	Ideal stage.....	56
17.2.	1-Stage method	57
17.3.	Scrubber base model	57
17.4.	PAH absorption modelling.....	57
18.	Results and discussion.....	59
19.	Results evaluation	62
19.1.	Sensitivity analysis evaluation.....	70
19.2.	Mass balance calculation.....	73
20.	PAH reduction.....	76
20.1.	Homogenizers.....	76
20.2.	Electrostatic precipitator	77
20.3.	Open loop water treatment system	78
21.	Conclusions	80
22.	Further study suggestions.....	82
	References.....	83
	Appendix A. Selected EPA 16 PAH (<i>Yan et al. 2003</i>).....	89
	Appendix B.....	90
	Appendix C. Fuel treatment, pressure loop and exhaust gas cleaning	91
	Appendix D. Absorption of contaminant.....	92

Appendix E.....	93
Appendix F.....	94
Appendix G. Known TDSF (°C).....	95
Appendix H.	96
Appendix i.....	97
Appendix J.....	98
Appendix J continued.....	99
Appendix K.....	100
Appendix L.	101
Appendix M.	102
Appendix N. Case III	103
Appendix O. Case III	104
Appendix P. Case III.....	105
Appendix Q. Case III	106
Appendix R. Case I.....	107
Appendix S. Case I	108
Appendix T. Case I.....	109
Appendix U. Case I	110
Appendix W. Case Extrapolated.....	111
Appendix V. Case Extrapolated	112
Appendix X. Case Extrapolated	113
Appendix Y. Case Extrapolated	114

Abbreviations

amu	Atomic mass units
EPA	Environment Protection Agency
GC-MS	Gas Chromatography – Mass Spectrometry
HACA	Hydrogen-Abstraction-C ₂ H ₂ -Addition
HFO	Heavy fuel oil
IFO	Intermediate fuel oil
IMO	International Maritime Organization
L/G	Liquid/Gas ratio
MARPOL	International Convention for the Prevention of Pollution from Ships
MDO	Marine Diesel oil
MEPC	Marine Environment Protection Committee
MGO	Marine gas oil
MS	Matrix spike
MSD	Matrix spike duplicate
PAH	Polycyclic Aromatic Hydrocarbons
PAH _{Aq}	Polycyclic Aromatic Hydrocarbons in aqueous phase
PAH _{PM}	Polycyclic Aromatic Hydrocarbons in PM
Phe _{eqv}	Phenanthrene equivalent
PM	Particulate matter
ppb	Parts per billion
PSU	Practical Salinity units
QA	Quality Assurance
QC	Quality Control
RSFR	resonance stabilized free radicals
SO _x	Sulphur oxides
TDC	Top dead center
TDSF	Temperature dependent solubility functions

UAF	unscaled approximation function
UNIQUAC	Universal Quasichemical

Symbols

C_s	Concentration of salt in [mol/dm ³]
$C_{sat\ i}$	Saturation solubility in mol/m ³
K_{ow}	Octanol-water partitioning coefficient
P_v	Vapor pressure of component in gaseous phase
S_0	Solubility of organic solute in fresh water [mol/dm ³]
k_s	Setschenow constant
c	Scaling coefficient
\mathcal{H}	Henry's law constant of component
\mathcal{H}_{sw}	Henry's law constant of component seawater
P_{vi}	Vapor pressure of the component in Pa
R	Universal gas constant
T	Temperature
V	Gas volume
V_{LeBas}	Molecular volume
S_0	Solubility in mol/m ³
S	Solubility of organic solute in saline water [mol/dm ³]

Introduction

In 1890's a German engineer Rudolf Diesel invented a single cylinder internal combustion reciprocating engine (*Vermeire, 2012*). Today over 200 million internal combustion engine units are produced annually with size ranging from fraction of horse power to five stories high 80 MW engines used in marine applications (*Catalog of CHP Technologies, 2017*).

As the potential of Diesel's engine has been discovered, the engines have been gradually replacing the steam engines in automobiles and ships, the fuel oil demand has been naturally increasing. Since the engines in ships are greater and slower in speed than in automobile engines, the ships received residual oil from crude oil distilleries as fuel (*Vermeire, 2012*).

As a result, the combustion of residual fuel generates numerous emissions, IMO and locals are stepping up to regulate the emissions coming out from stacks. One of the most important emissions are the sulphur oxides emissions (SO_x), which are responsible for example the acid rain. As the SO_x react with the water steam, they react forming a sulphurous acid H₂SO₃. As the vapor condenses, it comes down as a rain with a low pH.

To minimize the SO_x emissions, International Maritime Organization (IMO) released MARPOL annex VI, to regulate air pollutions and affecting so the SO_x emissions from stack must be equivalent to the 0.1 S% fuel. Currently, there are so called Emission Control Areas (ECA), where such requirement is in power. Outside of these areas, ships can sail without any restrictions on the SO_x emissions. However, currently the gaze is towards year 01.01.2020, when the SO_x emissions are going to be restricted down to 0.5 w-S% globally in accordance with MARPOL Annex VI. (*International Chamber of Shipping, 2019*) The ECA areas with 0.1 w-S% restrictions will remain.

One of the most economically and efficiently approved method to reduce the SO_x emissions, even below the given restrictions are the wet exhaust gas scrubbers. Even more so, the open loop scrubber is frequently used technology, in which the scrubber utilizes the ambient seawater for the absorption. (*EPA, 2011*). The seawater at the outlet of the scrubber is filtered from the particulate matter and then released back into the sea as it contains no additional chemicals. For the purposes of the thesis, the open loop scrubbing system will be referred as DeSO_x. According to *Ship&Bunker 2019*, it is expected that the demand of open loop

scrubbers will increase by 2020 due to the sulfur cap, as during the longer trans-voyages, the ships utilizing closed loop scrubbers, won't have enough storage space on board for the dirty wash water.

The DeSOx towers are unfortunately not selective processes and thus absorb to some extent everything that comes along with the exhaust gases. One specific emission group, which is extremely closely monitored, by order of IMO, is the group consisting of the condensed unburnt polycyclic aromatic hydrocarbons (PAH). These have been identified to include carcinogenic components. A specific group called polycyclic aromatic hydrocarbons (PAH) is among the monitored emissions from scrubbers. PAH emissions have been identified as carcinogens and to monitor these emissions, in Resolution MEPC.259(68) it is stated that depending on the wash water flow in DeSOx tower and assumed concentration, PAH must be monitored with in line fluorescence, if the tower wash water flow rate is above 5 t/MWh. (MEPC.259(68)) The readings must be reported as phenanthrene equivalence [Phe_{eqv}] and converted to ppb.

During commissioning and acceptance period of scrubber, a wash water sampling for third party laboratory must be conducted. (MEPC.259(68)) For PAH MEPC reserved detailed Gas Chromatography Mass Spectrometry (GC-MS) -analysis according to EPA or ISO standards. The usual method of EPA 8270 does not require analysis of solid phase, such as soot. EPA has listed 16 priority PAH, which are listed in **Appendix A**. The samples are collected at relevant sampling points for seawater inlet, scrubber outlet and overboard discharge. The samples are collected into amber glass bottles, sealed, cooled down and delivered to the laboratory for analysis. Usually the delivery to the laboratory lasts over 24 hours after the sampling. Unfortunately, it has turned out, that the laboratory analysis and optical sensor readings can differ significantly from each other (EPA, 2011; Lahtinen, 2016). Authors report, that optical sensors give much higher readings than the laboratory results. This trend has been seen in several other articles and studies.

In this thesis, a different approach has been taken towards the difference in readings between laboratories and sensors. It is supposed, that there are some internal influence on PAH concentration in the sampling bottle during delivery to the laboratory. In addition to analysis

issue problems, it is suspected that the salinity of water has significant impact on the absorption of PAH into the wash water, resulting in different readings depending on the surrounding seawater, even if the fuel quality and engine configuration remain the same.

The scope of the thesis is to propose a possible method to determine mass balance of PAH in the exhaust gases with spread sheet (Excel) calculation method and to compare the method by simulating the process in flow sheet (Aspen Plus) with UNIQUAC method. For this, the effect of wash water salinity must be considered. Currently there is no viable method on the field, that could measure the amount of PAH in the exhaust gases and the methods for measuring the concentration of PAH in the wash water are contradicting with each other.

Literature part

1. Structure of emission regulating and monitoring organizations

In year 1948 an international conference in Geneva adopted a convention to establish Inter-Governmental Maritime Consultative Organization (IMCO). After entering into force in 1958, the aim of the organization was to provide safety on board, efficiency of ship operation and to control and prevent the pollution generated on ships. The name changed to International Maritime Organization (IMO) in year 1982 (*Safety4sea, 2016*). IMO assembly contains at the moment of 172 member states. For the pollution regulations, a supportive Marine Environment Protection Committee (MEPC) is responsible for emissions generated by ships.

To verify that the ships indeed are operating in the compliance with IMO safety regulations and limits of MARPOL according to MEPC guidelines, there are organizations called classification societies such as Lloyds Register, DNV GL and others. After ship undergoes any modification in their operation or process, they must apply for class approval from the class they are registered to. Class verifies the proper installation of equipment. In addition, the class verifies on behalf of the Flag state the performance of the reduction of emissions. This verifications end in a system specific Marine Equipment Directive Certificate (MED-G) and into ship specific International Air Pollution Prevention Certificate (IAPP) The network of different parties and their interaction is presented in **appendix B**.

Currently there are so called Sulphur Emission Control Areas (SECA), in which the ship SO_x emissions must be equivalent to the 0.1 S% containing fuel. There is discussion that the emission control areas (ECA) should be expanded further. In Figure 1, the current and possibly future ECA areas are presented.

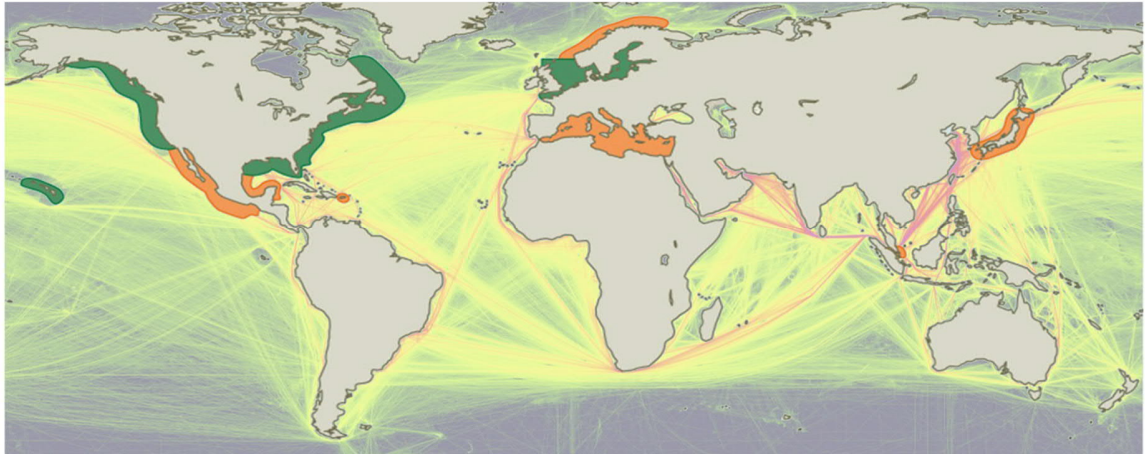


Figure 1. Shipping activities and routes. Green areas are existing ECA areas and orange are possibly future ones. In the ECA areas sulphur emissions must be equivalent to 0.1 S%. (*Endres et al. 2018*)

Currently the hot topic is the sulphur cap regulation for year 2020. The current resolution is that by the year 2020 the sulphur emissions must be 0.5 S% equivalent all over the sea. Taking into consideration the fuel price gap and the proven technology of scrubbers, it also expected to increase the EGCS demand.

2. Process

Comparable to other combustion power plants, the energy is coming from fuel combustion process, while EGCS reduces the emissions coming from the combustion unit. Process is presented in the **appendix C**. Thesis concentrates mainly on the exhaust gas cleaning section of the process, but the functions of the previous sections are also shortly discussed to give an insight of their functionality and influence.

In simplest form, a scrubber is an absorption column, which utilizes the seawater for the absorption process. The exhaust gases are steered from the engine to the column and enter it from lower section of the scrubber. As the gases travel through the column, they encounter downwards stream of wash water. Water is finely dispersed across the whole column and travels towards the bottom by means of gravity and if necessary, is treated accordingly before the overboard discharge. The cleaned exhaust gas escapes the column through the top of the column.

3. Seawater

The composition of the seawater varies around the globe, from low salinity brackish waters in the Baltic Sea to the hypersaline Dead Sea. The most investigated properties of the seawater for the exhaust gas scrubbing are the components of the ions present in the sea. Especially the amount of carbonates and bicarbonates is essential, as those are the components for the neutralization of the lowered pH after scrubbing (*Andreasen et al. 2007*). Authors propose generalized seawater model in Table 1.

Table 1. Components of Standard Seawater at a Salinity of ~35 ppt. (*Andreasen et al.2007*)

constituent	mass fraction (g/kg seawater)	molality (mol/kg H ₂ O)
Cl ⁻	19.35	0.5658
Na ⁺	10.78	0.4861
SO ₄ ²⁻	2.71	0.0293
Mg ²⁺	1.28	0.0548
Ca ²⁺	0.41	0.0107
K ⁺	0.399	0.0106
HCO ₃ ⁻	0.108	0.00183
Br ⁻	0.067	0.00087
Sr ²⁺	0.08	0.00009
B(OH) ₃	0.0198	0.00033
CO ₃ ²⁻	0.016	0.00027
B(OH) ₄ ⁻	0.0079	0.00010
F ⁻	0.0013	0.00007

Below in the figure 2 the world-wide salinity map presented by NASA.

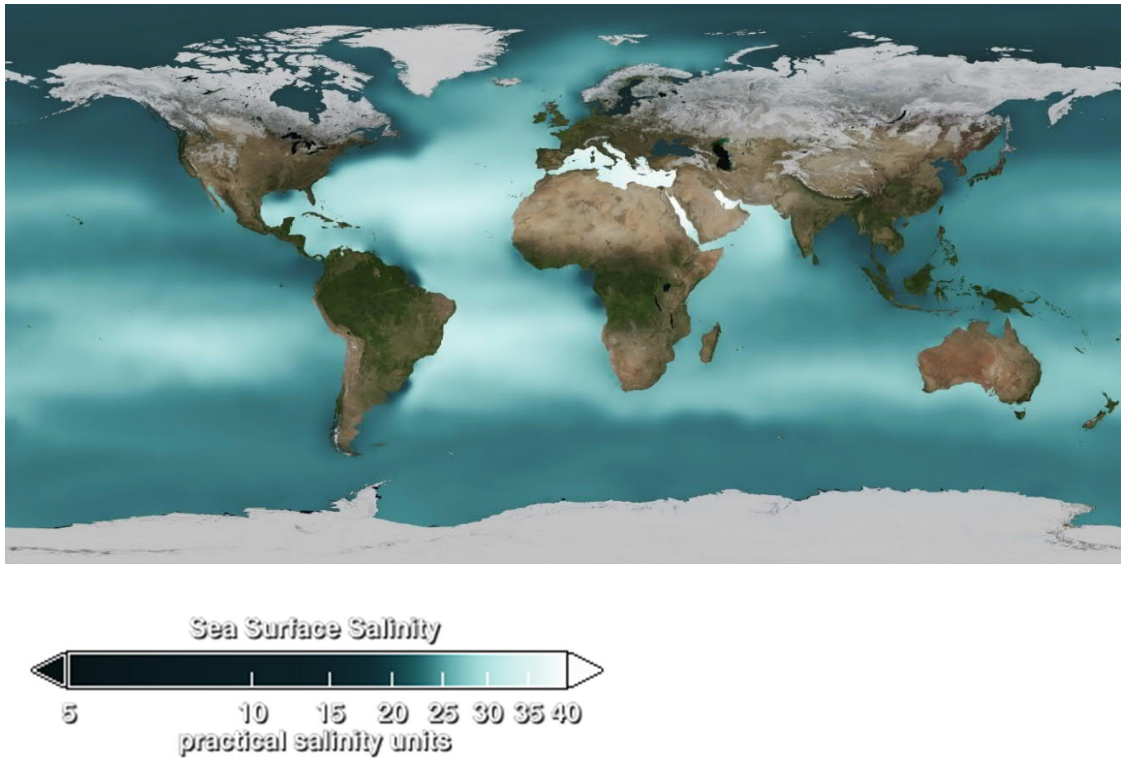


Figure 2. Worldwide salinity according to NASA. (NASA, 2019)

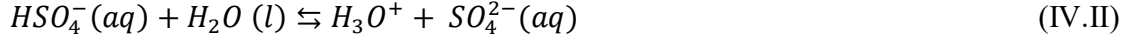
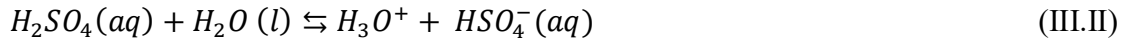
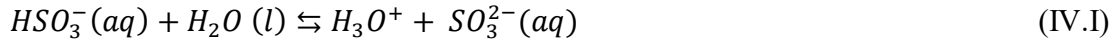
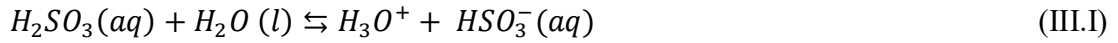
As one can see, there is a distinct fluctuation regarding the salinity of surface waters worldwide and it increases towards the equator.

4. Scrubber reaction

Absorption of SO_x is a reactive process. In the following sequence, the reactions in seawater scrubber are presented. The SO_x molecules undergo following reaction with available water:



As one can see, the absorption forms sulphuric and sulphurous acids, which reduce the general pH of the wash water after the dissociation.



In the open loop scrubbers, there are no further additives for the neutralization. The neutralization occurs due to the presence of the carbonates and bicarbonates, which function as buffering solution (*Andreasen et al. 2007*). It is assumed, that with the increasing sulfur content, the salinity of the wash water is increased. The principle of absorption is presented in **appendix D**.

5. Fuel

As the more diverse engines were developed, specific fuels were required for designated engine. This resulted in the development of efficient distillation plants, which compared to the straight run plants further distilled previous residue of the straight run distilleries (*Vermeire, 2012; Burak, 2010*) in the vacuum distillation units.

In straight run distilleries approximately 50 % of the original crude oil barrel ended to the residual fuel for the ship engine operation. With the improved distilleries, in which the vacuum distillation, visbreaking and catalytic cracking is applies, approximately 16 % of original crude oil barrel winds up to the residual fuels and so to the ships (*Burak, 2010*). This has several impacts on the fuel quality:

- Lower hydrogen amount
- Increased trace metal concentration
- Increased amount sulphur, oxygen and nitrogen
- Higher density
- Lower calorific value
- Increased asphaltenes
- Tendency for incompatibility (*Burak, 2010*).

Due to its current state and properties as listed above, fuel cannot enter the engine as such and therefore must be purified onboard. Because of the increased density and viscosity, the fuel is usually blended with the distillate, sulphur free marine gas oil (MGO) as a cutter stock and heated up to get it at least to the pumpable state (*Catalog of CHP Technologies, 2017*). The resulting mixture is called often intermediate fuel oil (IFO) with viscosity of 380 cSt.

As mentioned earlier, the increased asphaltene content and density of the fuel results in possible incompatibilities. The asphaltenes is temperature and pressure sensitive fraction of the fuel and are one of the primary reasons for sludge generation in the purification units (*Burak, 2010*). In other words, blending too much MGO into IFO, may result in poorer combustion and even increase fuel loss.

As the IFO is the residual fuel oil it is by definition cheaper than the distillate MGO and with continuously increasing fuel prices, using IFO has economic benefits. Due to the increased sulfur content the sulphur scrubbers or MGO must be used in the ECA areas and ports with local restrictions.

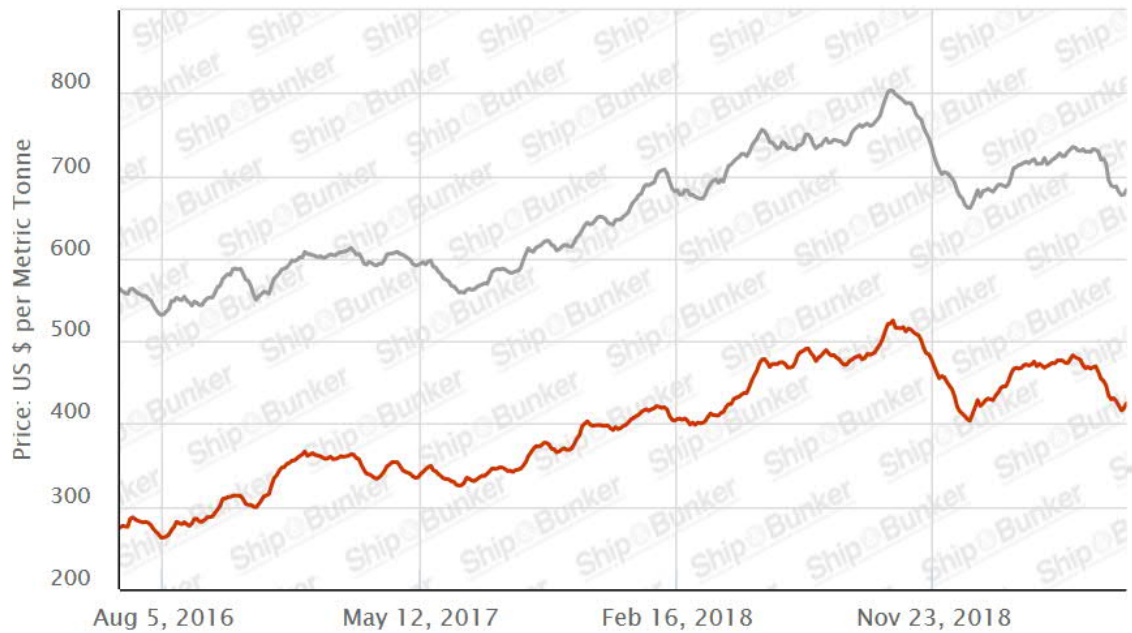


Figure 3. Price development of global average bunker fuel price. HFO (red) and MGO (gray). Site visited on 27.6.2019. (*Ship&Bunker, 2019*)

Although there is much effort in transferring to the more carbon neutral fuels, according to Lloyds Register review, the IFO will still be present in around of 60 % in used fuels (*Lloyds Register*). As one can see, the price difference of the fuels is significant enough to consider installation of the scrubbing equipment, which enables the vessel to operate on the sulphur containing fuel. One open loop scrubber installation cost roughly 1-1.3 M\$. The span varies for whether the scrubber is installed for main engine only or will it cover also the boilers and auxiliary engines. Depending on the fuel prices, the scrubber payback period is estimated to be around 1 year. (*Tanker Shipping and Trade, 2018*)

6. Polycyclic aromatic hydrocarbons and soot

To investigate in depth the topic of the thesis, some aspects must be studied more thoroughly. The essential aspect is to find the correlation between PAH and other organic carbonous emissions that are escaping from the engine. For this, the sequence from fuel preparation and injection into the combustion cylinder all the way to the absorption in the desulphurization unit.

Not every section will be discussed in depth, but only the most relevant ones that have relevant relation to the scope of this thesis. The sections with most chemical impact on the process. In addition, some thoughts will be presented regarding the analysis of the aqueous emissions in the laboratory.

7. Fuel treatment process

In **appendix C**, in blue box, the fuel treatment process is presented. It is responsible to deliver treated fuel that fulfils the specifications for engine operation. Specifications are presented in the **appendix E**.

7.1. Settling tank

The fuel is loaded in port into a bunker tank, from which it is directed to the settling tank. The settling tank is a large reservoir, which is used for pre-cleaning of fuel by gravity – heavier impurities settle to the bottom of the tank due to the gravity. Usually the settling tanks are large enough for 24-hour full load operation of all consumers.

The tanks are usually equipped with baffles, preventing formed sludge mixing with the fuel. Bottom of the settling tank is sloped towards the sludge tank, so that the sludge accumulates in vicinity of sludge drain. Tanks are temperature regulated and usually operate below 75 °C to prevent asphaltene agglomeration and above 7 °C, which is usually the pour point. (*Babicz, 2015*)

7.2. Purifier

From the settling tank, the fuel is pumped towards the more effective cleaning system as known as purifiers. The principle of the purifier is similar to the settling tank, but instead of the gravitational forces the purifier utilizes centrifugal forces. As the impurities have higher density than the actual surrounding fuel, they can be relatively easily ejected from the fuel. According to the Wärtsilä Encyclopedia, a separator is a structure consisting of a frame, electrically driven vertical shaft and a bowl assembly, which is mounted on the frame. In case of heavier fuels, the separators are operated as purifiers (*Babicz, 2015*)

7.3. Service tank

After the purifiers, the fuel is directed to the service tanks. The service tanks contain only the quality of fuel suitable for engine operation. In other words, the service tanks are reservoirs of already processed fuel meeting the specifications as shown in the **appendix E**. According to Lloyds Register:

“Each tank is to have a capacity for at least eight hours operation, at sea, at maximum continuous rating of the propulsion plant and/or generating plant associated with that tank. The arrangement for oil fuel service tank is to be such that one tank can continue to supply oil fuel when the other is being cleaned or opened for repair” (Babicz, 2015)

7.4. Pressure loop

To ensure the full fuel injections, the fuel is supplied to the engine in excessive amounts. The over flow fuel is then recirculated back to the mixing tank, which is connected to the freshly delivered fuel. The loop contains booster pumps, final heaters, engines and mixing tank. The booster pumps increase the velocity of the circulating fuel, the final heaters heat the fuel until the required viscosity has been reached and the mixing tube mixes the overflowing fuel with the freshly delivered fuel from service tank.

8. Combustion

After the fuel is treated and is ready for use, it is finally heated up for high pressure injection into the combustion chamber of the cylinder. The high pressure breaks down the fuel into a fine droplet jet. Another reason for the high-pressure injection is, that the fuel jet is properly mixing with the charged air in the cylinder during combustion. The initial fuel is undergoing a preparation of combustion by evaporating and the fuel molecules dissociate under high pressure and temperature into free radicals and form a radical pool. Simultaneously, the charged air undergoes similar break-up reaction. As the radical pool exceeds its critical threshold, the fuel vapors ignite and combust the further coming fuel jet. In the figure 4, the radical pool formation is presented.

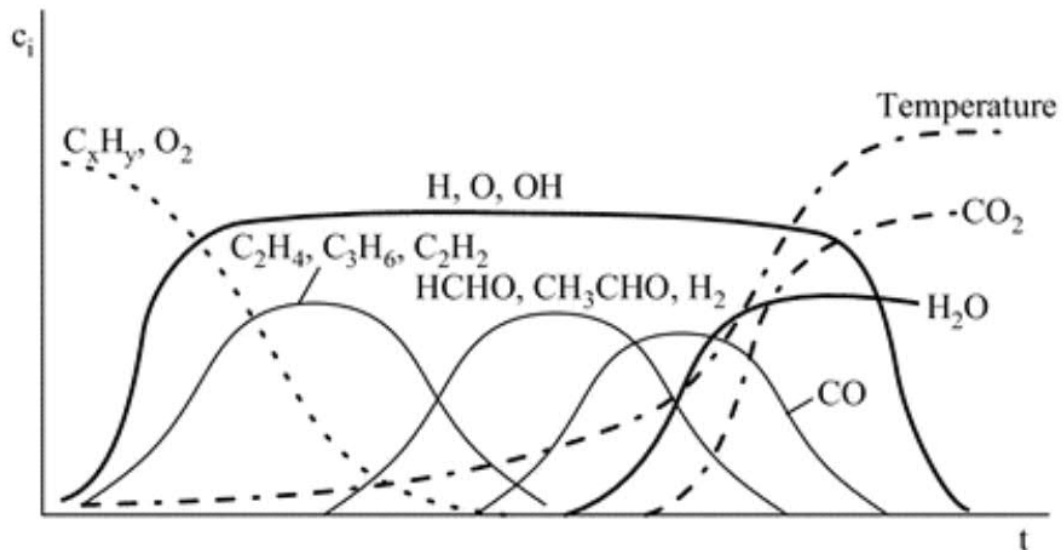


Figure 4. The radical pool formation and depletion during combustion in respect to time. (Van Basshuysen et al. 2004; Warnatz et al. 1996)

The injection is timed so, that the combustion occurs slightly past the TDC. As the combustion occurs, it generates rapid temperature rise, which further creates rapid pressure rise. The sudden pressure rise pushes down on cylinder bore and the down movement of the bore generates power.

The internal engine combustion is usually designed for a specific load range, within which the combustion is most efficient. Usually the load range is between 75-85 %. Outside the load range, the fuel mixing with charge air is less efficient, resulting in higher specific fuel consumption and increased emissions.

9. Soot and PAH formation

As not a single process reaches 100 % conversion, same issue applies also for fuel combustion. When fuel enters the combustion chamber, it undergoes preparation for combustion, in which a radical pool is formed. As the premixed combustion initiates, it also ignites the forth coming remainder of the fuel jet, which further combusts as diffusion combustion. Although surplus charge air is led into the combustion chamber, small fraction of fuel remains uncombusted, even though it went through the preparation for combustion process.

As a result, the active radicals initiate the termination process, which includes recombination, condensation and agglomeration. As a result, carbon rich particulates are formed, which upon further collisions form visible soot. Although the result is clearly visible from stack, the path for soot formation is not as straight forward and undergoes several pathways, depending on the used fuel.

Although there are various hypothesis and theories available, as presented in an extensive review by *Richter et al. 2000*, all studies agree that soot is formed from condensation of aromatic hydrocarbons. In the figure 4, the building blocks for formation of aromatic hydrocarbons, are presented. In the figure 5, *Omidvarborna et al. 2015* presented a chronological development of soot particles.

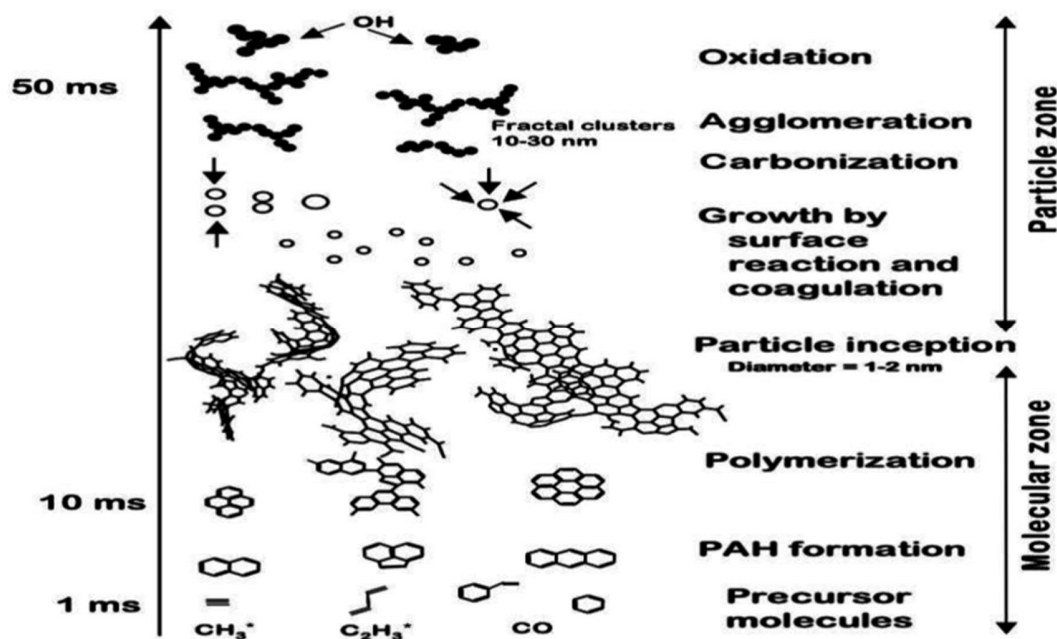


Figure 5. Chronological development of soot from precursor molecules all the way up to particle zone. (Omidvarborna et al. 2015)

In following chapters, the PAH and soot formation in different flames is briefly discussed. Although the PAH is in central role of this thesis, soot plays essential role regarding the field laboratory analysis and therefore soot formation is also reviewed alongside the PAH formation. It also must be noted, numerous pathways for soot formation are presented in the found articles. In the following chapters, the pathway that includes the PAH formation is discussed and described majority of current studies support the principles, that soot is incepted from PAH as one of the key gaseous precursors.

9.1. Flame

Before going deeper in the building block mechanisms, a few words regarding the flame and its structure are necessary. As the fuel is injected, it undergoes previously discussed preparation for combustion. The initial fuel is not immediately combusted but is first premixed with the charge air. As the combustion initiates, it ignites the forth coming fuel jet. In the following figure, a structure of a jet flame is presented.

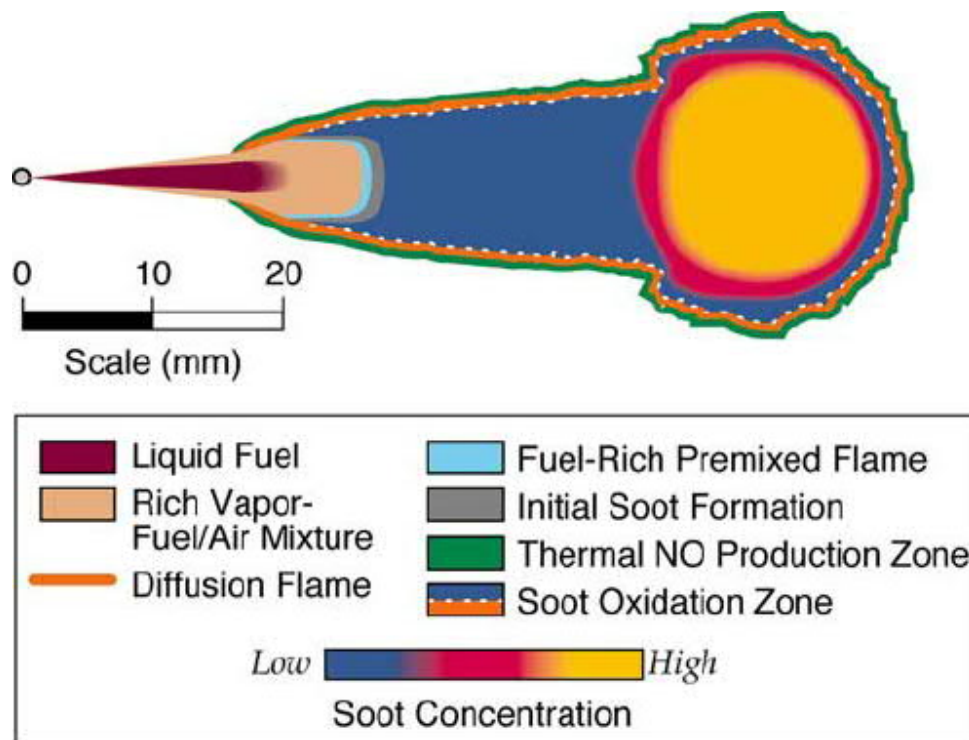


Figure 6. Phenomological flame structure (*Dec, 1997*)

As the initial blast of compressed fuel ignites the forth coming fuel jet, the combustion transforms from premixed combustion into diffusion combustion. The premixed combustion is when the fuel is properly mixed with surrounding air and as the combustion commences, there is enough oxygen to convert fuel to CO_2 with practically no soot formation.

In case of diffusion flames, the situation is different. To initiate fuel combustion, the oxygen must diffuse through the oxidation region to the forth-coming fuel. An example of diffusion combustion is wood combustion or candle flame. Such mechanism results in uncombusted fractions of the fuel. As one can see form figure 6, the premixed combustion initiates at the light blue region and followed by the initial soot formation, which follows by low soot concentration throughout the jet. The higher soot concentration is in the fireball region the flame. The light that is emitted from the diffusion flames is originated from the soot oxidation.

9.2. PAH formation

In the most recent articles, it is often stated, that PAH is an important gaseous soot precursor that is formed in flames. For PAH molecules to build up in the flame, certain molecules, which are listed below, must be formed by fuel chain splitting during the fuel preparation for combustion.

1. Acetylene [C_2H_2] (*Richter et al. 2000; Hansen et al. 2012*)
2. Propargyl [C_3H_3] (*Hansen et al. 2012; Frenklach, 2001*)
3. Allyl [C_3H_5] (*Hansen et al. 2012*)
4. *i*- C_4H_5 (*Hansen et al. 2012*)
5. Phenyl (*Hansen et al. 2012; Frenklach, 2001; Richter et al. 2000*)

These are the most often mentioned molecules in the studies found and regarding the initiation of the reaction most important are components from 2-5. The importance in these components is, that these are Resonance Stabilized Free Radicals (RSFR), which means that their life time in hostile surroundings is longer than the one of the regular free radicals. In the figure 7 below, the resonance structures of the components 2-4 are presented.

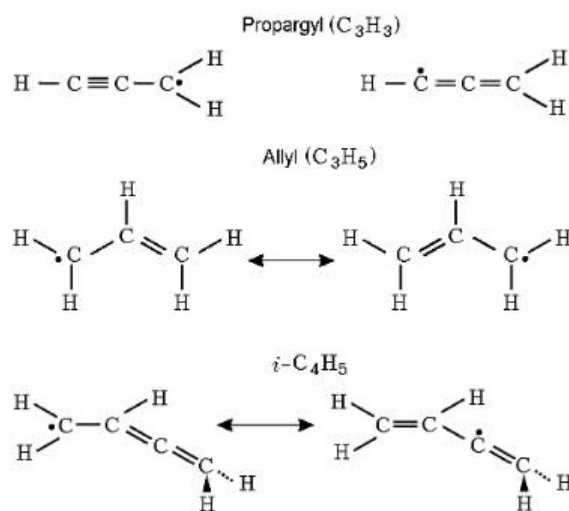


Fig 7. Resonance stabilized structures of propargyl, allyl and *i*- C_4H_5 . Due to the resonance stabilization, the reaction rate coefficient of such radicals with O_2 is by orders of magnitude smaller than by regular radicals.

As the RSFR pool grows during fuel preparation for combustion, these radicals undergo cyclization reactions, forming first aromatic ring of benzene [C₆H₆] or phenyl radical, depending on the source reactants.

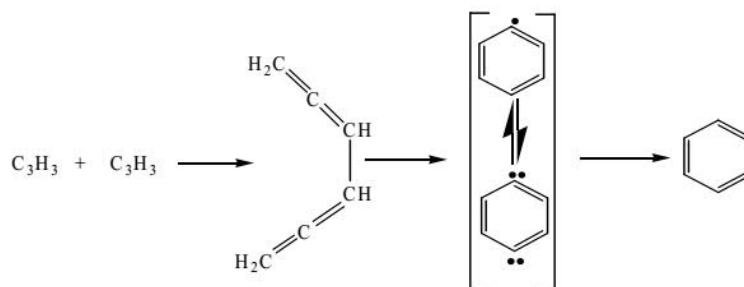


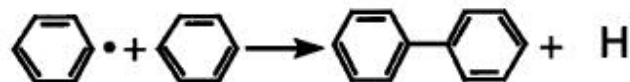
Figure 8. Reaction of propargyl radicals into benzene (*El-Sinawi, 2011*)

As a result, a molecule with weaker bond energy is formed, which can therefore easier react with remaining radicals and initiate a radical growth chain. (*Hansen et al. 2012*). The PAH growth reaction mechanism is known as a mechanism (HACA), which poses the ethylene molecule into the central role in aspect of PAH growth.

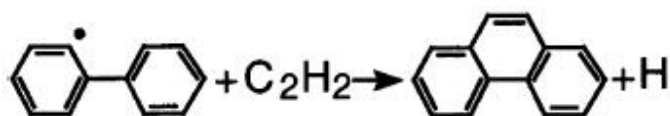
9.2.1. HACA

HACA is a repetitive reaction sequence that has been widely recognized as the major pathway for aromatic rings to grow into PAH molecules. (*Frenklach, 2001; Omidvarborna, 2015*). Due to its repetitive nature, the following sequence presents the formation of phenanthrene from benzene molecule. After first rings are formed, they are subjected to vast amount of free radical attacks, from which the essential and dominant for the PAH formation is the hydrogen radical. As the hydrogen radical approaches benzene ring, it abstracts hydrogen from the aromatic C-H bond and forms gaseous H₂ molecule, leaving phenyl radical behind. This first step converts benzene into a RSFR phenyl and the HACA growth process has been initiated. (*Frenklach, 2001*)

1. As a second step, the newly formed phenyl radical reacts with following benzene molecule, by abstracting the hydrogen and attaching itself to the benzene molecule. The abstracted hydrogen can so initiate a new chain with other molecules.



2. The formed diphenyl molecule is subjected to another hydrogen radical attack and new radical is formed, which is met by ethylene molecule. The radical disrupts the triple bond of the ethylene and the radical electron is so propagated to the attached side chain.
3. The “dangling” side chain radical abstracts hydrogen from the neighboring phenyl ring and forms a phenanthrene, which due to its multiple aromatic rings falls under general description of PAH.



The HACA process can continue from phenanthrene into larger molecules following this sequence and is known to be also reversible, meaning that the rings can be disrupted as well, until entropy barrier is reached, and the reaction becomes irreversible and finally stops (*Frenklach, 2001*). As one can see, the HACA process is fueled by the hydrogen abstraction and occasionally by another hydrogen. In such case, when the PAH growth by HACA proceeds, more hydrogen molecules are formed, resulting in depletion of oxygen that is used for combustion. This results in less oxygen available in the immediate vicinity of growing PAH, resulting in enhanced PAH growth. (*Frenklach, 2001*).

9.2.2. Physical growth

The path from PAH to incipient soot is discussed stage-wise as presented in the figure 9 below.

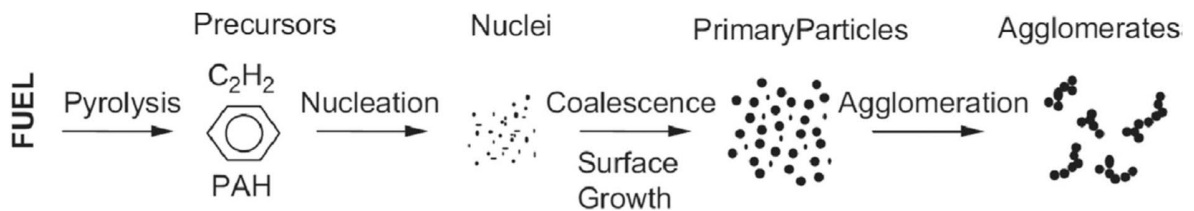


Figure 9. Five development stages from fuel to soot. (Omidvarborna *et al.* 2015)

The individual stages are not discussed as in depth as the PAH formation, but the essentials are presented.

9.2.3. Nucleation

When HACA mechanism has proceeded to such extent, that the heavier PAH molecules are formed, the transition from gaseous to solid phase initiates. (Omidvarborna *et al.* 2015). According to majority of studies, there are experimental difficulties regarding the nucleation process as the measurement equipment limits only to the particles larger than 1.5 nm. (Richter, 2000; Omidvarborna *et al.* 2015).

Due to the fact of difficulties, Mao *et al.* 2017 studied to nucleation of PAH by means of simulation of coronene nucleation into soot. They state in their study, that the physical nucleation occurs after the temperature is cooled down to 800K. A sequence of the nucleation is presented in the figure 10 below.

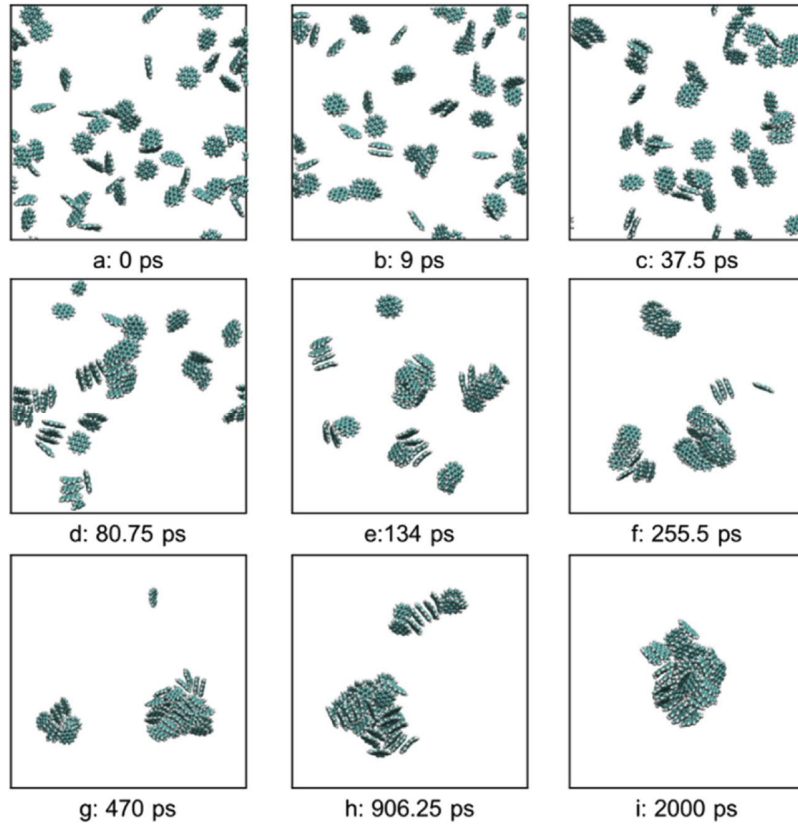


Figure 10. Physical nucleation of coronene to soot at 800 K from 0-2000 picoseconds. (Mao, 2017)

The same authors reported in their study, that if the exhaust gases exceed the temperature 1600 K, the nucleation would not occur as the collided PAH particles would dissociate back into monomer state (Mao, 2017). In general, the studies agree that the first nuclei of the nascent soot occurs, when it reaches atomic mass of 2000 amu. (Richter, 2000; Omidvarborna et al. 2015). The mass growth however is not terminated at the formation of nascent soot particle, but the mass growth can continue by condensation of gaseous PAH onto the surface of the soot particle. (Omidvarborna et al. 2015)

9.2.4. Coagulation and agglomeration

Coagulation occurs as soon as the first nascent soot particles are formed. (Omidvarborna et al. 2015). As the first particles are still light enough to have the attraction forces, these particles bind to each other, forming larger units, which at some point are stable enough not to coagulate with particles of its size.

The agglomeration has similar basic principle as coagulation, but of larger particles. The larger particles collide and stick together due to the weaker intermolecular forces.

9.2.5. Oxidation

So far, soot formation has been discussed, starting from molecular building blocks all the way up to the visible particles. One should however not forget, that the combustion and soot formation process occurs while surrounded by vast amount of oxygen. This means, that the oxygen can disrupt the carbon bonds of the molecules at any moment and convert them into CO₂ or CO depending on the amount of oxygen present. In essence, unlike the other five steps described above, oxidation can occur at any point of the soot formation process. Oxidation occurs on the surfaces of the soot particles.

However, the oxygen is not the only specie that can oxidize soot, although it is most important component regarding the soot mass loss and reduction of carbon accumulation on soot. In flames that are rich in fuel, species such as O, O₂ and OH are the oxidizing species, while in lean flames, components such as H₂O, CO₂, N₂O, NO and NO₂ also are viable oxidizers. (*Omidvarborna et al. 2015*). The formation of the oxidizers is not in the scope of this thesis.

9.2.6. Influence of various parameters

In the chapters above, the most discussed reaction pathways are presented in a simplified form and the reaction conditions are not taken into account. The amount of PAH generated depends on various parameters, such as is the used fuel aliphatic or is it aromatic. For instance, *Richter et al. 2000* state in their study, that the PAH formation in aliphatic fuels is much lower than in the aromatic fuels and the maximum PAH formation is never reached in aliphatics. Meanwhile in aromatic fuels, the rate of PAH formation is up to 200 times higher. This of course can be explained by the fact that the aromatic rings do not have to be formed, as the fuel itself contains them.

In respect of fuels, it is difficult and tedious work to assess which mechanism is dominant for which type of fuel and therefore falls out of scope of this thesis. The used IFO is a mixture of aliphatic and aromatic substances and in addition, IFO contains a fraction of asphaltenes, which are presented in the figure below.

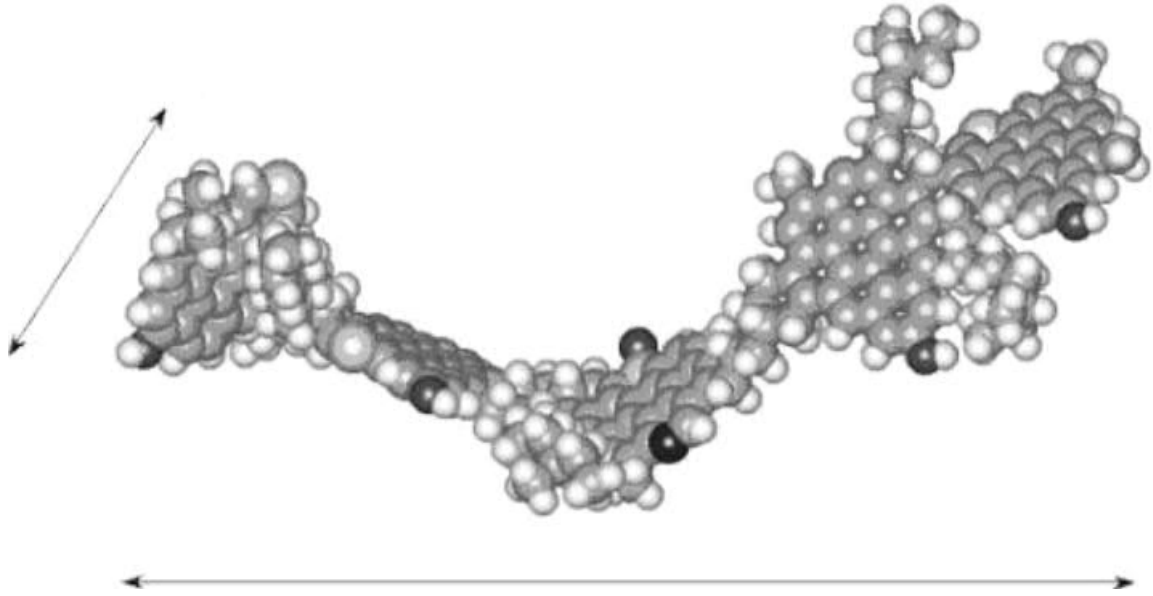


Figure X. Asphaltenes are aromatic molecules, with mass of about 700 amu (*Auflem, 2002*). Black atoms are representing heteroatoms such as oxygen and sulphur.

These asphaltenes tend to form more soot and PAH (*Mastral et al. 2000*), during the fuel pyrolysis, i.e. fuel preparation of combustion (*Aakko-Saksa et al. 2017*). This means that depending on the region in flame, different mechanisms are proceeding simultaneously. In case of MGO, longer saturated chains prevail in the composition and therefore the combustion does not generate as much PAH, as the first benzene rings must be formed for further increase of PAH.

Another important aspect, that has great influence on PAH formation is pressure. According to *Frenklach 2001*, under higher pressure, more PAH is formed than in atmospheric. This observation feels intuitive as PAH formation reduces the number of gaseous molecules and thus, relieving the pressure. In terms of pressure, the cylinder pressure is a function of engine crank angle. Although, the bore is near top dead center (TDC), when the ignition commences, the pressure is not constant. The main aim of this whole chapter is to establish the link between PAH and soot.

10. PAH and Soot in Exhaust Gas

The soot formation does not deplete all PAH as the rule of the processes never to reach 100 % conversion applies also here. After the expansion stroke is finished, the piston bore rises back up for the discharge stroke and the cylinder valves are opened for the exhaust gas to escape the combustion chamber to the turbine of the turbo compressor unit. There the exhaust gases are cooled down to approximately 670 K.

In study by *Cooper 2003*, author measured different amount of PAH in the exhaust gases of smaller auxiliary engines of passenger ferries. There are also extensive studies conducted by *Aakko-Saksa et al. 2017*. and *Teinilä et al. 2018* regarding the general ship emissions and the influence of the installed cleaning equipment on the emissions.

It is important to highlight, that PM is not equivalent to soot. PM does contain soot, but it also consists of ash, sulphates, metals and other impurities, that have escaped from the engine after combustion. (*Teinilä et al. 2018*). Soot can also be fractionized into two fractions – organic carbon (OC) and elemental carbon (EC) (*Li et al. 2018*). In the figure 11 below, a composition of PM of certain ship is presented.

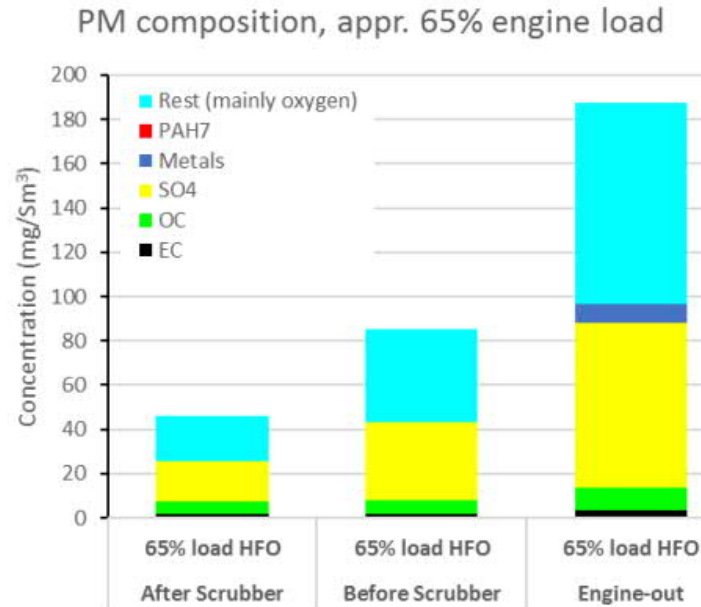


Figure 11. Concentration and composition of PM at various locations of the exhaust gas delivery process. Used fuel is HFO combustion. Before the scrubber, there was a Diesel Oxidation Catalyst installed, which reduced the amount of PM in the exhaust gas. The PAH fraction of PM is miniscule. (*Teinilä et al. 2018*)

In the set of studies by *Aakko-Saksa et al. 2017* and *Teinilä et al. 2018* the PM samples were collected straight from the gases and prepared for GC-MS analysis. In one measurement of PAH on PM by *Aakko-Saksa et al. 2016* over 20 PAH were analysed. Based on the profile of PAH on PM in the figure 12, it can be observed, that the PAH compounds that were found on the PM primarily were part of heavier PAH.

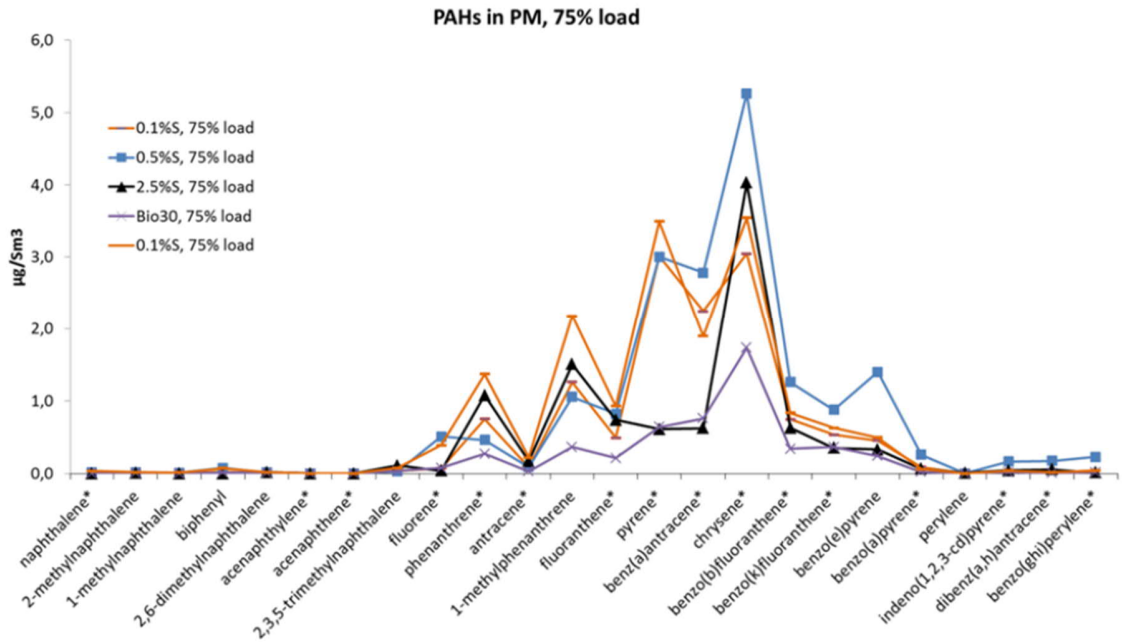


Figure 12. PAH concentrations of various fuels in PM per normalized m³ of gas. The relevant EPA 16 PAH for this thesis are marked with asterisk *. (*Aakko-Saksa et al. 2017*)

The highest peaks of the profile are set at the heavier compounds, which is intuitive when considering previous chapters, where it was determined that the PAH with higher molecular mass tend to coagulate on surface of soot particles. In the study by *Cooper 2003*, the PAH were measured directly from the gaseous phase and not from the mitted PM. The reported values were in microgram/kWh, but for better comprehension, the results are converted into mg/h and g/h. In the following table 2, the calculated results are presented.

Table 2. A table of light EPA 16 PAH in mg/h, using the engine specifications and measurement results found in the article of *Cooper 2003*. Yellow cells are MGO, green are MDO and grey are IFO.

Engine	B/AE1	B/AE1	C/AE1	C/AE1	D/AE1	D/AE2	E/AE1	E/AE3
Load	55.00 %	56.00 %	51.00 %	48.00 %	43.00 %	48.00 %	41.00 %	39.00 %
Naphthalene	295.68	251.66	46.98	32.49	470.94	348.10	5198.60	4574.41
Acenaphthylene	1.11	0.42	0.19	0.18	0.41	0.75	1.10	1.56
Acenaphthene	2.85	1.56	0.14	0.14	0.35	0.64	32.90	19.55
Fluorene	23.76	17.98	0.77	0.50	21.00	29.84	164.51	117.29
Phenanthrene	46.46	47.94	0.34	0.23	95.46	127.16	888.37	766.31
Anthracene	0.48	0.15	0.05	0.05	0.45	0.82	15.35	1.95
sum mg/h	370.34	319.70	48.47	33.57	588.61	507.30	6300.83	5481.08

In the table 3 below, the fraction of heavy PAH in exhaust gases are presented.

Table 3. A table of heavy EPA 16 PAH in mg/h and g/h, using the engine specifications and measurement results found in the study by *Cooper 2003*. Yellow cells are MGO, green are MDO and grey are HFO.

Engine	B/AE1	B/AE1	C/AE1	C/AE1	D/AE1	D/AE2	E/AE1	E/AE3
Load	55.00 %	56.00 %	51.00 %	48.00 %	43.00 %	48.00 %	41.00 %	39.00 %
Fluoranthene	1.16	0.36	0.02	0.05	5.09	9.95	10.97	77.41
Pyrene	0.26	0.06	0.02	0.02	3.82	9.24	61.42	25.80
Benz(a)anthracene	0.24	0.15	0.14	0.14	0.32	0.57	8.77	4.69
Chrysene	0.05	0.09	0.07	0.09	0.25	7.10	29.61	25.02
Benzo(b)fluoranthene (UNECE)	0.08	0.12	0.10	0.09	0.29	0.57	1.10	1.76
Benzo(k)fluoranthene (UNECE)	0.13	0.21	0.17	0.16	0.25	0.50	1.10	0.16
Benzo(a)pyrene (UNECE)	0.13	0.21	0.17	0.18	0.48	0.89	2.19	3.52
Indeno(1,2,3- c,d)pyrene (UNECE)	0.32	0.45	0.41	0.38	3.50	5.33	9.32	17.20
Dibenzo(a,h)anthracene	0.40	0.57	0.50	0.47	3.18	5.33	8.77	16.81
Benzo(g,h,i)perylene	0.13	0.21	0.17	0.16	0.04	0.05	0.09	17.20
sum mg/h	2.90	2.43	1.77	1.74	17.22	39.52	133.35	189.58

When comparing the tables 2 and 3 to the figure presented in the figure 13, it leads to conclusion, that in the PM mainly heavy PAH are present and that the lighter fraction of PAH escapes as gaseous emissions from the stack. Small fraction of heavier PAH however remains in the exhaust gases.

Based on the results, there is a substantial amount of PAH present in the exhaust gas as gaseous emissions. Especially it must be highlighted, that the mass amount of lighter PAH in exhaust emissions is much higher compared to the mass of heavier PAH. In addition, it can also be seen that different fuels emit different amount of PAH, in following order: MGO<MDO<HFO

11. PAH and soot solubility in water

As the exhaust gas enters the scrubber, it is encountered by vast counter flow of wash water. The wash water cools rapidly the temperature of the exhaust gas down from approximately 520 K down to 300 K, depending on the temperature of the used water. The amount of wash water varies from 400-800 m³/h depending on the engine load.

As the water droplets collide with the soot particles, they envelop the soot into the aqueous phase. The process is however not as straight forward with gaseous PAH emissions, so observing their behavior with the wash water and the chemical thermodynamics must be taken into account.

11.1. Solubility in pure water

One of the most basic principles in chemistry is “similar dissolves similar”. Since PAH are organic compounds, they have poor solubility in inorganic water, due to the differences of attraction forces. In case of organics, the Van-der-Waals forces are dominant and in case of water, the strong dipole hydrogen-oxygen -bridges prevail. As the soot is mainly carbon, it does not dissolve in water but remains as suspension in the aqueous phase. Some of the parameters for the PAH solubilities were not found in the literature and thus were estimated relying on the literature.

11.2. Solubility in saline water

Since the scrubbers can use saline water from sea chest while operating, the regular solubility does not apply as it has been long established, that the increasing concentration of salts and other electrolyte compounds will have a reductive effect on the solubility of organic compounds. In year 1889 Russian scientist Setchenow presented an empirical equation to describe so called salting-out effect (*Eganhouse et al. 1976*):

$$\log \left(\frac{S_0}{S} \right) = k_s C_s \quad (3)$$

where:

- S_0 is the solubility of organic solute in fresh water [mol/dm³]
- S is the solubility of organic solute in saline water [mol/dm³]
- k_s is the Setschenow constant
- C_s is the concentration of salt in [mol/dm³]

Since the Setchenow constants are dependent on temperature of the sea water, there has been no data found on Setchenow constants for every component. Since there is data available for solubility of PAH compounds in fresh water, *Xie et al. 1997* suggest a simple estimation of solubility of seawater solubility, by simply dividing the fresh water solubility by factor 1.36. Authors highlight, that there can be some irregularities in cases of some solutes, but none were mentioned regarding PAH and that the estimation is valid with NaCl solutions of 3.0-3.5 %.

Another possibility how to estimate Setchenow constants is mentioned in the study of *Ni et al. 2003*. Authors present an equation basing on the PAH octanol-water partitioning coefficients (K_{ow}) (*Ni et al. 2003*):

$$k_s = 0.040 \log K_{ow} + 0.114 \quad (4)$$

In their study, authors proposed also equations basing on the molecular volume (V_{LeBas}) and solubility in fresh water, but the K_{ow} yielded best R^2 -value of the plot.

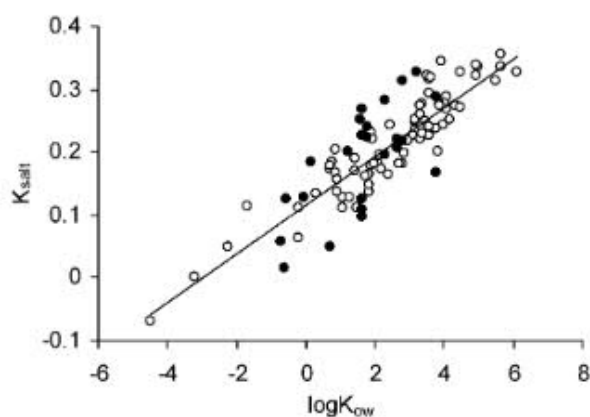


Figure 13. Plot $\log K_{ow}$ vs k_s . ($n=101$, $R^2=0.7717$, S.E. = 0.0410) (Ni *et al.* 2003)

The values of $\log K_{ow}$ for selected 16 PAH are found in pubchem.com and are presented in **Appendix F**.

At this point it must be highlighted, that only the effect of NaCl is observed in this review of salinity effect on the PAH solution. The sea water composes from several other ions, which have different activity from Na^+ and Cl^- . Although, in their study Xie *et al.* 1997 stated, that the obtained Setchenow constants were approximately the same for artificial sea water and natural sea water. Therefore, the effect of the other ionic species is not considered nor discussed in this review.

12. PAH quenching

In this chapter the adsorption of PAH to soot surface is discussed. It is an essential phenomenon in respect to the thesis. As it was earlier discussed, that there is contradiction between in line fluorescent sensors and the laboratory analysis of the wash water samples. As reported by *Lahtinen 2016* and *Hensen 2012*, the laboratory analysis indicates much lower values, which are barely detectable, compared to the sensors. In case of MV Ficaria Seaways the sensor was sent to the manufacturer for maintenance and recalibration, but no issue has been detected in sensor operation. In PhD thesis *Lahtinen 2016* reports method 8310 (USEPA 1986) was used to analyze for PAH, it was however not reported if the soot samples were analysed for PAH. In report on MV Ficaria Seaways (*Hensen, 2012*), it is suspected that PAH is trapped in soot. According to numerous articles, PAH adsorbs onto the soot particles – quenched – but the usual sample preparation method as asked in the IMO guidelines does not take it into account. The interaction of PAH and soot can be dynamic or static. Although dynamic quenching is not in the scope of the thesis it is still shortly discussed.

12.1. Dynamic quenching

Dynamic quenching affects primarily the sensor measurement as its measuring principle is based on the fluorescence of PAH. The UV rays from sensor excite the PAH molecules, the molecules emit light with longer wavelengths after a short time delay. The sensor measures the intensity of the emitted light and converts it to the PAH concentration. (*Hach, 2010*)

In essence, the dynamic quenching occurs when the smaller PAH molecule collides with much larger molecule, such as humic acid or fulvic acid (*Wang et al. 2015*). The humic acids and fulvic acids are present in the seawater by nature. Their source is still not exactly known, but it is assumed that they are derived from dead organic matter – such as dead fish or strayed wood trunk – which has been dissolved to a molecular state over time. Humic acids are larger molecules than fulvic acids. (*Pettit, 2004*)

As the PAH molecule collides with such molecule, its energy level shifts. As it passes the sensor detector, the sensor excites molecules energy level even further. The reflected radiation back to the analyzer does not correspond then with the expected PAH radiation range. Therefore, the PAH remains unregistered and sensor shows lower concentration of PAH in the flow.

Even though the sensor shows lower values, it still exceeds the results that are obtained from laboratory wash water sample analysis. In the following chapter, the discussion concentrates on static quenching.

12.2. Static quenching in fresh water

Unlike the dynamic quenching, static quenching occurs when PAH molecules physically or chemically adsorb on the surface of the soot and dissolved organic carbon. In this chapter, the adsorption isotherms are not discussed in depth, as according to *Tremblay et al. 2005*, too many parameters have influence on most of the isotherms. Some results are presented as a possible guideline of graphical presentation of the adsorption phenomenon.

It has been observed that the adsorption of PAH to the soot particle in aqueous surroundings is exceptionally strong, when comparing the adsorption of other hydrophobics into natural organic carbon. (*Jonker et al. 2002; Bucheli et al. 2000*). This is not in contradiction to the discussion in earlier chapters on soot formation from PAH. If one observes the soot structure, one can see the increased surface of the soot particle. The suggested soot structure is presented in the figure 14 below.

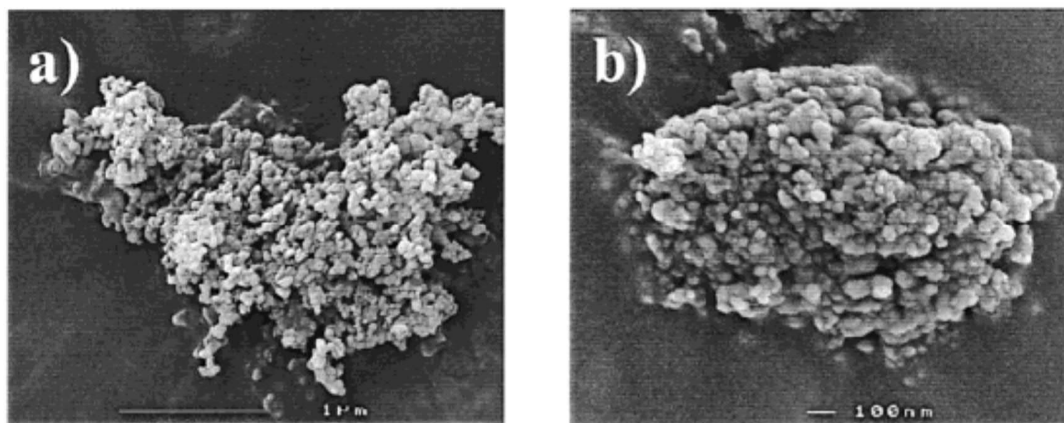


Figure 14. Electron scanning microscope images of traffic and oil soot. According to the source (*Jonker et al. 2002*), the diesel soot is similar to the examples in this figure. “Grape bunch”-like structure supports the qualitative discussion in chapters 4 and 5. (*Jonker et al. 2002*). In the following table, the properties of the Diesel soot are presented. Same soot was used in studies of *Jonker et al. 2002* and *Bucheli et al. 2000*.

Table 4. Properties of used NIST standard reference material SRM-1650. (*Bucheli et al. 2000*)

Parameter	Value	Unit
Average aggregate size	180±20	nm
Primary soot sphere diameter	30	nm
External geometric surface area (2D)	100	m ² /g
BET surface area (3D)	48	m ² /g
Average pore volume	150	Å
Average pore diameter	0.180	cm ³ /g
total organic carbon content	0.770±0.018	[gC/gSolid]
soot carbon content	0.481±0.005	[gC/gSolid]
amorphous carbon content	0.289±0.019	[gC/gSolid]

In their study *Jonker et al. 2002* investigated the solid-liquid equilibrium of PAH, by adding to the solution deuterated PAH isotopes. It was observed, that not all native PAH were available for equilibrium measurements, as their desorption rate was practically nonexistent in water solution. This let the authors to conclude, that the native PAH adsorbed to the high energy containing sites of soot particle, leaving for added PAH the weaker energy sites. Authors also state, that the unavailable fractions of the native PAH support the hypothesis, that the more voluminous components end up into the narrow-slit pores of the soot, resulting in extremely low desorption. This however does not mean that the PAH couldn't be extracted from the soot particle with suitable solvent. (*Jonker et al. 2002*)

Further discussion in the study of *Jonker et al. 2002* it is suggested, that part of the PAH components is trapped within the soot particle already in the gaseous phase. The formed exterior of the soot particle provides a suitable adsorption surface for PAH in aqueous surroundings. It is also speculated, that the soot-like substances, such as PAH are planar and therefore can penetrate through the narrow-slit pores of soot and that their planar structure interacts well with the similarly planar surface of soot particle, causing π -cloud overlapping. During the penetration to the pores, it is suggested that PAH molecules experience enhanced adsorption energies due to the multiple contact points within the soot molecule. (*Jonker et al. 2002*)

The study of *Jonker et al. 2002* provided a good insight on the events of PAH with soot interactions. Nevertheless, since the experiment was to determine the equilibrium of PAH and soot in fresh water, the case with seawater is much different as presented in the study of *Tremblay et al. 2005*.

12.3. Static quenching seawater

Tremblay et al. 2005 did an extensive study on effects of temperature, salinity and humic substances on PAH adsorption on estuarine particles. It must be emphasized, that the approach to the influence of these parameters on PAH adsorption is different from this thesis. In the study by *Tremblay et al. 2005*, the solution of PAH and other parameters was done in prior to altering the parameters values, resulting in observable changes of adsorption mechanism. In this thesis, PAH is directly transferred in ready solution (seawater) and no post alterations are performed on the matrix, except for temperature. The temperature change will be discussed in following chapter of sampling.

The sorbent in the study of (*Tremblay et al. 2005*) are estuarine particles, which are sediment of river mouths and differ from soot by structure and chemical composition. Authors indicate, that the field-based studies are in contradiction with laboratory-based results. For instance, in laboratories a linear correlation is obtained for adsorption isotherm, while field data indicates poor correlation and even opposite trend is possible. The non-linearity can be explained by the presence of a second sorbate, which causes competing sorption of PAH. In both cases, presence of sorbate – dissolved or suspended – results in a higher apparent solubility of the PAH. (*Tremblay et al. 2005*).

Since the adsorption is enthalpy driven process, increasing temperature increases solubility of PAH. With increasing salinity, the fraction adsorbed to the sorbate increases, as expected. In figure 15, the partition coefficients K_p of phenanthrene and fluorene at different temperatures and salinities are presented.

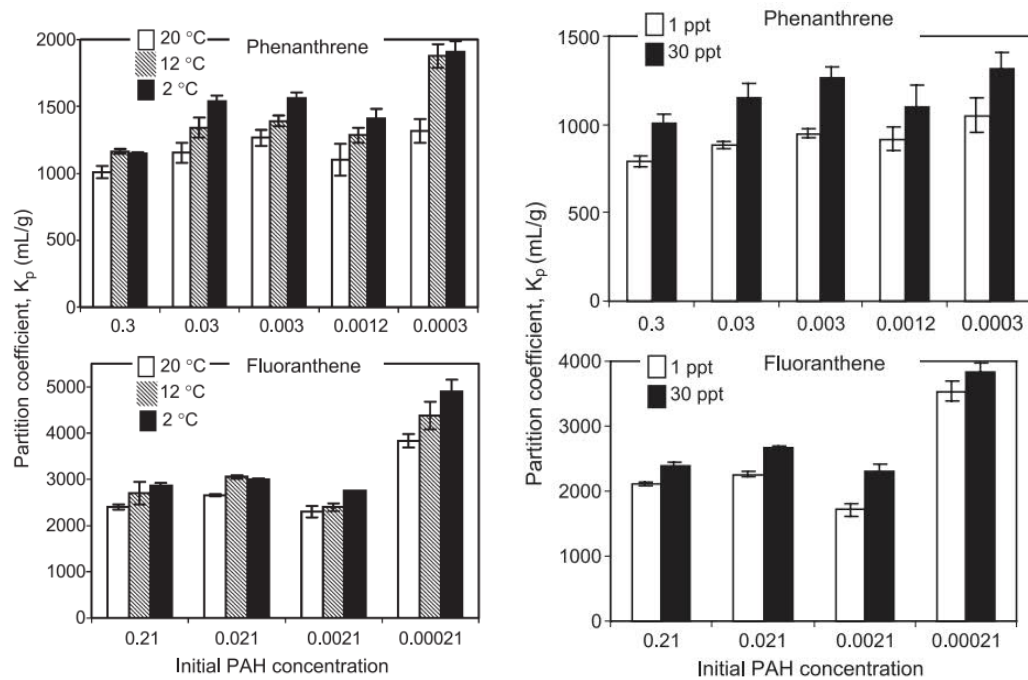


Figure 15. Partition coefficients of phenanthrene and fluoranthene at different temperatures and salinities respectively. (Tremblay et al. 2005).

The influence of dissolved organic compounds has been detected not to have ability to compete with the estuarine particulates for PAH sorption.

Applied part

13. Estimating unknown solubilities

For establishing the mass balance of the PAH species, the solubility of PAH is necessary to know at different temperatures. The temperature dependent solubility functions (TDSF) were not available for all PAH species, especially for the heavier PAH. Nevertheless, the data found in literature, provided sufficient information to estimate the TDSF for the remaining PAH species. The used method was 3rd degree polynomial regression analysis, that provided encouraging results. The selected temperature range for this analysis was 15-30 °C. The known TDSF were reported by *May et al. 1978* and are presented in **appendix G**.

For all known PAH species, the average solubility was calculated over the selected temperature range. The average of TDSF was calculated and every value of corresponding TDSF was divided by its average. This yielded a set of averaged TDSF. Then, using 3rd degree polynomial regression analysis an unscaled approximation function (UAF) was generated, containing all values of averaged TDSF. The reason for 3rd degree polynomial is, that the original TDSF as reported by *May et al. 1978*, are presented as 3rd degree polynomials. The plot for the unscaled approximation function fitted for all averaged available TDSF is presented in the figure below.

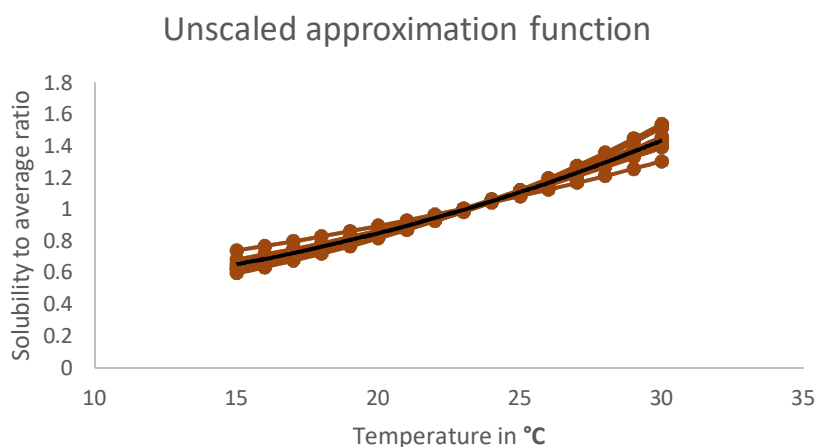


Figure 16. Averaged available TDSFs of individual PAH species and UAF trend. The UAF is $UAF(T) = 10^{-5}t^3 + 0.0005t^2 + 0.0104t + 0.3373$ and the coefficient of determination $R^2 = 0.9783$. The residuals are presented in **appendix H**.

The unknown TDFS of remaining PAH were estimated by introducing the additional scaling coefficient “**c**” into UAF. As the solubilities of all individual PAH are known at 25 °C, the scaling coefficient **c** is iterated, so that the UAF generates equal solubility as reported. The iteration scaling coefficient is done with Excel’s “goal seek” function. With scaling coefficient **c**, the UAF takes following form:

$$f(T) = c * (UAF(T)) \quad (5)$$

The **c** values for each individual PAH are presented in the **appendix i**. The obtained solubility curve was compared with the solubility curve of known PAH species. In the figures 17 below, results for phenanthrene and anthracene are presented. All remaining results are presented in **appendix J**.

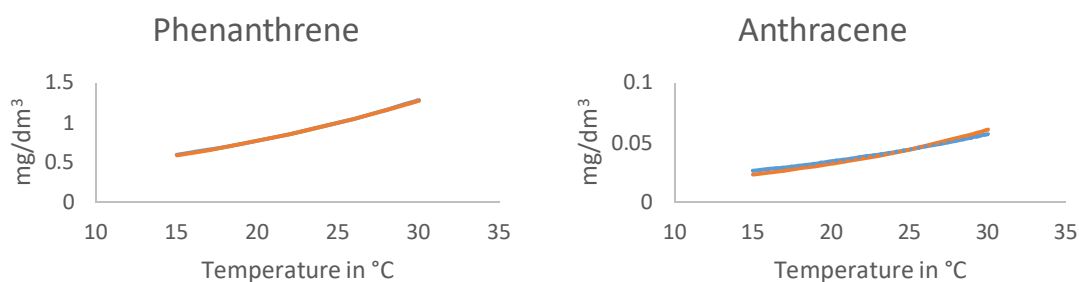


Figure 17. Left: Phenanthrene $c=0.94$. Orange line *May et al. 1978*, blue line: equation 5. Right: Anthracene $c=0.042$. Orange line *May et al. 1978*, blue line: equation 5.

The estimates fit well with the solubility equations presented by *May et al. 1978*, suggesting that solubilities of the unknown species can be estimated with good confidence. In addition, the solubilities of the presented species vary significantly, suggesting that this estimation is applicable on wide range of solubilities. These estimations are only valid on the selected temperature range. In case new solubility equations must be calculated, one must bear in mind that the equations of *May et al. 1978* are valid on the range of 5-30 °C. Therefore, it is not recommended to apply reported values past the initially selected temperature range.

For further calculations of the seawater solubility and Henry's constants, estimated solubilities are used only for the species that were previously unknown. Otherwise, the equations by *May et al. 1978* are implemented.

14. Henry's law constants calculation

In the study by *Cooper 2003*, it is presented, that what magnitude of PAH mass flow it is expected. Although the used engines were smaller, the exhaust gas flow still ranged between 2600-7150 Nm³/h. This yields, that the PAH are extremely diluted and Henry's Law is applicable as presented in the figure below.

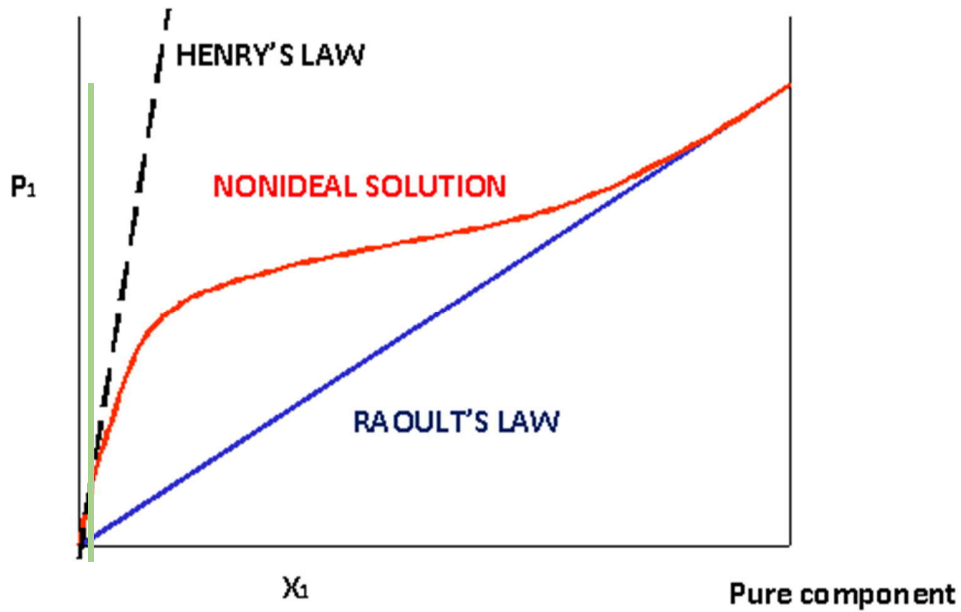


Figure 18. The space between the y-axis and the green line represents the range, within which the Henry's law is applicable. Green line is a modification to the figure from *LibreTexts, 2019*.

Since the PAH while entering the scrubber are in the gaseous state, the absorption by Henry's law applies and ideal gas conditions are assume. Henry's law is presented as follows (*Alaee et al. 1996*):

$$\mathcal{H} = \frac{P_v}{S} \quad (6)$$

where:

- S is solubility in mol/m^3
- \mathcal{H} is Henry's law constant of component
- P_v is vapor pressure of component in gaseous phase.

Although the Henry's Law applies at constant temperature, it is often assumed, that the seawater cools the gases down rapidly to constant temperature and therefore the Henry's Law can be applied. In case of PAH, their solubility in distilled water alone is extremely low, so an assumption can be made, that no absorption of PAH occurs while exhaust gas is hot.

There were numerous methods presented in the literature, which proposed methods for calculating Henry's law constant \mathcal{H} for different PAH species. Unfortunately, majority of the obtained Henry's constants differed from each other, depending on the method with which they were determined. Another problem is, that the Henry's constant is often determined for one temperature only. However, a study by *Bamford et al. 1999* was performed for determining the Henry's law constant \mathcal{H} of several PAH over temperature range $4.1 - 31^\circ\text{C}$. *Parnis et al. 2015* authors determined the Henry's law constant \mathcal{H} over wide range of components and temperatures using the COSMO-RS method and presented the equations for each component in the following form:

$$\log \mathcal{H} = A + B/T \quad (7)$$

where:

- \mathcal{H} in $\text{Pa m}^3 \text{ mol}^{-1}$
- A and B measured coefficients
- T in K

The coefficients A and B for equation 7 are presented in the **appendix K**.

To estimate the Henry's law constant in saline water \mathcal{H}_{SW} the calculated regular Henry's law constant \mathcal{H} is used. First, the vapor pressure P_v of individual PAH over the temperature range is calculated, by multiplying the Henry's constant \mathcal{H} with the saturation solubility – converted to mol/m^3 – of the PAH component.

$$P_{vi} = \mathcal{H}_i \cdot C_{sat\ i} \quad (8)$$

where:

- P_{vi} is the vapor pressure of the component in Pa
- \mathcal{H}_i is the Henry's law constant in $\text{Pa m}^3 \text{ mol}^{-1}$
- $C_{sat\ i}$ is the saturation solubility in mol/m^3 .

After obtaining the vapor pressure P_{vi} the Henry's law constant for saline water \mathcal{H}_{SW} can be calculated using solubility into seawater, which can be calculated by using equation 3.

To validate the approach by directly substituting the sea water solubility into equation 8 for Henry's law constant for saline water \mathcal{H}_{SW} , the study by *Alaee et al. 1996* is used for reference. In their study, authors investigated the effect of NaCl and temperature on \mathcal{H} of phenanthrene. In the determination of effect of NaCl, the authors stepwise increased the salt concentration and evaluated the Henry's constant \mathcal{H} with gas stripping apparatus. Before going into the results of evaluation, it must be emphasized, that initial Henry's constant \mathcal{H} in *Alaee et al. 1996* study was lower compared to the obtained by using *Parnis et al. 2015* estimates. The investigated Henry's constant \mathcal{H} is at 25 °C. Taking this into account, three curves are presented in the figure 19 below:

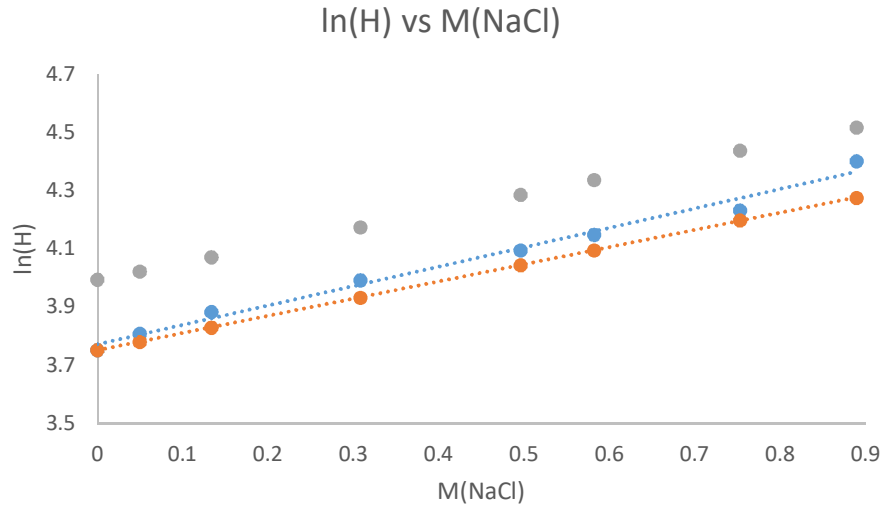


Figure 19. Plots of $\ln(\mathcal{H})$ depending on the salt concentration. Blue: Measurements by *Alaei et al. 1996*. Orange: Calculation of $\ln(\mathcal{H})$ with initial $\ln(\mathcal{H})$ by *Alaei et al. 1996*. Grey: $\ln(\mathcal{H})$ based on the estimates by *Parnis et al. 2015*.

Based on the results, it appears that *Parnis et al. 2015* method overestimates the $\ln(\mathcal{H})$, while calculations with Setchenow constants underestimates it slightly. The latter can be explained, by inaccuracy of Setchenow constants, as the influence of temperature on these constants is not reviewed in this thesis. Setchenow constant are presented in the literature part chapter 11.2. The deviation is however very low and therefore the previously presented calculation method can be used with good confidence. Regarding the overestimation of *Parnis et al. 2015* the obtained initial Henry's law constant falls still in range of constants found in the study of *Xie et al. 1997*. The constants are collected in **appendix L**. It appears, that the Henry's law constant values vary depending on the method, that has been used for the analysis.

Regarding the implementation of this method on field results, the corresponding \mathcal{H}_{SW} for every component considering the salinity and temperature of the absorbing water. After the constants are calculated, they can be implemented on the reported concentrations in the wash water analysis, to calculate the corresponding vapor pressure. From the vapor pressure, the mass of the individual PAH can be calculated with the ideal gas law:

$$pV = \frac{m}{M}RT \quad (9)$$

Where:

- p is vapor pressure in Pa
- V is exhaust gas volume in m³
- m is mass of PAH component g
- M is molar mass of component g/mol
- R is ideal gas constant J/molK
- T is temperature in K

The obtained mass of PAH represents the amount of PAH in the exhaust gas before the scrubber. Since the wash water flow rate and the PAH concentration in wash water is analyzed, the discharged PAH mass can be calculated. Resulting in one last unknown parameter, which is the PAH mass after scrubber in exhaust, a simple mass balance is presented below.

$$m_{PAH \text{ exhaust gas}} = m_{PAH \text{ washwater}} + m_{PAH \text{ after DeSO}_x} \quad (10)$$

Before the implementation of the method, the field study methods, results and evaluation are introduced.

15. Sampling

Two ships were selected for sampling procedure on three different dates. The ship specifications are presented in the following table 5.

Table 5. Analysis and ship operation parameters

Vessel	L/G mass based
Case I	8.15
Case II	8.03
Case III	11.5

The sampling was collected from following locations, that are also presented in appendix C:

- Sea suction
- DeSOx outlet before wash water filtration
- DeSOx outlet after wash water filtration
- Overboard discharge

The samples were drawn from a sampling point that was located at each stream. The samples were then put into polystyrene containers that were transferred to cold storage room at approximately +6 °C. On the day of disembarking the samples, the storage containers were loaded with freeze packs, to maintain the cold temperature during transportation.

The samples were checked several times during remaining transit. The PM fell out on the bottom of the flask by gravity and the remaining solution did not contain any visible suspended solids. The flasks were the carefully placed back into the container to avoid excess mixing as some of lighter components may have been accumulated on the surface and would have otherwise be adsorbed on the cap of the flasks.

For this Thesis a bit different analysis was requested compared to the annual analysis as suggested by IMO. Instead of just analysing the aqueous phase of the sample, the analysis of

solid phase, such as PM, was additionally requested, because it is suspected, that PM adsorbs PAH from the aqueous phase.

15.1. Annual analysis

Annual analysis is usually done accordingly: a sample bottle is first filtered with 0.45 micron mesh to filter out the PM and particulates. Then the aqueous sample is prepared with method EPA 3510 C 1996 with separatory funnel liquid-liquid extraction. After separatory funnel, the sample is analysed according to method EPA 8270E 2017 and the results are reported.

15.2. Analysis for this thesis

For this thesis, an expansion in analysis methods was requested. In addition to the EPA 3510 C 1996 and EPA 8270E 2017 methods, the method EPA 3550C 2007 for analysing the filtered particulates is added. In this method the particulate matter samples are transferred to a dichloromethane (DCM) solvent and are ultrasonically extracted. The sample is then analysed according to method EPA 8270E 2017 with GC-MS.

15.3. Quality control

In addition to the additional method, a quality control of the methods was requested. Here the matrix spike (MS) and matrix spike duplicate (MSD) were added to the extracts and to simulate the conditions of sample delivery from ship to the laboratory, the samples were cooled down for 24 hours, which is usual time for the annual samples to be delivered to the external laboratory.

The MS and MSD contain the same EPA 16 PAH and a known number of spikes are added to the samples. The aim of these is to measure the recovery of the aforementioned methods. The recoveries are then reported and cross evaluated. If the recovery falls outside the predetermined recovery control limit, the analyte compound is flagged. The usual recovery limits are 80-120 % (*R&D systems, 2014*). If the recoveries differ from each other by more than 20 %, the analyte compound is flagged.

15.4. Laboratory results evaluation

In the following figure 20, the dependence on the fraction of coloured cells compared to the amount of PAH in the wash water is presented.

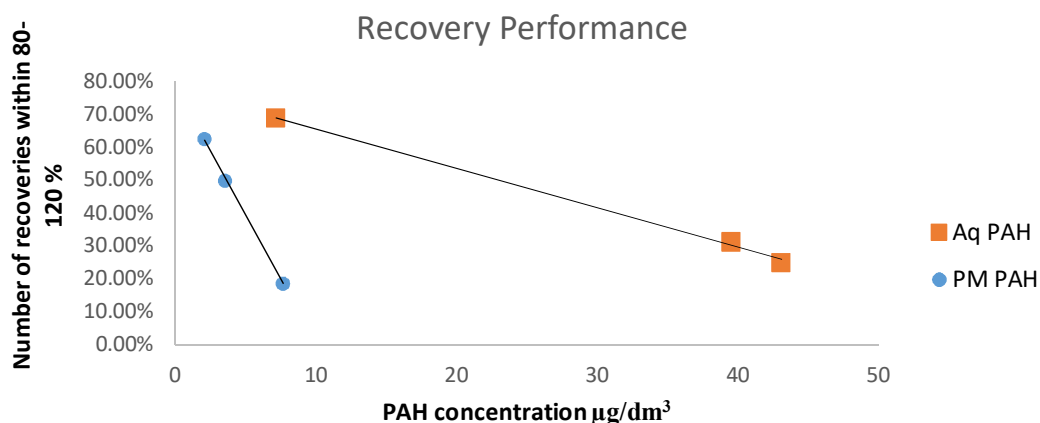


Figure 20. Amount of recoveries that fall outside 80-120 % recovery limits in respect to the PAH found. Blue data is the PAH found on PM and orange is the amount of PAH found in the aqueous phase.

It appears that the more components there are present in the sample, the more recovery rates deviate from 100 % recovery. This may be explained with the evaporation of the PAH, but on the other hand, the PAH that are bound to the PM, are at lower concentrations compared to the aqueous PAH. Prolonged extraction times may be necessary or other recovery method should be implemented. Figure 20 does not however indicate that what recoveries were obtained, but it must be noted, that the recoveries for heavy PAH components were better, than for the lighter PAH.

The poor recoveries for lighter PAH could also be explained with the adsorption to the PM. As it was discussed earlier, that the heavy PAH can adsorb onto the PM/soot structures by attaching to the surface of the pores in prior to aqueous PAH. After the adsorption of heavy PAH has proceeded to such extent that the soot is saturated with heavy PAH, meaning that the only PAH that can adsorb onto soot are the lighter PAH species.

This hypothesis is however in contradiction with the obtained results, as very little of lighter PAH are found in the PM phase. This may be explained, that the ultrasonic extraction couldn't desorb lighter PAH from PM due to the enhanced adsorption of salinity and temperature reduction. There is also a possibility, that the lighter PAH adsorb in quantities

onto sorbates smaller than 0.45 μm , which is the filter mesh size, which are then filtered out. Therefore, they are lost to the remaining analysis.

Another hypothesis for poor light PAH recoveries, is that they are thermally and sonolytically decomposed. This depends on the analysed phase. In the article of *Leonhardt et al. 1998*, it is reported, that ultrasonic extraction with dichloromethane and water can oxidize the acenaphthylene into other components, which cannot be anymore included in the group of EPA 16 PAH. Similar observations were reported in the article of *Sun et al. 2006* on phenanthrene. On the other hand, in the review of *Mastral et al. 2000*, it is reported, that the ultrasonic extraction yields good results when extracting PAH from particulates, meanwhile *Jonkers et al. 2002* advice against it.

Also thermal decomposition of PAH is possible as it was discussed in prior to the field sampling and therefore the ultrasonic extraction was chosen. In addition, the ultrasonic extraction was used for PAH analysis in source articles, therefore the results are somewhat comparable in this aspect. As one can see, there are numerous factors that can influence the recovery of PAH and therefore bias the laboratory results.

16. Laboratory results

The values were corrected by dividing individual PAH species by their reported recovery rate, as the analysis performing laboratory granted permission to do so. However, the correction is an estimation. Below in the figures the result is presented as a percentage.

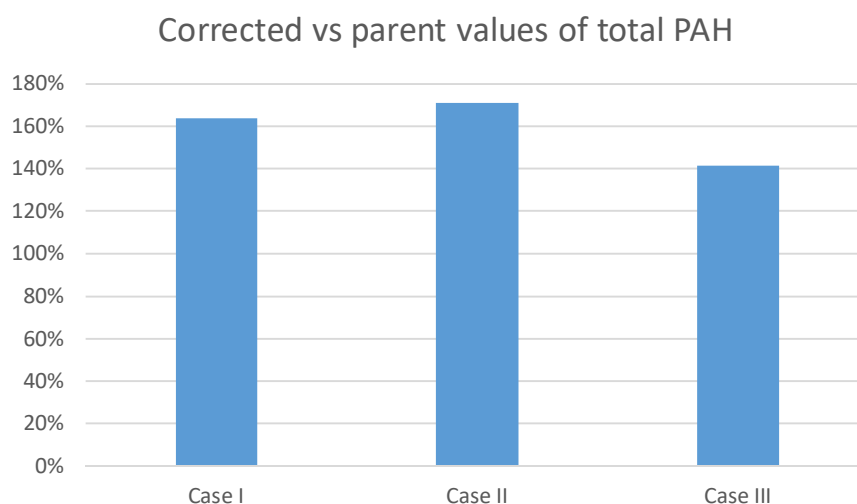


Figure 21. Corrected vs parent total PAH concentrations as percentages.

In the figure below, the percentage of PAH found in the PM compared to the total PAH.

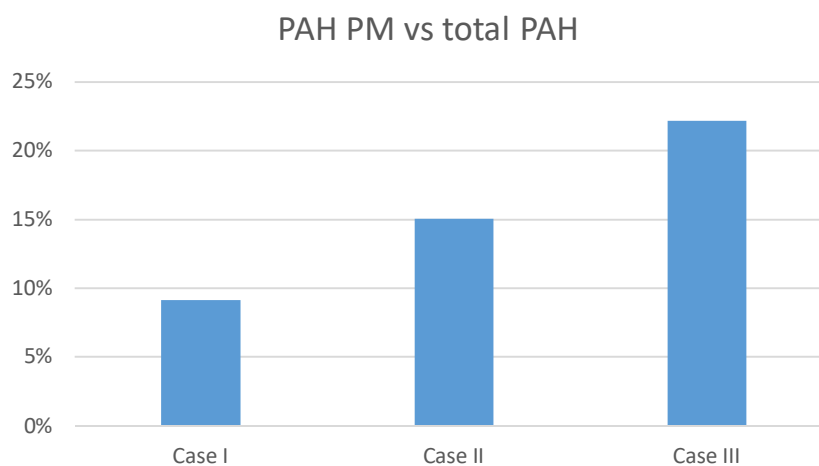


Figure 22. PAH_{PM} vs total PAH.

Considering that the major error does not originate from the adsorption of PAH onto soot, although the adsorption is evidently undeniable, the implementation of recovery rates as means for estimating the parent sample concentrations is from here on viewed more sceptically.

Unfortunately, the analysis results do not differentiate which PAH_{PM} were already in PM and which originated from the gaseous phase and since the results have a significant variation among each other, the proper evaluation would have required the separate PM mass analysis and separate sampling. However, the fraction of PAH in PM is significantly lower, and it is assumed, that only small fraction of PAH is adsorbed onto PM during transportation. Therefore, in this thesis, the PAH_{PM} is not differentiated into solid phase and aqueous phase and the absorption calculations are carried out with PAH_{AQ} .

17. PAH simulation

17.1. Ideal stage

An ideal stage is a theoretical section in which the fluids leaving that section are in equilibrium with each other. Usually the heavier fluid (liquid) is denoted as L and lighter fluid (vapor) is denoted as gas. The principle is presented in the figure below. The mole fractions of solute in aqueous phase are denoted as X and in vapour phase as Y.

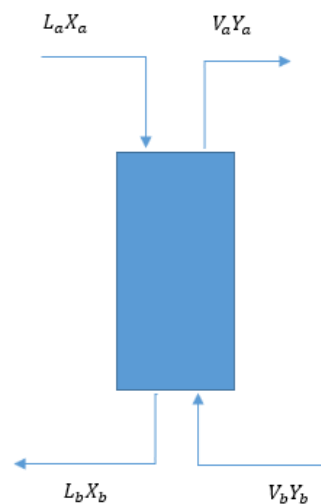


Figure 23. Schematic representation of ideal stage.

It is assumed, that the equilibrium is achieved by means of Henry's law. However, to apply the Henry's law, the system must fulfil some requirements:

- Solute must be dilute enough
- Solute must be supercritical

The Henry's law constants for PAH have been determined among the found literature and in case with PAH, the components are semi volatile, meaning they can vaporize also under room temperature and pressure. According to *Skogestad, 2008*, Henry's law is applicable also on supercritical components. This lets to conclude that also semivolatiles below the critical point can be modelled with Henry's law. It can be debated, whether the latter requirement is fulfilled when regarding PAH and therefore the simulation has been carried out with Henry's law and with pure solubility.

17.2. 1-Stage method

A 1-Stage method in essence is a calculation of mass balance of PAH in the leaving vapour phase. The method assumes no heat transfer, the constant temperature equivalent to the temperature of wash water and constant pressure of 1 atm. In this method the Henry's law constants are implemented. The Henry's law constants must be corrected for the out-salting according to the Setchenow equation as described in literature part in chapter 11.2.

17.3. Scrubber base model

For the base model of a scrubber, the exhaust gas data was collected and modelled. The key component was the SO₂ as scrubbers are initially designed to remove sulphur emissions. The ENRTL is chosen for the thermodynamic model for reactions simulation. Based on the simulation results the SO_x removal efficiency exceeds the 97% requirement with four ideal stages. The obtained model with four stages is used to simulate the PAH absorption.

17.4. PAH absorption modelling

The spreadsheet calculations were done before the flowsheet simulation. Unfortunately, Aspen Plus did not have all required 16 PAH in its databanks and therefore part of the PAH species must have been excluded from the analysis. The remaining PAH had to be regressed individually for their solubility and Henry's law constants with varying salinity and temperature. The UNIQUAC thermodynamic model has been selected for this purpose. The regression did not converge due to the missing binary parameters between inorganic species such as NaCl. The model in Aspen Plus was simplified by removing electrolytic components from water as it is assumed, that the renewed regression bypasses the estimation of binary component interaction of other species. Renewed regression composed out of newly calculated Henry's law constants and solubilities.

Unfortunately, the concentrations of some species were too low for Aspen Plus. As the flowsheet program rounded the values down, divisions by zero occurred in some cases and the program crashed. Such species were again excluded from the simulation and therefore the analysis proceed hereafter with only four species, which are listed below:

- Naphthalene
- Acenaphthene
- Fluorene
- Phenanthrene

Fortunately, these species form most of the mass of formed PAH.

18. Results and discussion

The aim is to compare the results obtained with spreadsheet calculation to the simulated model, which is presented in the figure 27 below.

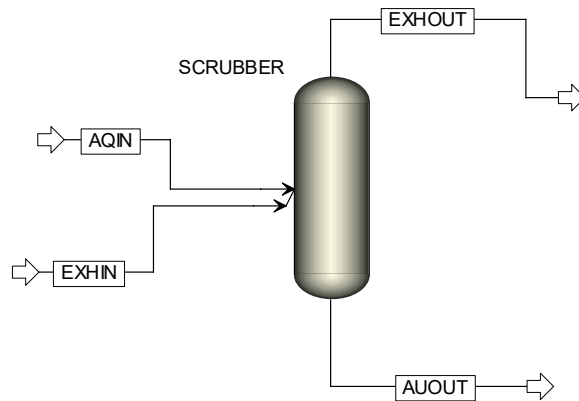


Figure 24. AspenPlus flowsheet, with RADFRAC column as scrubber and design specification blocks for individual PAH.

The used thermodynamic model is UNIQUAC as it is most suitable model for prediction of the activity coefficient in Henry's law. RADFRAC column is used to model the scrubber. The inlet streams are introduced on-stage. Four design specification blocks are included for individual PAH species. The purpose of these blocks is to vary the amount of individual PAH in the exhaust gas so, that it would match with the PAH concentrations reported in the corrected laboratory analysis. Simulations with Henry's law and solubility-based absorption were performed in parallel. In the table 6 below, the error to the hand calculated method is presented.

Cooper 2003, has reported in his study, the PAH emissions as mg/kWh, which were measured directly from stack without scrubber. However, the more closely investigated engine load in that study was in the region of 39-41%, resulting in higher PAH emissions per kWh, which occurs mainly due to the poor mixing of the charge air and the fuel in the combustion chamber. The PAH were also measured across wider load range and are presented in the figure 25. The chosen ship for the comparison between study of *Cooper 2003*

and this thesis is Case III. In the figure below, the lines represent different PAH in mg/kWh. The lines values and purpose are presented in the table below.

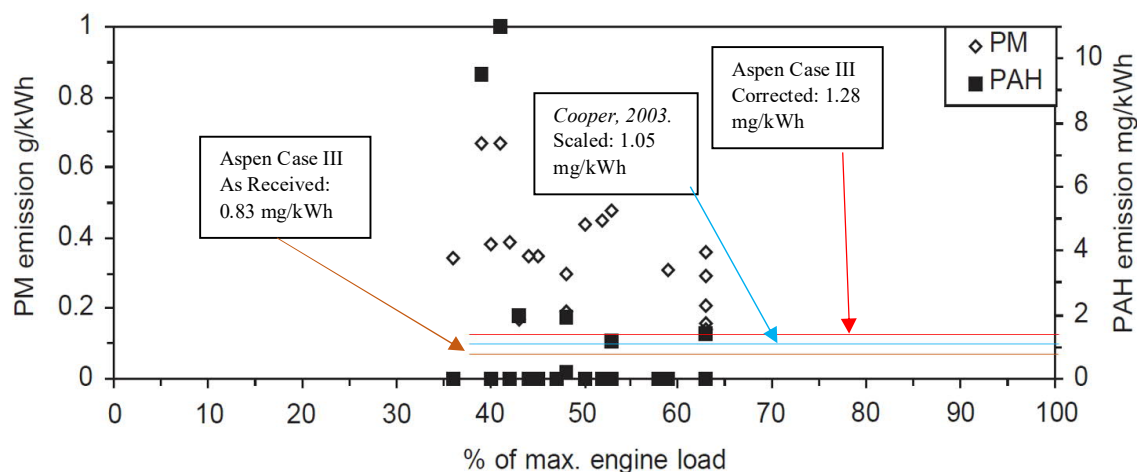


Figure 25. The different PAH values in mg/kWh and estimated sum of naphthalene, acenaphtehene, fluorene and phenanthrene in study by *Cooper 2003*, in mg/kWh.

The study by *Cooper 2003* contains 29 PAH species, which contain also such species as methylated naphthalenes, which contribute significantly to the overall mass. This would indicate that the results based on the four PAH species would be lower than the depicted results by *Cooper 2003*, in figure 25. The results are somewhat discouraging as the scaled value presented by *Cooper 2003*, falls neatly in between the laboratory reported and corrected parent PAH values. Therefore, based on the results, it cannot be determined, which results are more valid. It is also unknown how the generated PAH trend would develop with increasing engine load in the study by *Cooper 2003*.

However, for proper results analysis, three measurements are not enough. In addition, the seawater salinity did not vary significantly to present the visible effect on PAH found. Therefore, for proper deviation evaluation additional points were simulated in Aspen Plus and calculated in spreadsheet.

In the following table 8, the selected parameters and their variation are presented. In the table X the “aqueous PAH”, are the mole fractions of total PAH in wash water. The first two values are based on the concentration found in the wash water of ships Case I and Case III. The last

value is an imaginary case, which estimated higher fraction based on the concentration of previous cases.

Table 8. Varied parameters

L/G (mass)	Salinity (PSU)	Temperature (°C)	Aqueous total four PAH mole fraction
14	0	15	2.76125×10^{-5}
12	20	17	1.59×10^{-4}
10	35	20	2.25×10^{-4}
8	40	25	
6		27	

Based on these values a sensitivity analysis was carried out with Aspen Plus and with hand calculated 1-Stage model. The error between the results of 1-Stage method and Aspen Plus are presented in the appendices N-Y. The error is calculated accordingly:

$$e = \frac{1 - \text{Stage method}}{\text{Aspen Plus simulation}} \quad (11)$$

19. Results evaluation

Based on the results, a certain pattern is observed. The One-Stage method tends to overestimate the PAH mass flow, where the L/G ratio is high and the temperature is low. In respect to salinity, the over-estimation decreases with the increasing salinity. The over estimation however can turn into under estimation, when the L/G ratio decreases and the temperature increases.

A possible explanation to such phenomenon can be the heat transfer between hot exhaust gas and wash water. Since the heat transfer is neglected in the spreadsheet method while Aspen Plus takes it into account. In the figure below, the temperature profile, stage composition in liquid and vapour phase are presented under two different water inlet temperatures. Observed ship is Case III. The main component that is observed is naphthalene, as it's mole fraction in both phases exceeds significantly the fractions of remaining acenaphthene, fluorene and phenanthrene.

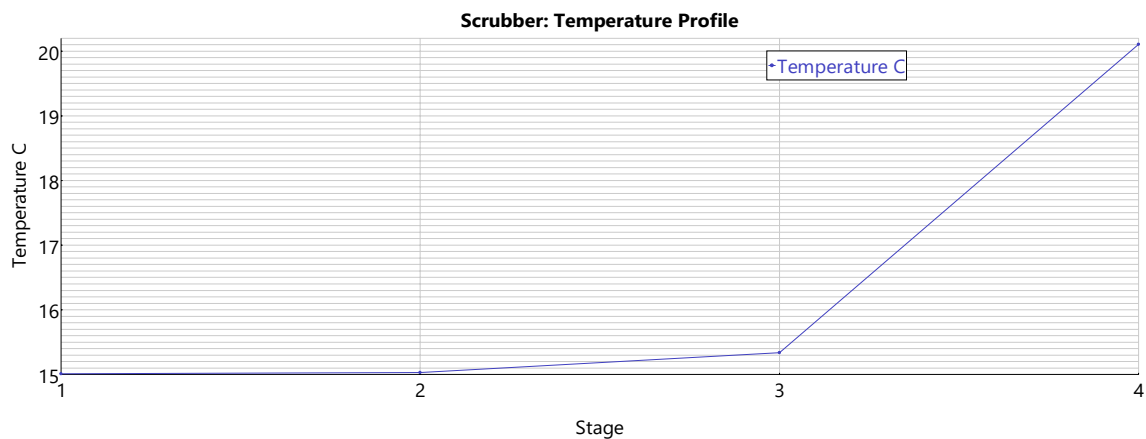


Figure 26. Temperature profile. Case III configuration. L/G 11,5. Salinity 20 PSU. Wash water inlet 15 °C.

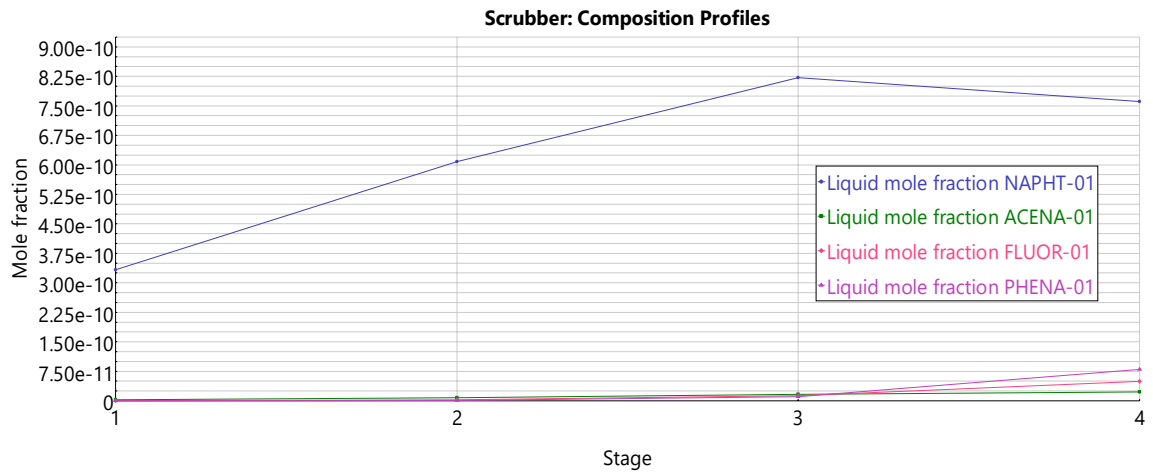


Figure 27. Liquid phase profile. Case III configuration. L/G 11,5. Salinity 20 PSU. Wash water inlet 15 °C.

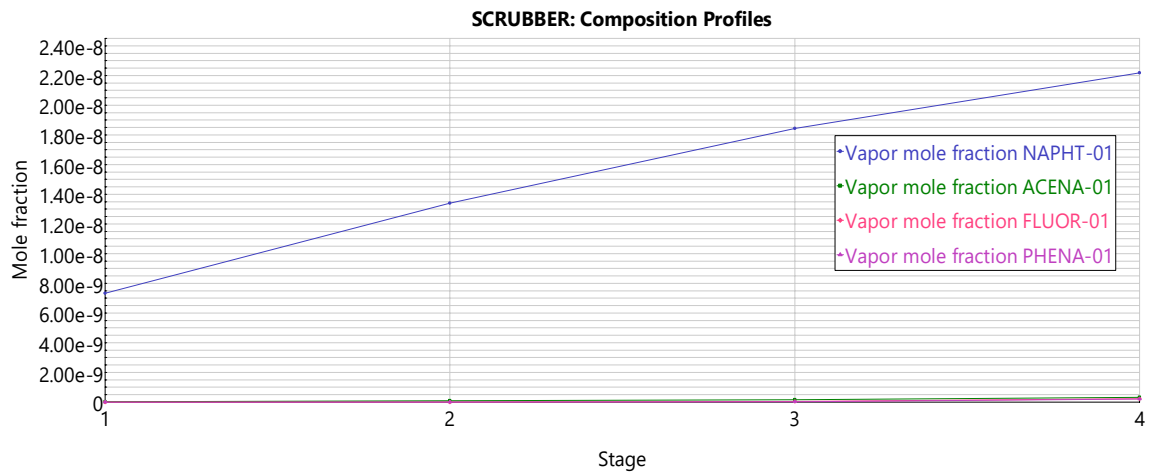


Figure 28. Vapor phase profile. Case III configuration. L/G 11,5. Salinity 20 PSU. Wash water inlet 15 °C.

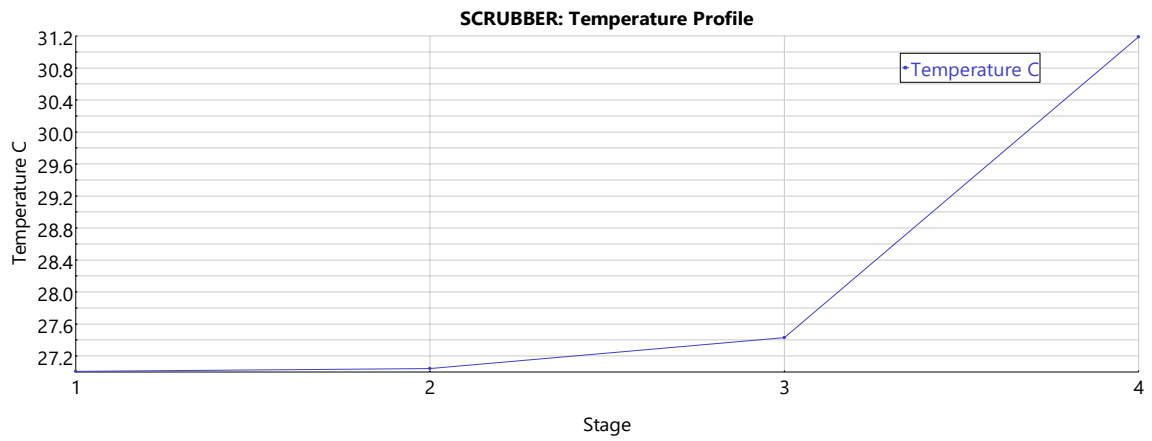


Figure 29. Vapor phase profile. Case III configuration. L/G 11,5. Salinity 20 PSU. Wash water inlet 27 °C.

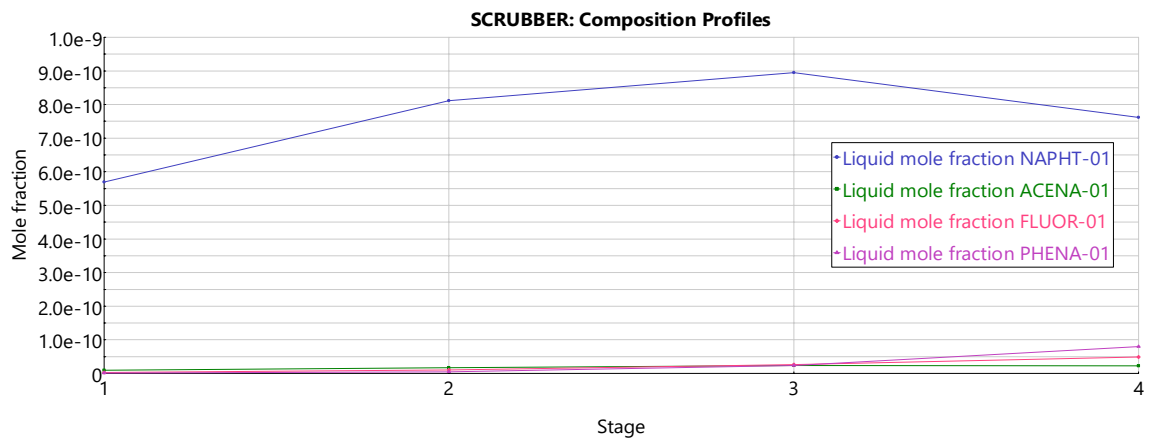


Figure 30. Liquid phase profile. Case III configuration. L/G 11,5. Salinity 20 PSU. Wash water inlet 27 °C.

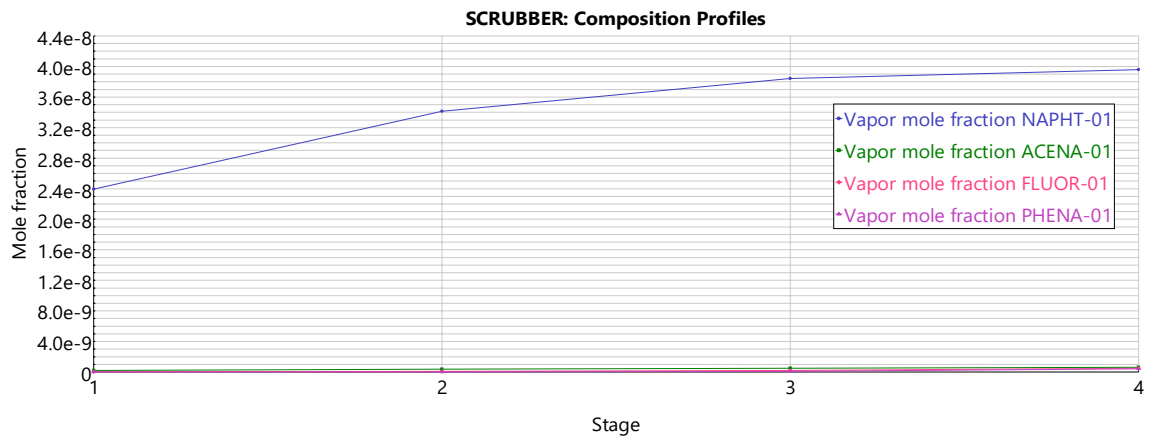


Figure 31. Vapor phase profile. Case III configuration. L/G 11.5. Salinity 20 PSU. Wash water inlet 27 °C.

Based on the figure above, the temperature has significant influence on the PAH absorption. The reduction of the naphthalene mole fraction in the aqueous phase between stages 3 and 4 indicates, that part of the absorbed naphthalene desorbs from the wash water as the hot exhaust gases exchange heat with water. In addition, the influence of the heat can be seen in the elevated mole fractions in the first equilibrium stage, when the wash water temperature is 27 °C, as more naphthalene is present in the vapour phase.

The influence of salinity is presented in the figures below. The used ship is again Case III. The wash water temperature of 20 °C is maintained constant.

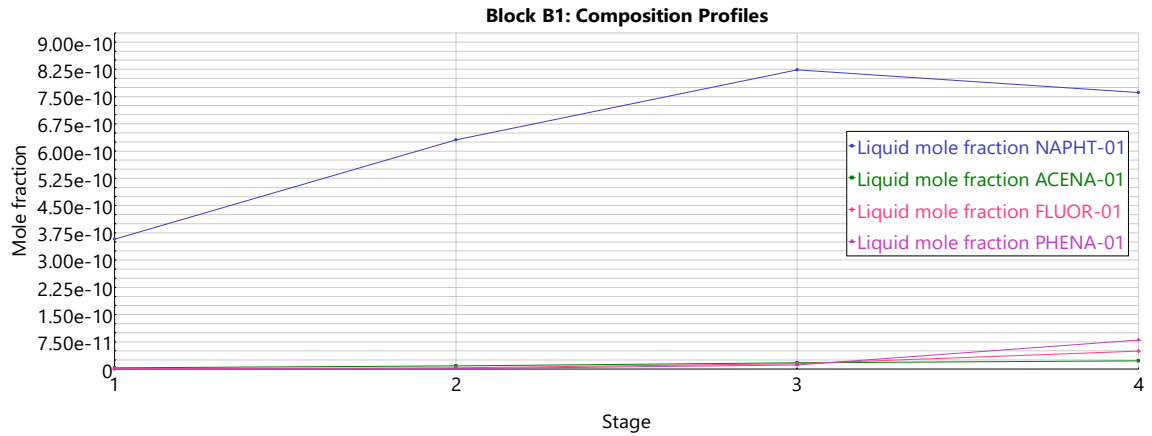


Figure 32. Liquid phase profile. Case III configuration. L/G 11.5. Wash water inlet temperature 20 °C. Salinity 0 PSU.

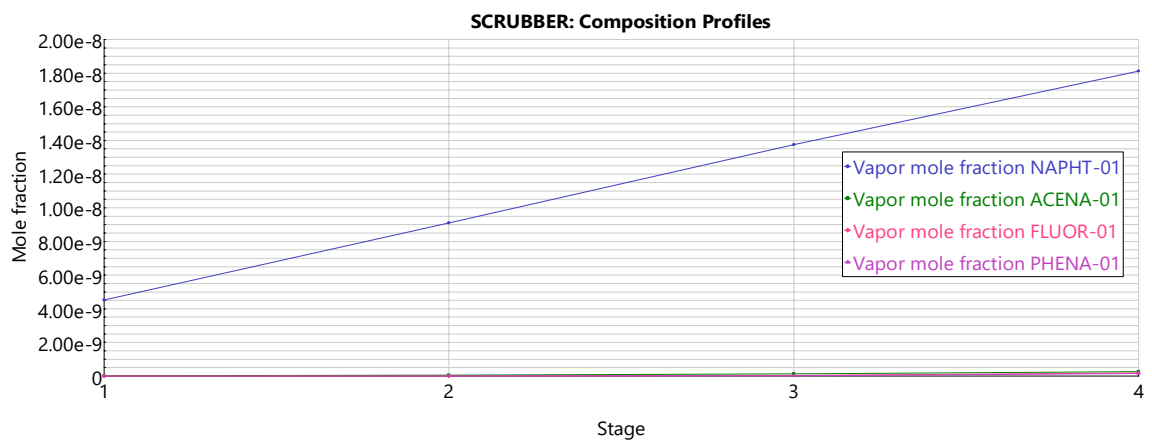


Figure 33. Vapor phase profile. Case III configuration. L/G 11.5. Wash water inlet temperature 20 °C. Salinity 0 PSU.

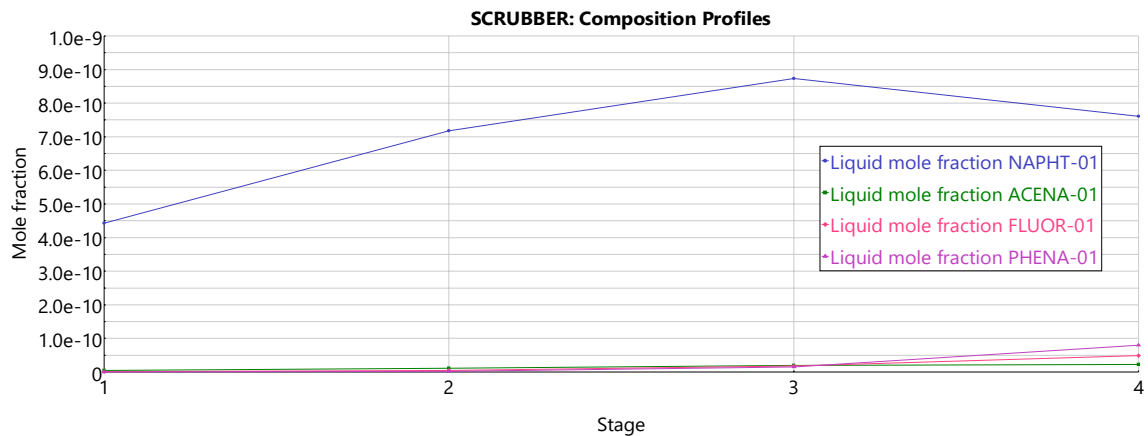


Figure 34. Liquid phase profile. Case III configuration. L/G 11.5. Wash water inlet temperature 20 °C. Salinity 20 PSU.

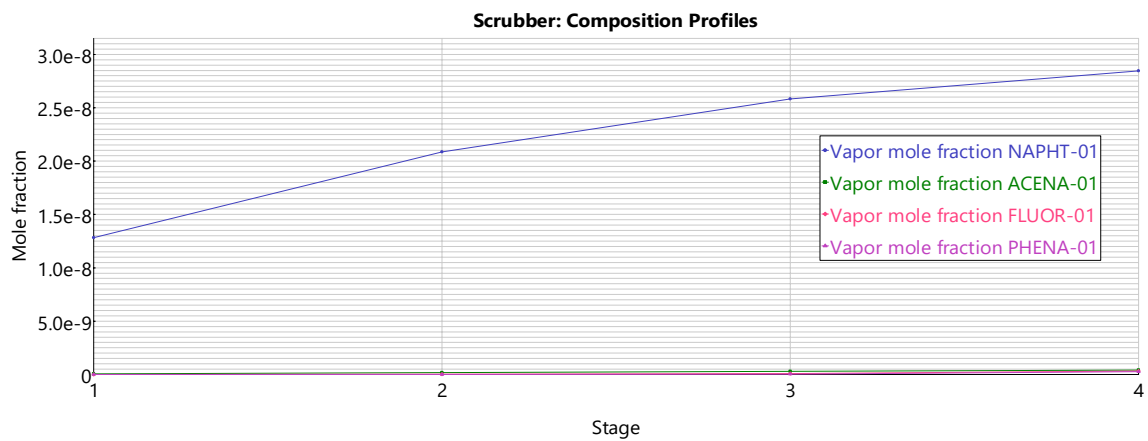


Figure 35. Vapor phase profile. Case III configuration. L/G 11.5. Wash water inlet temperature 20 °C. Salinity 20 PSU.

The absorption stage efficiency is also decreased with increasing salinity. As less naphthalene is absorbed in to the aqueous phase, the more naphthalene is available in the vapour phase in the later stages.

The so called “perfect fit”, when the results in 1-Stage method and the Aspen Plus simulations are equal to each other. The case observed is again based on Case III.

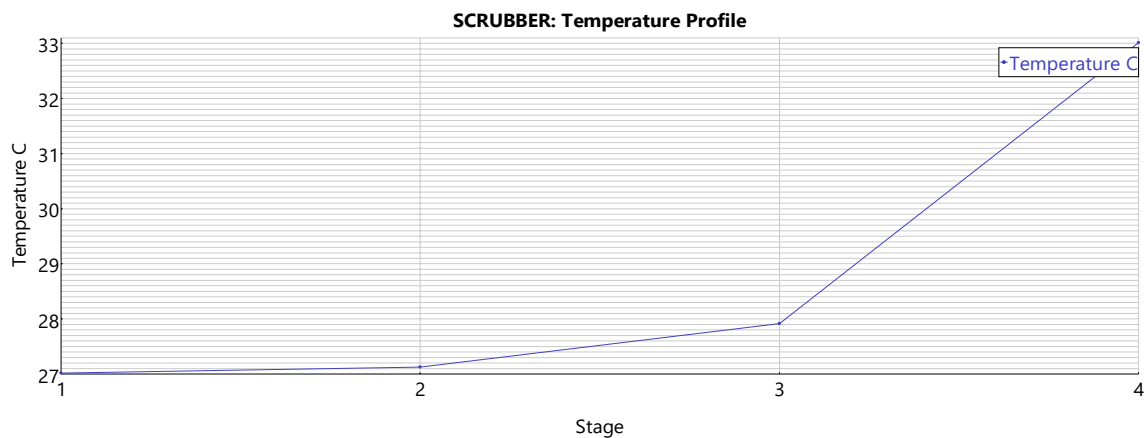


Figure 36. Temperature profile. Case III configuration. L/G 8. Wash water inlet temperature 27 °C. Salinity 20 PSU.

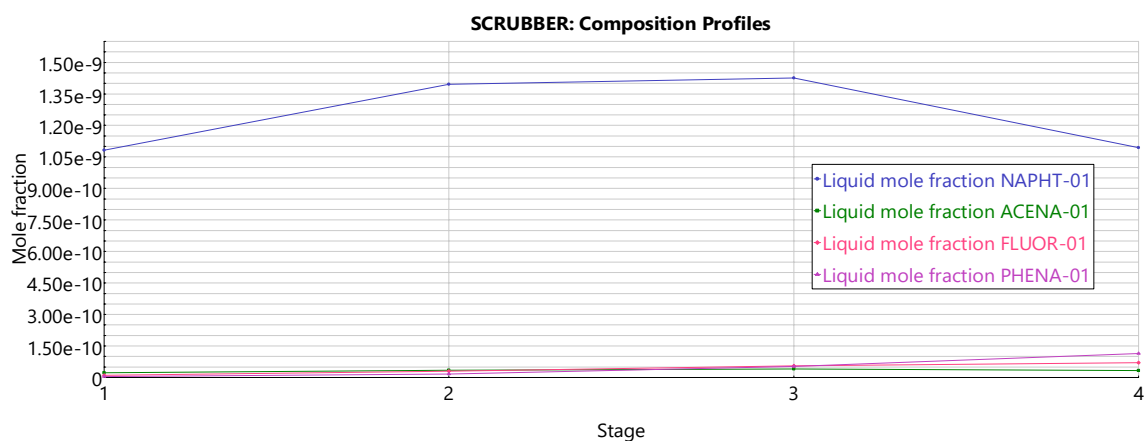


Figure 37. Liquid phase mole fraction profile. Case III configuration. L/G 8. Wash water inlet temperature 27 °C. Salinity 20 PSU.

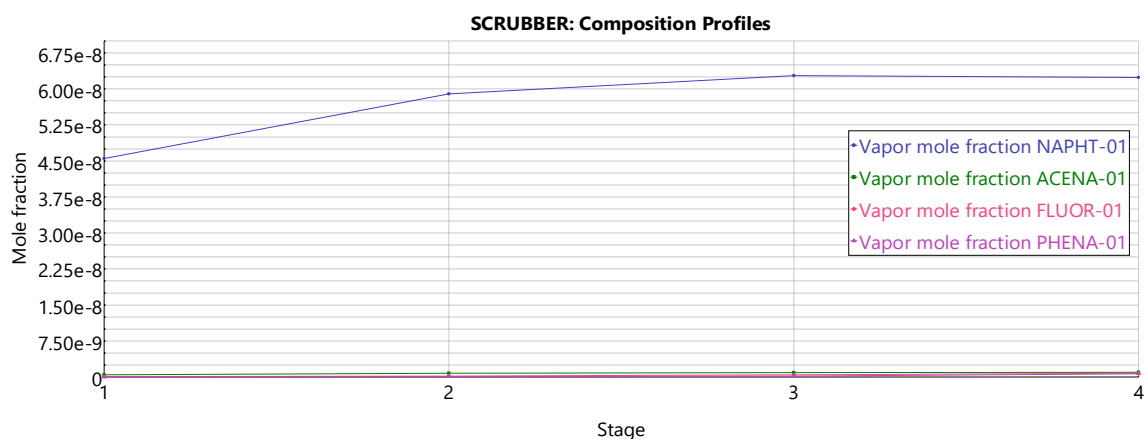


Figure 38. Vapor phase mole fraction profile. Case III configuration. L/G 8. Wash water inlet temperature 27 °C. Salinity 20 PSU.

In the last case, the desorption caused by the heat transfer between exhaust gas and wash water, caused the naphthalene vapor mole fraction in stage 3 to increase above the mole fraction in stage 4. The increase of the mole fraction in the vapour phase and the loss of the naphthalene in the liquid phase reduces the PAH absorption significantly, reducing the stage efficiency to such extent, that the one stage absorption approximation can be estimated with one stage only.

In addition, as can be observed from the figures 30 to 42 above, mole fraction of naphthalene is much higher than the mole fractions of acenaphthene, fluorene and phenanthrene. This indicates, that the major error of total PAH estimation derives from the error of naphthalene estimation. The contribution of remaining species contributes only a little in the gaseous phase to the total mass. This may be due to the molecular weight of the molecules. As the naphthalene is the lightest species it is most affected by the temperature and may desorb at the lower stages.

Table 9. Extrapolated case. Lowest total error between 1-Stage method and Aspen Plus simulation. L/G 8, Salinity: 20 PSU, T: 27 °C.

T 27 °C	Exhaust in	Exhaust out	Wash water out
Naphthalene	93 %	92 %	100 %
Acenaphthene	120 %	137 %	100 %
Fluorene	145 %	615 %	100 %
Phenanthrene	130 %	2810 %	100 %
Sum	100 %	100 %	100 %

As for individual PAH, the one-stage method underestimates the naphthalene mass flow but overestimates the mass flow of the remaining PAH. The errors compensate each other, resulting low deviation between two calculations. Based on the results of sensitivity analysis, the gaseous PAH can be initially calculated with 1-Stage method and then corrected with correction factor from **appendices N-Y**.

19.1. Sensitivity analysis evaluation

Sensitivity analysis in Aspen Plus and with 1-Stage method were carried out. The error between Aspen Plus simulation and 1-Stage method was evaluated. Sensitivity analysis results were imported to IMB SPSS 25. Variance and regression analysis were carried out to evaluate which wash water parameters predict the error. In addition to the wash water parameters presented in the table 8, the two-way parameters of L/G –ratio, salinity and temperature were included into regression. The regression resulted in the approximation function coefficients as presented in the table below.

Table 10. Regressed coefficients for general error equation.

Coefficients ^a						
		Unstandardized Coefficients		Standardized Coefficients		
Model		B	Std. Error	Beta	t	Sig.
1	Constant	-5,225	,354		-14,739	,000
	PSU	-,014	,004	-,294	-3,781	,000
	T (°C)	,054	,008	,341	6,456	,000
	L/G –ratio	,593	,017	2,335	35,867	,000
	L/G*T (°C) (averaged)	-,016	,001	-1,671	-21,507	,000
	PSU*T (°C) (averaged)	,002	,000	,771	11,838	,000
	L/G*PSU (averaged)	-,003	,000	-,827	-15,628	,000

a. Dependent Variable: Error

The obtained equation is presented below.

$$e_{General} = -0.014PSU + 0.054T + 0.593\frac{L}{G} - 0.016\frac{L}{G}T + 0.002PSU * T - 0.003\frac{L}{G}PSU - 5.225 \quad (12)$$

The remaining error has a standard deviation of 25.6 % as presented in the figure below.

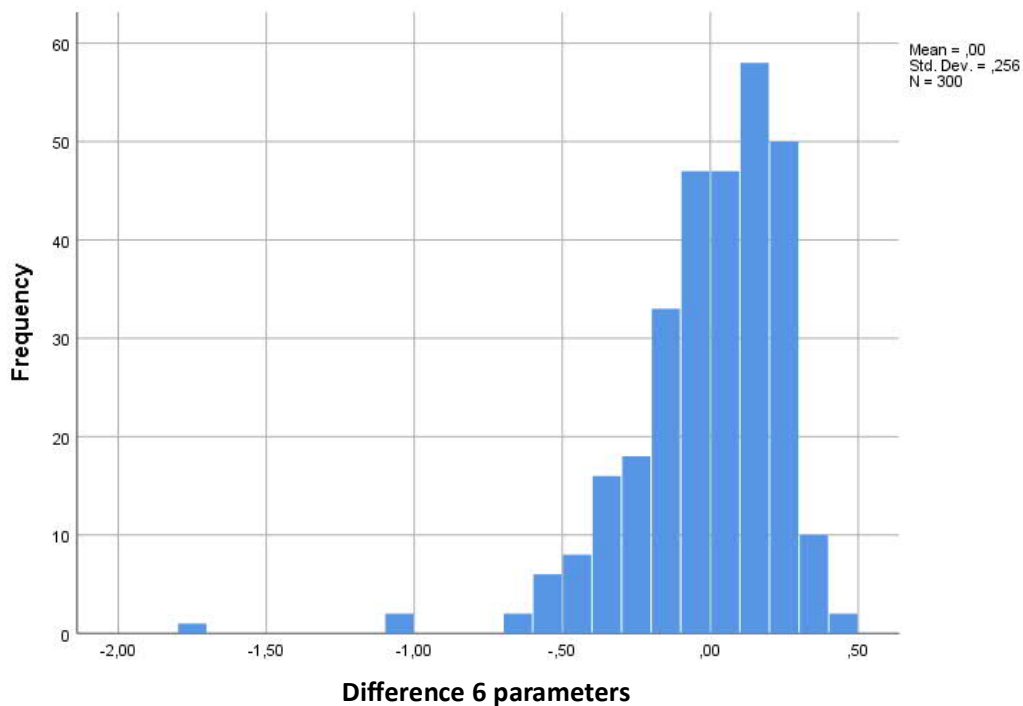


Figure 40. Remaining error and standard deviation.

It is assumed, that the ships with open loop scrubbers will not travel in waters with 0 PSU and operate the EGCS with L/G –ratios of 14 and 6. Therefore, these parameters are excluded from the following error approximation function. The new variance and regression analysis states, that with the excluded parameters, the main effect of parameter PSU is no longer statistically significant. A new regression with only five parameters was carried out. Results are presented in the table below.

Table 11. Regressed coefficients for refined error function.

Coefficients ^{a,b}					
		Unstandardized Coefficients		Standardized Coefficients	
Model		B	Std. Error	Beta	t
1	(Constant)	-4,586	,394		-11,636
	T (°C)	,041	,011	,498	3,874
	L/G	,517	,022	2,249	23,323
	LG*T(°C) (averaged)	-,013	,001	-1,914	-13,343
	PSU*T(°C) (averaged)	,001	,000	,668	7,442
	L/G*PSU (averaged)	-,003	,000	-,890	-10,902

a. Split = 1.00

b. Dependent Variable: Error

The obtained function is following.

$$e_{Refined} = 0.041 T + 0.517 \frac{L}{G} - 0.013 \frac{L}{G} T + 0.001 PSU * T - 0.003 \frac{L}{G} PSU - 4.586 \quad (13)$$

The remaining error standard deviation is 8.8 %.

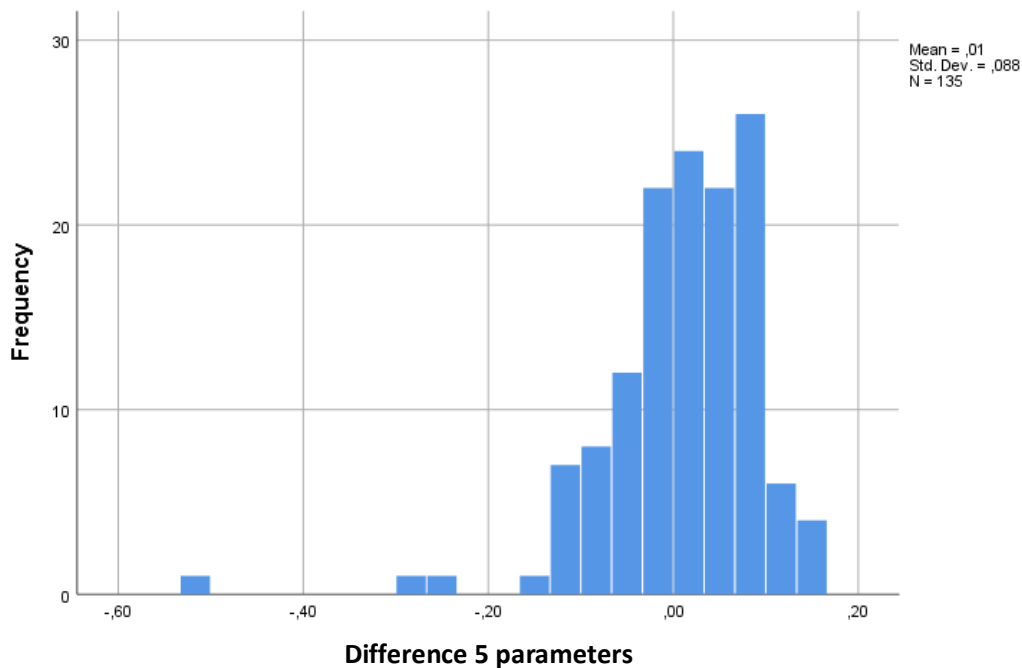


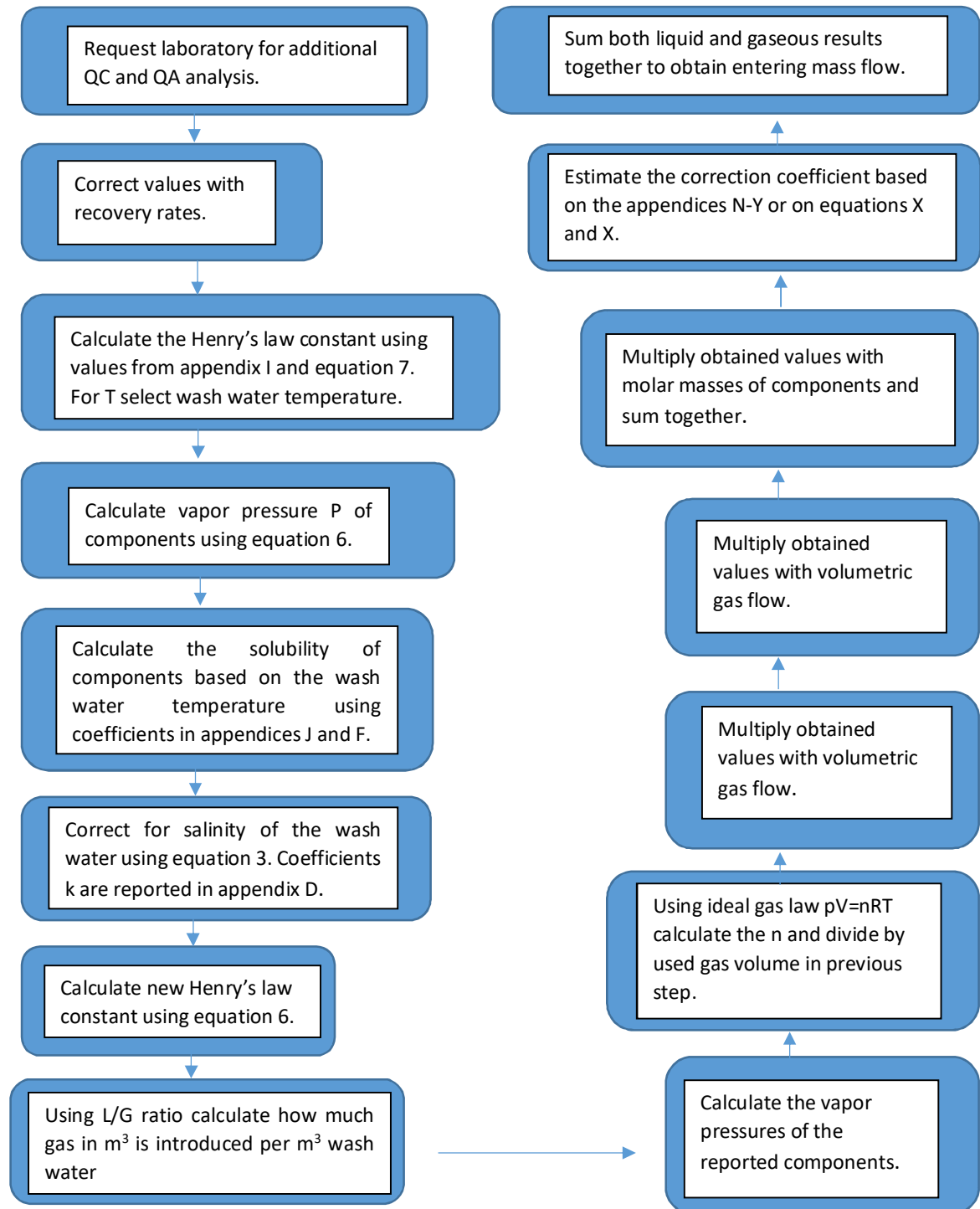
Figure 41. Remaining error and standard deviation.

In both cases, the residuals were examined and it is determined, that linear approach is sufficient. The proposed two equations can be used to estimate the error between the sensitivity analysis of Aspen Plus and 1-Stage method, which can be used in correcting the 1-Stage method results closer to the Aspen Plus results. In case ship operates within the parameters

19.2. Mass balance calculation

However, because the method is based on the extrapolated conditions of the ships, it does not necessarily predict the true concentrations of other possible cases, where the temperature of the wash water might be below 15 °C or where the PAH concentrations found in the aqueous phase deviate from the reports used in this thesis. Below a flow diagram of the proposed method:

Step by step flow diagram for PAH mass balance calculation



Above the step by step method is presented. As said previously, this method is now based on the extrapolated results and to make it more accurate, multiple additional measurements and samplings should be made based on real cases. The mass balance calculation presented in the flow chart above does not include the PAH bound to the PM.

20. PAH reduction

To reduce the PAH emissions several possibilities are suitable. Unfortunately, none of them is specifically designated to PAH reduction, but can be influenced indirectly at various stages of the process.

20.1. Homogenizers

Heavy fuel oil is a heterogeneous mixture of different hydrocarbons. The HFO can be fractionized into four following phases:

- Saturates (Aliphatics)
- Aromatics
- Resins
- Asphaltenes

As the asphaltenes contain also hetero-atoms, such as oxygen, they tend to agglomerate. These asphaltene agglomerates form usually denser fuel droplets preventing oxygen to reach the centre of the droplet, generating pyrolysis formed PAH emissions during combustion.

A homogenizer is a device that utilizes shearing forces to spread the in each other immiscible liquid phases into an even solution. A homogenizer consists of a dynamic rotor and static stator. As the unevenly distributed fuel enters the homogenizer, the shearing forces disrupt the asphaltenes across the bulk fuel phase. This is often called “fuel conditioning”, which is done in prior to the engine. The structure of homogenizer is presented in the figure below.

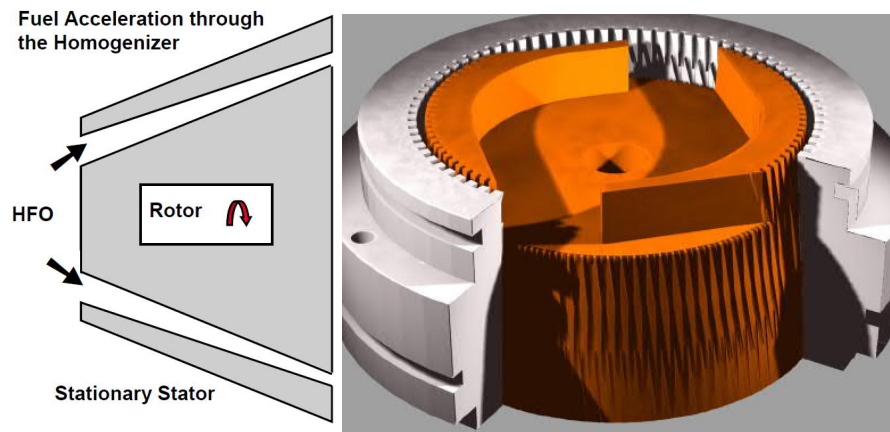


Figure 42. Rotor and stator of homogenizer. The small carvings generate pressure fluctuation causing ultrasonic waves, that further disintegrate asphaltene agglomerates. (Burak, 2010)

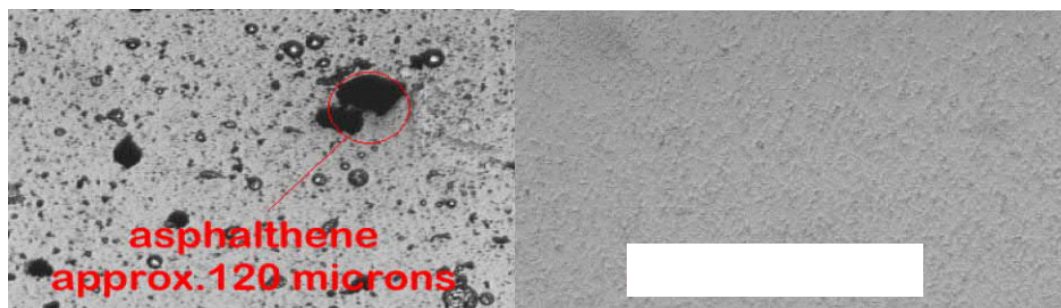


Figure 43. Unconditioned before and conditioned fuel after the homogenizer. (Burak, 2010)

As the conditioned fuel is injected into a combustion cylinder, the fuel droplets evaporate more rapidly. This shifts the PAH formation more towards the pyrosynthesis path and thus lowering their concentration.

20.2. Electrostatic precipitator

An electrostatic precipitator (ESP) is equipment, which is installed after the engine. The ionizing corona ionizes the PM, that are found in the exhaust gas and afterwards the collection plates remove the PM from the exhaust gas.

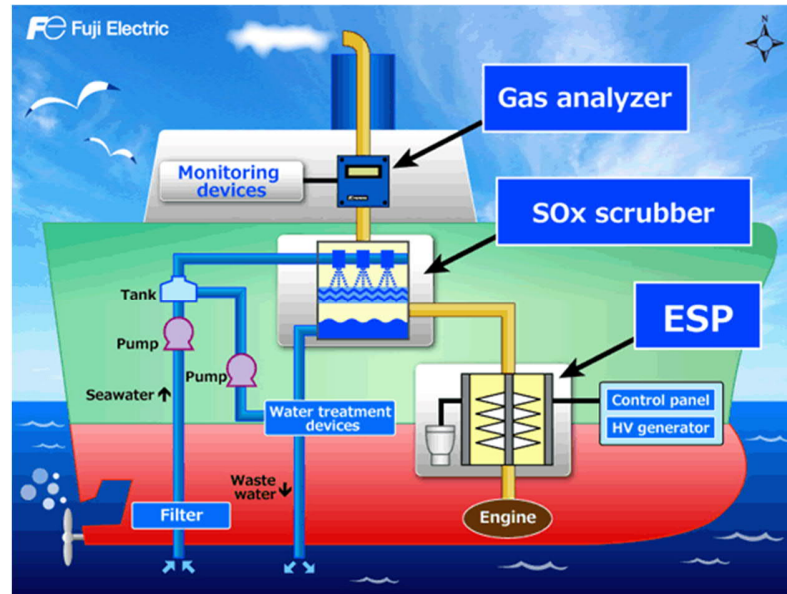


Figure 44. Location of ESP on ship. (FE)

The ESP must be installed in prior to scrubber.

20.3. Open loop water treatment system

As an alternative to aforementioned homogenizers, a baffle tank system combined with hydrocyclone that can treat open loop wash water from PM and PAH. The PM settles down at the first stage and to reduce the PM accumulation, part form the water is directed to the hydrocyclone for removal. The effluent from hydrocyclone is then returned back to the tank.

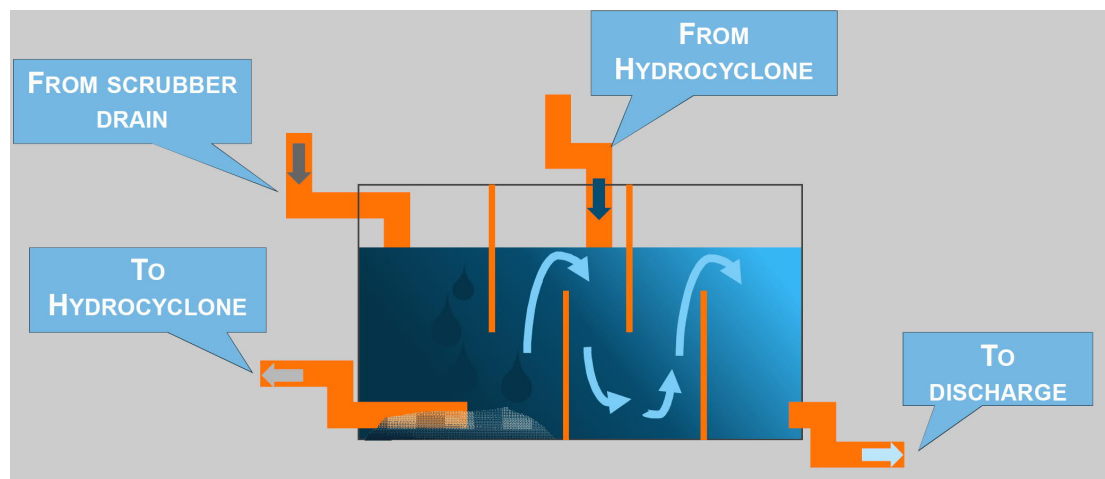


Figure 45. Open loop water treatment – residence tank. (Wärtsilä, 2017)

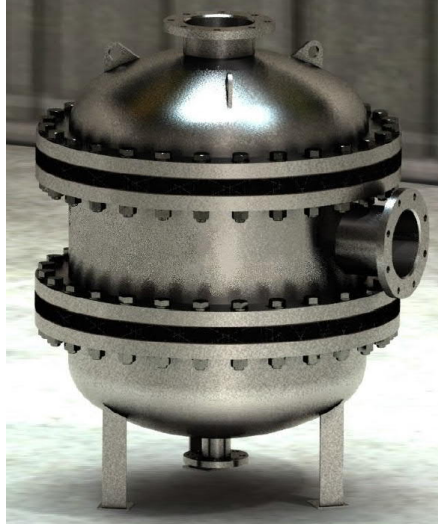


Figure 46. Hydrocyclone (*Snickars-Nykamb, 2017*)

The effluent from hydrocyclone is then returned back to the tank.

21. Conclusions

Three samples for PAH analysis were drawn from ships. The analysed phases were aqueous and PM phase. Initially, it was assumed that a fraction of PAH adsorbs on the surface of the PM during transportation from ship to the laboratory. In addition to the analysis a quality control and quality assurance analysis were requested for proper evaluation of the initial concentration. The QC and QA results revealed, that the laboratory analysis underestimate the PAH concentrations severely and that the used recovery control limits allow such large deviation, resulting in unflagged results in the laboratory.

It is observed, that the more PAH is found in the aqueous phase the more the recovery rates deviate from 100% recovery, especially in case of lighter PAH. This appears to generate severe error in the total PAH amount as light PAH components dominate the mass fraction of the total PAH sum. Another possible explanation to such inaccuracy may originate from the ratio of the added spike to the parent sample concentration. In Cases I and II, the added matrix spike and matrix spike duplicate are dwarfed out by the concentration of the parent PAH concentration.

The possible reason for this is that during the extraction from the inorganic water phase heat is used, which may cause the PAH desorption. Another possible reason for lighter PAH loss, especially while extraction from PM, is that ultrasound may cause cavitation bubbles, that cause the PAH to react with the solvent into methylated PAH. Such PAH are not included into the EPA 16 PAH species and therefore are not reported.

Simulations were carried out with Aspen Plus simulation program. Unfortunately, not all PAH species were present in the Aspen Plus databanks and in some cases, the solubility was too low for Aspen Plus to process it. The solubilities and Henry's law constants for different salinities and temperatures were calculated based on Setchenow and Henry's law equations and plugged into Aspen Plus each time a different salinity was observed. The results matched well with the found literature.

Henry's law has been determined to be suitable for absorption modelling and it was determined, that scrubber has four stages. The aim was to determine the influence of the salinity on the absorption and the results indicate that the salinity decreases the absorption of

the PAH species. Simultaneously also other parameters such as L/G ratio and temperature were investigated. Based on the results, the highest absorption occurs at highest L/G ratio, lowest salinity and lowest temperature. It has been observed, that the heat exchange between gaseous and aqueous phase can cause a desorption of PAH to such extent, that the mole fraction of PAH can increase above the fourth (gas inlet) stage. The major error derived from the naphthalene. While the PAH that are heavier than naphthalene can be assumed to wash from gaseous phase completely, the naphthalene must be evaluated according to Henry's law.

As the 1-Stage method does not take into account heat exchange and thus must be corrected. Depending on the assumed wash water parameters, the error can be estimated with equations 12 or 13. The obtained value with 1-stage method must be then divided with the values obtained with equations 12 or 13.

22. Further study suggestions

It is evident, that to propose the correct method for PAH mass balance calculation, more samplings are required. In addition, to compare the results samples should be drawn directly from exhaust gas. In such case, the result can be directly compared with real time value. In addition, this would also determine the magnitude of the error in the analysis laboratory during recovery.

Another important aspect would be to measure the PM amount at the same locations. In this thesis, the PAH found in PM couldn't been added into total mass balance as the amount of PM before and after the scrubber is unknown.

In addition, it is suggested to study the operation of PAH sensors, taht measure the PAH concentration in water. Before this thesis, it was believed that the sensors record values higher than the actual PAH amount, but the situation may actually be reversed. It was originally assumed, that the in-line sensors record values too high due to possible interferences found in wash water that magnify the PAH. However, literature suggests, that the sensors might indicate too low values due to dynamic quenching. Dynamic quenching occurs when PAH interact with possible present humic substances. As the interaction of PAH with humic substance changes the initial excitation level of PAH and then the UV light from sensor "over excites" the PAH, the sensor does not register light with too high intensity and the PAH molecule goes past the sensor unnoticed. It is suggested to investigate the possible presence of humic substances and their influence on the sensor readings and compare the results with the laboratory analysis results.

References

- Aakko-Saksa P, Vesala H, Koponen P, Nyyssönen S, Puustinen H, Lehtoranta K, Timonen H, Teinilä K, Hillamo R, Karjalainen P, Kuittinen N. Black carbon measurements using different marine fuels. In 28th CIMAC World Congress 2016.
- Aakko-Saksa, P., Murtonen, T., Vesala, H., Koponen, P., Timonen, H., Teinilä, K., Aurela, M., Karjalainen, P., Kuittinen, N., Puustinen, H. and Piimäkorpi, P., 2017. Black carbon emissions from a ship engine in laboratory (SEA-EFFECTS BC WP1).
- Alaee, M., Whittall, R.M. and Strachan, W.M., 1996. The effect of water temperature and composition on Henry's law constant for various PAH's. *Chemosphere*, 32(6), pp.1153-1164. DOI: 10.1016/0045-6535(96)00031-8
- Andreasen, A. and Mayer, S., 2007. Use of seawater scrubbing for SO₂ removal from marine engine exhaust gas. *Energy & Fuels*, 21(6), pp.3274-3279.
- Auflem, I. 2002. Influence of Asphaltene aggregation and Pressure on Crude Oil Emulsion Stability. Doctor Ingeneur Thesis.
- Babicz, J. 2015. Wärtsilä Encyclopedia of Ship Technology. Second Edition.
- Bucheli, T.D. and Gustafsson, Ö., 2000. Quantification of the soot-water distribution coefficient of PAHs provides mechanistic basis for enhanced sorption observations. *Environmental Science & Technology*, 34(24), pp.5144-5151. DOI: 10.1021/es000092s
- Burak, S.R., 2010. Improving heavy fuel oil usage by homogenization. Ashland Specialty Chemical Company. Drew Marine Division, pp.1-9.
- Catalog of CHP Technologies. 2017. U.S. Environmental Protection Agency Combined Heat and Power Partnership.
- Cooper, D.A., 2003. Exhaust emissions from ships at berth. *Atmospheric Environment*, 37(27), pp.3817-3830. DOI: 10.1016/S1352-2310(03)00446-1
- Dec, J.E., 1997. A conceptual model of DI diesel combustion based on laser-sheet imaging (No. 970873). SAE technical paper.

Eganhouse, R.P. and Calder, J.A., 1976. The solubility of medium molecular weight aromatic hydrocarbons and the effects of hydrocarbon co-solutes and salinity. *Geochimica et Cosmochimica Acta*, 40(5), pp.555-561. DOI: 10.1016/0016-7037(76)90223-4

El-Sinawi, A. H. 2011. Impact of Combustion of Water in Fuel on Polycyclic Aromatic Hydrocarbon (Pah's) Precursors' Formation. *International Journal of Chemical, Molecular, Nuclear, Materials and Metallurgical Engineering*. Vol. 5. No. 8

Endres, S., Maes, F., Hopkins, F., Houghton, K., Mårtensson, E., Oeffner, J., Quack, B., Singh, P. and Turner, D. 2018. A New Perspective at the Ship-Air-Sea-Interface: The Environmental Impacts of Exhaust Gas Scrubber Discharge. *Frontiers in Marine Science*. DOI: 10.3389/fmars.2018.00139

EPA. United States Environmental Protection Agency Office of Wastewater Management. 2011. Exhaust Gas Scrubber Washwater Effluent.

FE: https://www.fujielectric.com/company/research_development/theme/egcs.html

Frenklach, M., 2002. Reaction mechanism of soot formation in flames. *Physical chemistry chemical Physics*, 4(11), pp.2028-2037. DOI: 10.1039/B110045A

Hach. 2010. FP 360 sc. User Manual. 01/2010, Edition 1.

Hansen, N., Miller, J.A., Klippenstein, S.J., Westmoreland, P.R. and Kohse-Höinghaus, K., 2012. Exploring formation pathways of aromatic compounds in laboratory-based model flames of aliphatic fuels. *Combustion, Explosion, and Shock Waves*, 48(5), pp.508-515. DOI: 10.1134/S0010508212050024

Hensen, J.P., 2012. Exhaust Gas Scrubber Installed Onboard MV Ficaria Seaways, Mijostryrelsen, Danish Ministry of the Environment. Environmental Protection Agency.

International Chamber of Shipping. 2019. Guidance to Shipping Companies and Crews on Preparing for Compliance with the 2020 'Global Sulphur Cap' for Ships' Fuel Oil in Accordance with MARPOL Annex VI.

Jonker, M.T. and Koelmans, A.A., 2002. Extraction of polycyclic aromatic hydrocarbons from soot and sediment: solvent evaluation and implications for sorption mechanism. *Environmental science & technology*, 36(19), pp.4107-4113. DOI: 10.1021/es0103290

Jonker, M.T. and Koelmans, A.A., 2002. Sorption of polycyclic aromatic hydrocarbons and polychlorinated biphenyls to soot and soot-like materials in the aqueous environment: mechanistic considerations. *Environmental science & technology*, 36(17), pp.3725-3734. DOI: 10.1021/es020019x

Lahtinen, J. 2016. Closed-Loop Exhaust Gas Scrubber Onboard a Merchant Ship: Technical, Economical, Environmental and Operational Viewpoints. *Acta Wasaensia* 342. *Energy Technology* 1. ISBN: 978-952-476-659-3.

Leonhardt, E. and Stahl, R., 1998. Decomposition of acenaphthylene by ultrasonic irradiation. *Analytical chemistry*, 70(6), pp.1228-1230. DOI: 10.1021/ac9710083

Li, M., Bao, F., Zhang, Y., Song, W., Chen, C. and Zhao, J., 2018. Role of elemental carbon in the photochemical aging of soot. *Proceedings of the National Academy of Sciences*, 115(30), pp.7717-7722. DOI: 10.1073/pnas.1804481115

LibreTexts. Site visited on 29.06.2019.

[https://chem.libretexts.org/Bookshelves/Physical_and_Theoretical_Chemistry_Textbook_Maps/Supplemental_Modules_\(Physical_and_Theoretical_Chemistry\)/Physical_Properties_of_Matter/Solutions_and_Mixtures/Ideal_Solutions/Dissolving_Gases_In_Liquids%2CHenry%27s_Law](https://chem.libretexts.org/Bookshelves/Physical_and_Theoretical_Chemistry_Textbook_Maps/Supplemental_Modules_(Physical_and_Theoretical_Chemistry)/Physical_Properties_of_Matter/Solutions_and_Mixtures/Ideal_Solutions/Dissolving_Gases_In_Liquids%2CHenry%27s_Law)

Mao, Q., van Duin, A.C. and Luo, K.H., 2017. Formation of incipient soot particles from polycyclic aromatic hydrocarbons: A ReaxFF molecular dynamics study. *Carbon*, 121, pp.380-388. DOI: 10.1016/j.carbon.2017.06.009

Mastral, A.M. and Callen, M.S., 2000. A review on polycyclic aromatic hydrocarbon (PAH) emissions from energy generation. *Environmental Science & Technology*, 34(15), pp.3051-3057. DOI: 10.1021/es001028d

May, W.E., Wasik, S.P. and Freeman, D.H., 1978. Determination of the solubility behavior of some polycyclic aromatic hydrocarbons in water. *Analytical Chemistry*, 50(7), pp.997-1000.

NASA: <https://svs.gsfc.nasa.gov/3652>

Ni, N. and Yalkowsky, S.H., 2003. Prediction of Setschenow constants. *International journal of pharmaceutics*, 254(2), pp.167-172. DOI: 10.1016/S0378-5173(03)00008-5

Omidvarborna, H., Kumar, A. and Kim, D.S., 2015. Recent studies on soot modeling for diesel combustion. *Renewable and Sustainable Energy Reviews*, 48, pp.635-647. DOI: 10.1016/j.rser.2015.04.019

Parnis, J.M., Mackay, D. and Harner, T., 2015. Temperature dependence of Henry's law constants and KOA for simple and heteroatom-substituted PAHs by COSMO-RS. *Atmospheric Environment*, 110, pp.27-35. DOI: 10.1016/j.atmosenv.2015.03.032

Pettit, R.E., 2004. Organic matter, humus, humate, humic acid, fulvic acid and humin: Their importance in soil fertility and plant health. CTI Research.

PubChem: <https://pubchem.ncbi.nlm.nih.gov/search/>

R&D systems. 2014. Spike, Recovery, and Linearity: Protocol for Validating Untested Samples in R&D systems ELISAs Experimental protocol only – not guaranteed.

Richter, H. and Howard, J.B., 2000. Formation of polycyclic aromatic hydrocarbons and their growth to soot—a review of chemical reaction pathways. *Progress in Energy and Combustion science*, 26(4-6), pp.565-608. DOI: 10.1016/S0360-1285(00)00009-5

Safety4sea, 2016: <https://safety4sea.com/strengthen-control-of-ships-sulphur-emissions/>

Ship&Bunker, 2019: <https://shipandbunker.com/prices/emea/nwe/nl-rtm-rotterdam>. Visited on 14.02.2019

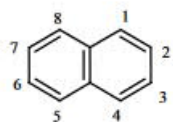
Skogestad, S., 2008. Chemical and energy process engineering. CRC press. P. 186. DOI: 10.1201/9781420087567

- Snickars-Nykamb, J. 2017. Treatment of wash water from open loop scrubbers. Scrubbers 360 ° - An overview of scrubber technology and a study visit to DFDS Primula Seaways. <https://static1.squarespace.com/static/56a0c84dfb36b1be19213613/t/592d3b94d2b857159c9fe9db/1496136617530/2+-+Wartsila+-+Treatment+of+wash+water+from+open+loop+scrubbers.pdf>. Visited on 01.06.2019
- Sun, P. and Weavers, L.K., 2006. Sonolytic reactions of phenanthrene in organic extraction solutions. *Chemosphere*, 65(11), pp.2268-2274. DOI: 10.1016/j.chemosphere.2006.05.029
- Tanker shipping and trade: https://www.tankershipping.com/news/view,new-tool-simplifies-evaluating-the-cost-of-tanker-compliance_52055.htm
- Teinilä, K., Aakko-Saksa, P., Jalkanen, J.P., Karjalainen, P., Bloss, M., Laakia, J., Saarikoski, S., Vesala, H., Pettinen, R., Koponen, P. and Kuittinen, N., 2018. Effect of aftertreatment on ship particulate and gaseous components at ship exhaust.
- Tremblay, L., Kohl, S.D., Rice, J.A. and Gagné, J.P., 2005. Effects of temperature, salinity, and dissolved humic substances on the sorption of polycyclic aromatic hydrocarbons to estuarine particles. *Marine Chemistry*, 96(1-2), pp.21-34. DOI: 10.1016/j.marchem.2004.10.004
- Van Basshuysen, R. and Schäfer, F., 2004. *Internal combustion engine handbook-basics, components, systems and perspectives* (Vol. 345)
- Vermeire, M.B., 2012. *Everything you need to know about marine fuels*. Published by Chevron Global Marine Products.
- Wang, L., Liang, N., Li, H., Yang, Y., Zhang, D., Liao, S. and Pan, B., 2015. Quantifying the dynamic fluorescence quenching of phenanthrene and ofloxacin by dissolved humic acids. *Environmental pollution*, 196, pp.379-385. DOI: 10.1016/j.envpol.2014.10.029
- Warnatz, J., Maas, U., Dibble, R.W. and Warnatz, J., 1996. *Combustion* (Vol. 3). Berlin: Springer.

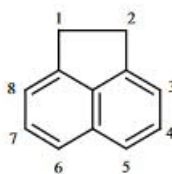
Xie, W.H., Shiu, W.Y. and Mackay, D., 1997. A review of the effect of salts on the solubility of organic compounds in seawater. Marine Environmental Research, 44(4), pp.429-444. DOI: 10.1016/S0141-1136(97)00017-2

Yan, J., Wang, L., Fu, P.P. and Yu, H., 2004. Photomutagenicity of 16 polycyclic aromatic hydrocarbons from the US EPA priority pollutant list. Mutation Research/Genetic Toxicology and Environmental Mutagenesis, 557(1), pp.99-108.

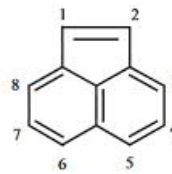
Appendix A. Selected EPA 16 PAH (Yan *et al.* 2003)



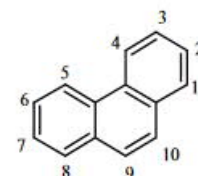
Naphthalene



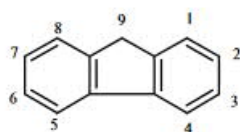
Acenaphthene



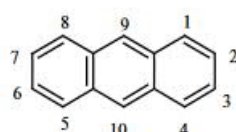
Acenaphthylene



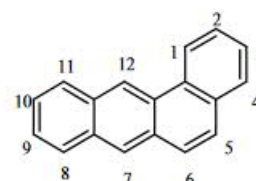
Phenanthrene



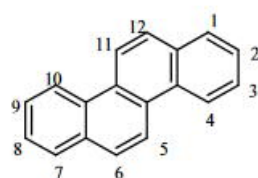
Fluorene



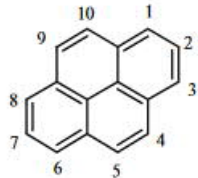
Anthracene



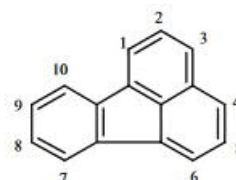
Benz[a]anthracene



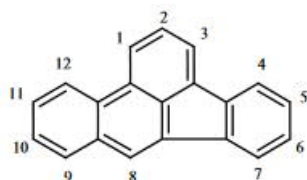
Chrysene



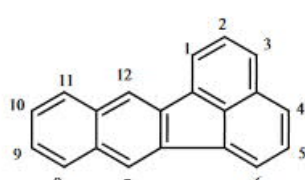
Pyrene



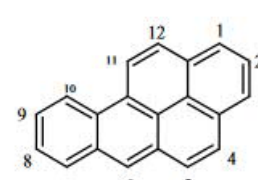
Fluoranthene



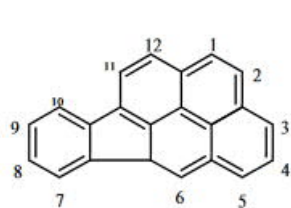
Benzo[b]fluoranthene



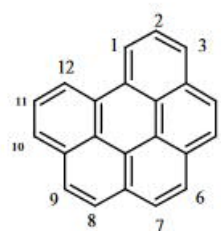
Benzo[k]fluoranthene



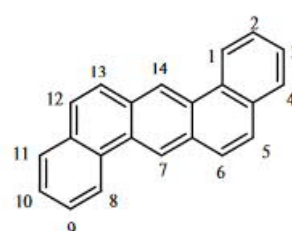
Benzo[a]pyrene



Indeno[1,2,3-*cd*]pyrene

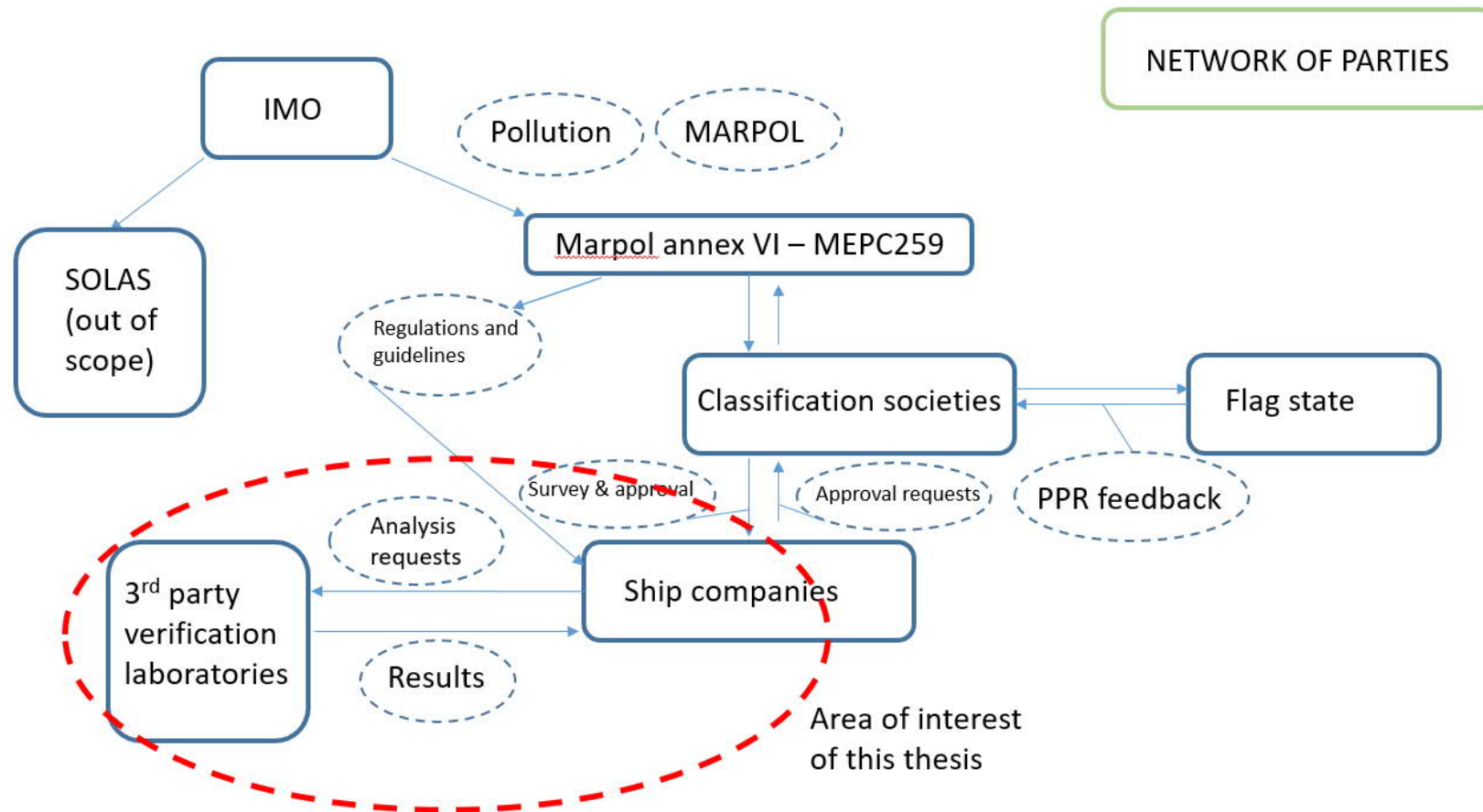


Benzo[*ghi*]perylene

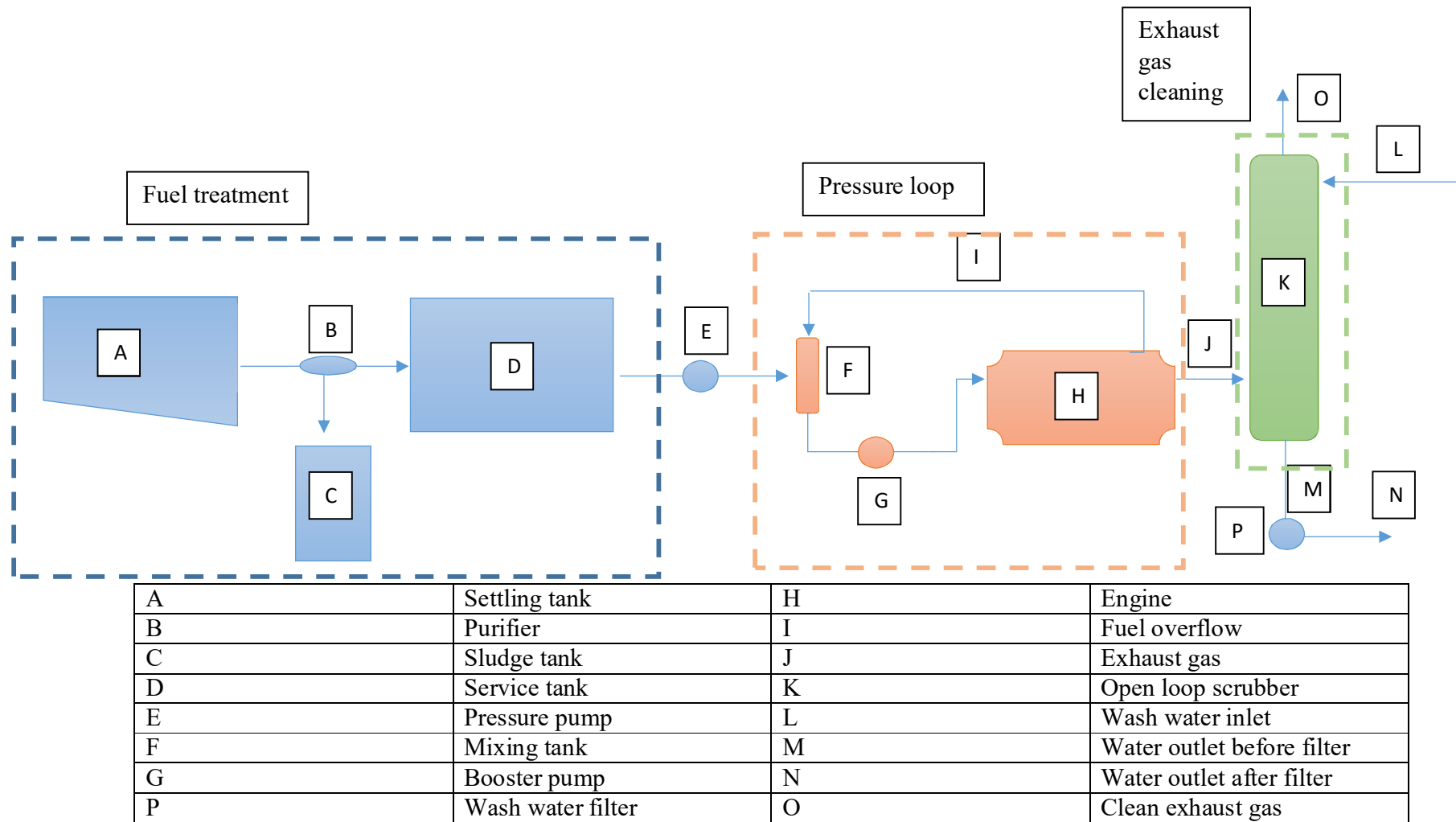


Dibenzo[*a,h*]anthracene

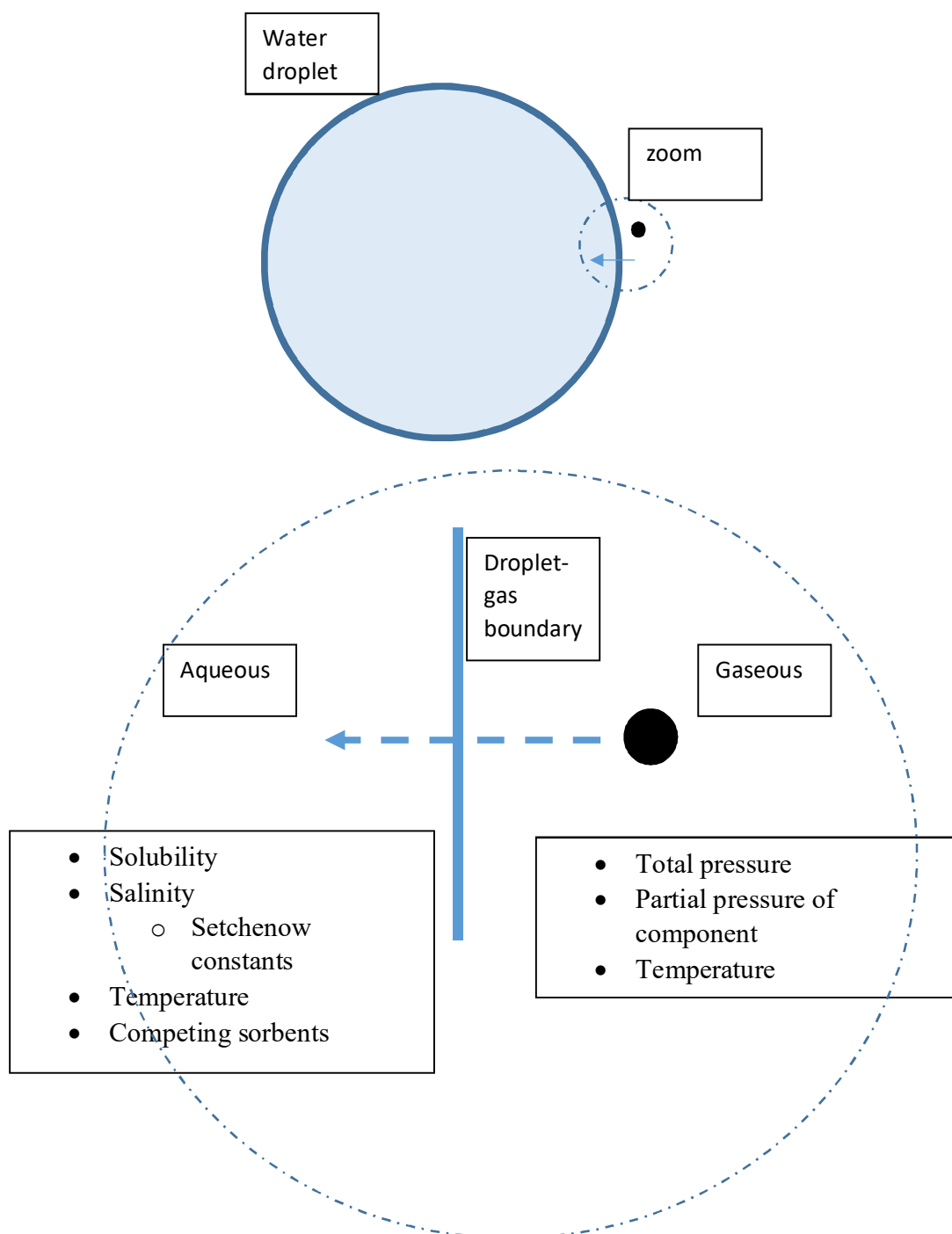
Appendix B. Network of parties



Appendix C. Fuel treatment, pressure loop and exhaust gas cleaning



Appendix D. Absorption of contaminant.



Appendix E

Table of fuel specification (*Vermiere, 2012*). Values of interest RMK.

Characteristics	Unit	Limit	Category ISO-F-											Test method reference	
			RMA	RMB	RMD	RME	RMG				RMK				
			10*	30	80	180	180	380	500	700	380	500	700		
Kinematic viscosity at 50°C*	mm ² /s	max.	10.00	30.00	80.00	180.0	180.0	380.0	500.0	700.0	380.0	500.0	700.0	ISO 3104	
Density at 15°C	kg/m ³	max.	920.0	960.0	975.0	991.0	991.0				1010.0			see 7.1 ISO 3675 or ISO 12185	
CCAI	—	max.	850	860	860	860	870				870			see 6.3 a)	
Sulfur*	mass %	max.	Statutory requirements											see 7.2 ISO 8754 ISO 14596	
Flash point	°C	min.	60.0	60.0	60.0	60.0	60.0				60.0			see 7.3 ISO 2719	
Hydrogen sulfide*	mg/kg	max.	2.00	2.00	2.00	2.00	2.00				2.00			IP 570	
Acid number*	mg KOH/g	max.	2.5	2.5	2.5	2.5	2.5				2.5			ASTM D664	
Total sediment aged	mass %	max.	0.10	0.10	0.10	0.10	0.10				0.10			see 7.5 ISO 10307-2	
Carbon residue: micro method	mass %	max.	2.50	10.00	14.00	15.00	18.00				20.00			ISO 10370	
Pour point (upper)*	winter quality	°C	max.	0	0	30	30	30				30			ISO 3016
	summer quality	°C	max.	6	6	30	30	30				30			ISO 3016
Water	volume %	max.	0.30	0.50	0.50	0.50	0.50				0.50			ISO 3733	
Ash	mass %	max.	0.040	0.070	0.070	0.070	0.100				0.150			ISO 6245	
Vanadium	mg/kg	max.	50	150	150	150	350				450			see 7.7 IP 501, IP 470 or ISO 14597	
Sodium	mg/kg	max.	50	100	100	50	100				100			see 7.8 IP 501 IP 470	
Aluminium plus silicon	mg/kg	max.	25	40	40	50	60				60			see 7.9 IP 501, IP 470 or ISO 10478	
Used lubricating oils (ULO): calcium and zinc; or calcium and phosphorus	mg/kg	—	The fuel shall be free from ULO. A fuel shall be considered to contain ULO when either one of the following conditions is met: calcium > 30 and zinc > 15; or calcium > 30 and phosphorus > 15											see 7.10 IP 501 or IP 470 IP 500	

Appendix F.

Parameters of EPA 16 PAH. Blue cells are calculated according to Eq. (4). Beige according to Eq. (5). Green according are found in website pubchem.com. Uncolored cells are from *May et al. 1978*.

compound		ks sele	ks in SW/NaCl	Distilled S0 mg/L	S seawater mg/L	salinity ‰	salinity %	mol/dm3	logKow
Naphthalene (w)	0.246	0.255842463	0.26	31.3	22	35	3.5	0.60	3.3
Acenaphthene	0.2708	0.238	0.238	3.9	1.84	35	3.5	0.60	3.92
Fluorene (w)	0.2812	0.267	0.267	1.685	1.166273655	35	3.5	0.60	4.18
Phenanthrene (w)	0.2924	0.371499749	0.371499749	1.0854	0.6505	35	3.5	0.60	4.46
Anthracene (w)	0.292	0.326	0.326	1.29	0.6	35	3.5	0.60	4.45
Acenaphthylene	0.2712	0.2712	0.2712	3.93	2.704452832	35	3.5	0.60	3.93
Pyrene (w)	0.3092	0.452790963	0.452790963	0.1215	0.0651	35	3.5	0.60	4.88
Fluoranthene	0.3204	0.339	0.339	0.206	0.129114732	35	3.5	0.60	5.16
Chrysene (w)	0.35	0.336	0.336	0.0018	0.001132861	35	3.5	0.60	5.9
Benzo (a) pyrene	0.3592	0.3592	0.3592	0.0015	0.0011	36.7	3.67	0.63	6.13
Benzo (a) Anthracene	0.3444	0.3444	0.3444	0.0094	0.005847962	35	3.5	0.60	5.76
Benzo (b) fluoranthene	0.3452	0.3452	0.3452	0.0012	0.000745726	35	3.5	0.60	5.78
Benzo (k) fluoranthene	0.3584	0.3584	0.3584	0.0008	0.000488189	35	3.5	0.60	6.11
Indeno (1.2.3-cd) pyrene	0.382	0.382	0.382	0.00019	0.000112235	35	3.5	0.60	6.7
Dibenzo (a,h) Anthracene	0.4052	0.4052	0.4052	0.000035	2.00242E-05	35	3.5	0.60	7.28
Benzo (g,h,i) Perylene	0.3792	0.3792	0.3792	0.00026	0.000154178	35	3.5	0.60	6.63

Appendix G. Known TDSF (°C)

Solubilities of light PAH (*May et al. 1978*)

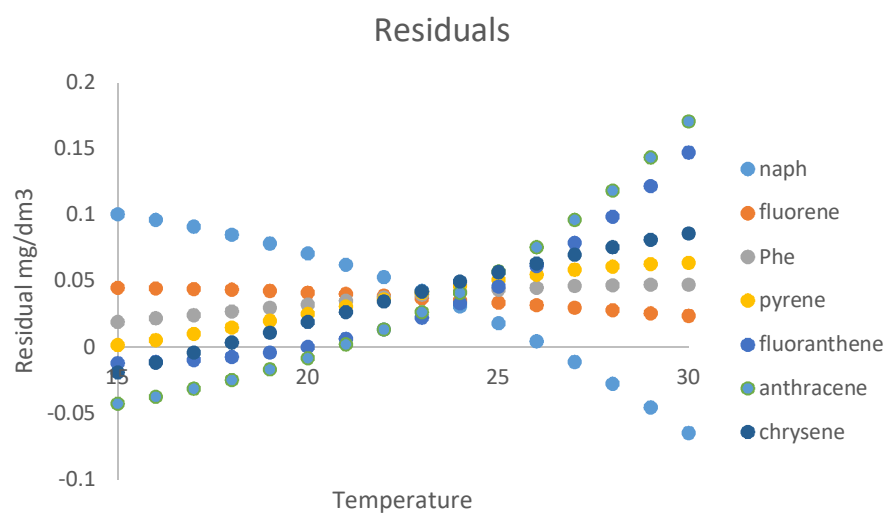
Compound	Solubility mg/dm ³	Source
Naphthalene	$0.0189t^2 + 0.2499t + 13.66$	May et al. 1978
Fluorene	$(0.0185t^3 + 0.4543t^2 + 22.76t + 543)10^{-3}$	May et al. 1978
Phenanthrene	$(0.0025t^3 + 0.8059t^2 + 5.413t + 324)10^{-3}$	May et al. 1978
Anthracene	$(0.0013t^3 - 0.0097t^2 + 0.8861t + 8.21)10^{-3}$	May et al. 1978

Solubilities of heavy PAH (*May et al. 1978*)

Component	Solubility mg/dm ³	Source
Pyrene	$(-0.0011t^3 + 0.2007t^2 - 1.051t + 50.4)10^{-3}$	May et al. 1978
Fluoranthene	$(0.0072t^3 - 0.1047t^2 + 4.322t + 50.4)10^{-3}$	May et al. 1978
Chrysene	$(0.0024t^2 + 0.0144t + 0.609)10^{-3}$	May et al. 1978

Appendix H.

Residuals of UAF



Appendix i

Table of c coefficient values for equation 5.

Light PAH

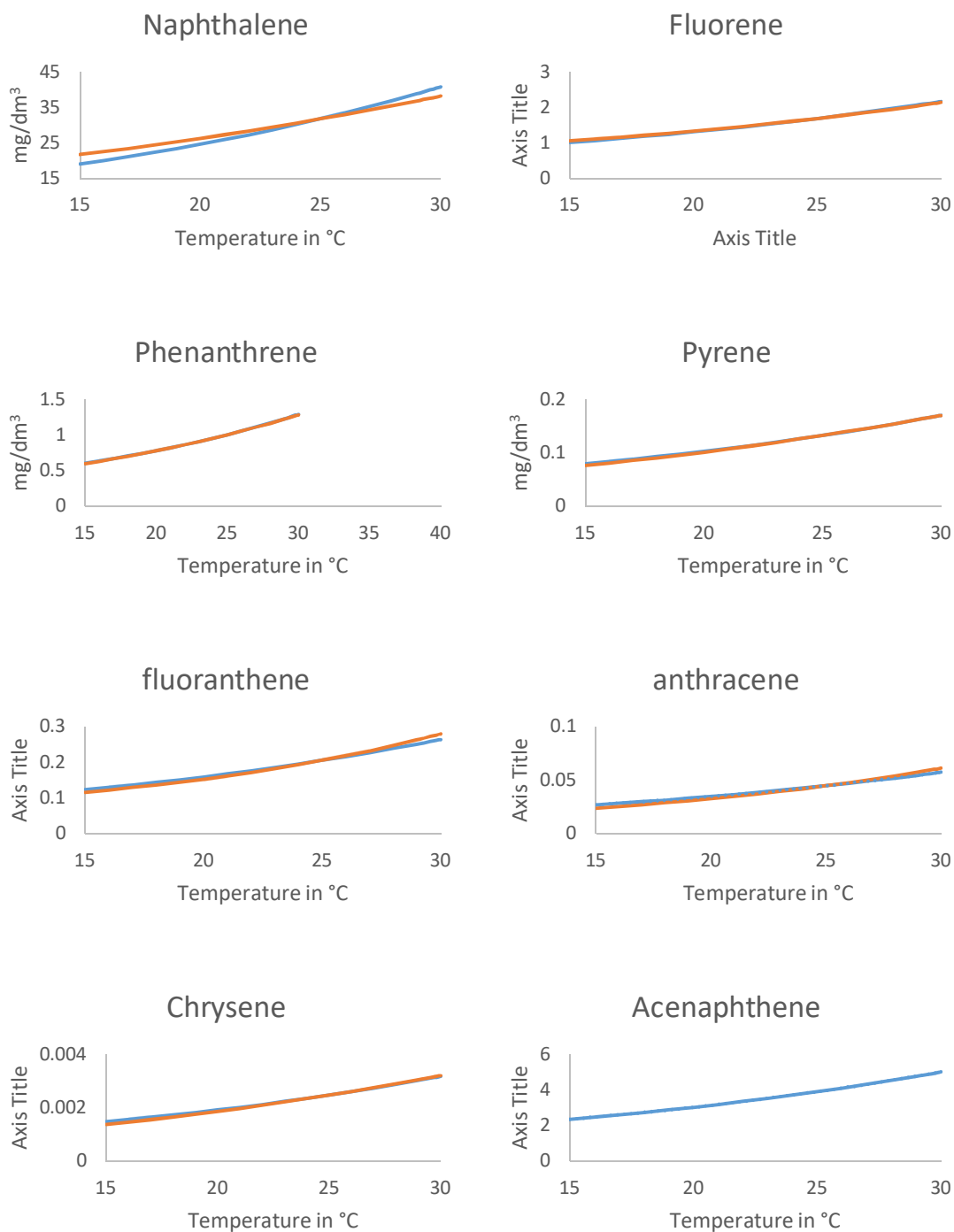
PAH	c value
Acenaphthene	3.6584
Acenaphthylene	3.6865

Heavy PAH

PAH	c value
Benzo[a]pyrene	0.001407
Benzo[a]anthracene	0.008818
Benzo[b]fluoranthene	0.001126
Benzo[k]fluoranthene	0.00075
Indeno[1,2,3-cd]pyrene	0.000178
Dibenzo[a,h]anthracene	3.2832×10^{-5}
Benzo[g,h,i]perylene	0.000244c

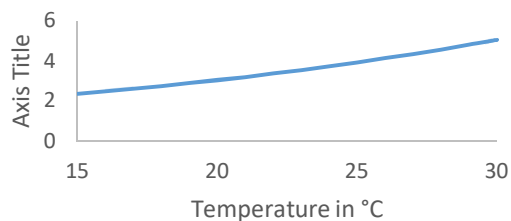
Appendix J.

Scaled TDSF and known TDSF. Blue line according to $f(T)$ and orange line from *May et al. 1978*.

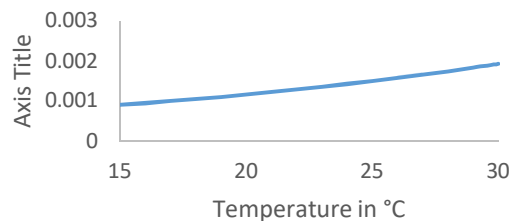


Appendix J continued

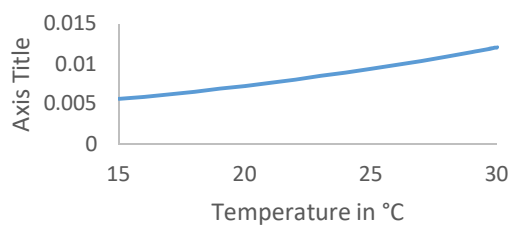
Acenaphthylene



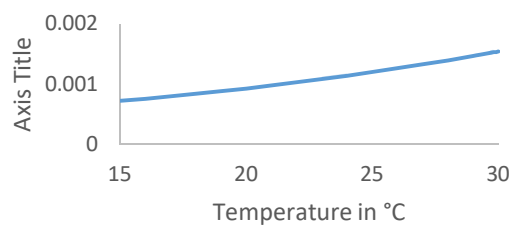
Benzo[a]Pyrene



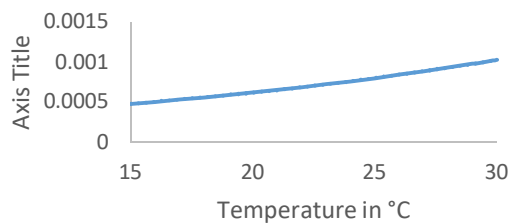
Benzo[a]Anthracene



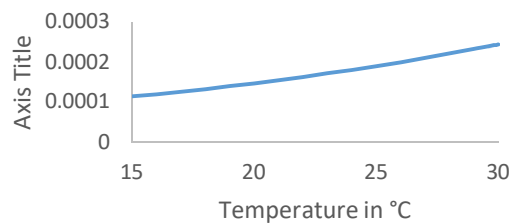
Benzo[b]Fluoranthene



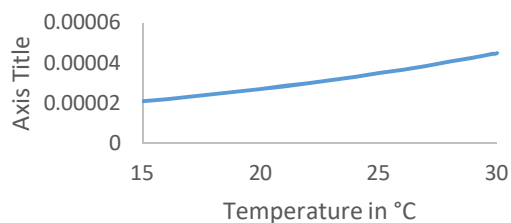
Benzo[k]Fluoranthene



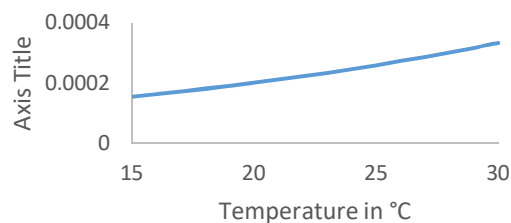
Indeno [1.2.3-cd] Pyrene



Dibenzo [a,h] Anthracene



Benzo [g,h,i] Perylene



Appendix K.

Henry's law constants by *Parnis et al. 2015*. estimates and in literature found constants over temperature range 20-25 °C according to review by *Xie et al. 1997*.

PAH	<i>Parnis et al. 2015</i> (Pa m ³ mol ⁻¹)	Literature (Pa m ³ mol ⁻¹)
Naphthalene	20 °C: 41.67 25 °C: 54.27	48.94 56 36.6 74.4 42.5
Acenaphthylene	11.67 15.74	11.55
Acenaphthene	21.37 28.74	14.79 24.42
Fluorene	7.07 9.81	11.86 6.45
Phenanthrene	3.32 4.68	3.98 5.55 2.38 4.68
Anthracene	3.59 5.07	6.59 7.40 7.40 1.96 3.30 4.94
Fluoranthene	1.17 1.70	0.65
Pyrene	1.45 2.09	1.89 1.10
Benzo[b]fluoranthene	0.10 0.16	0.051
Benzo[k]fluoranthene	0.11 0.17	0.044
Benzo[a]pyrene	0.12 0.19	0.034
Benzo[ghi]perylene	0.05 0.09	0.027
Indeno[1,2,3-cd]pyrene	0.05 0.07	0.029
Benz[a]anthracene	0.27 0.4	-
Dibenzo[a,h]anthracene	0.02 0.04	-

Appendix L.

Collected coefficients from *Parnis et al. 2015*.

Component	A	B
Napthalene	8.459	-2004.9
Acenaphthene	9.0081	-2250.9
Fluorene	9.3181	-2482.51
Phenanthrene	9.413	-2606.56
Anthracene	9.4938	-2620.3
Acenaphthylene	8.8156	-2271.52
Pyrene	9.644	-2780.21
Fluoranthene	9.7903	-2850.2
Chrysene	10.3614	-3204.84
Benzo[a]pyrene	10.5985	-3373.71
Benz[a]anthracene	10.3614	-3204.84
Benzo[b]fluoranthene	10.7422	-3438.16
Benzo[k]fluoranthene	10.8171	-3457.54
Indeno[1.2.3-cd]pyrene	10.981	-3613.54
Dibenzo[a.h]anthracene	11.3258	-3804.62
Benzo[g.h.i]perylene	10.7566	-3525.61

Appendix M.

Recovery for MS and MSD and RPD% calculation example and correction of the parent sample. Used values are from result report of Case I.

Component	Conc X_0	Spike added X_S	MS result X_{MS}	MSD result X_{MSD}	R% MS	R% MSD	RPD%
Unit/Formula	$\mu\text{g}/\text{dm}^3$	$\mu\text{g}/\text{dm}^3$	$\mu\text{g}/\text{dm}^3$	$\mu\text{g}/\text{dm}^3$	$\frac{X_{MS} - X_0}{X_S} 100\%$	$\frac{X_{MSD} - X_0}{X_S} 100\%$	$\frac{ R_{MS} - R_{MSD} }{((R_{MS} + R_{MSD})/2)} 100\%$

The corrected result is then calculated by dividing the parent sample concentration of anthracene by the average of R%MS and R%MSD:

This calculation is done on the permission of laboratory and is only an estimation.

Appendix N. Case III

PSU	Case III	Liq																						
	LG14					LG12				LG10				LG8				0	LG6					
	O T 15	ExhIn	ExhOut	Aqout		T 15	ExhIn	ExhOut	Aqout		T 15	ExhIn	ExhOut	Aqout		T 15	ExhIn	gas	aq		T 15	ExhIn	ExhOut	aq
	Naphthalene	150 %	423 %	100 %		Naphthalene	148 %	315 %	100 %		Naphthalene	141 %	229 %	100 %		Naphthalene	133 %	168 %	104 %		Naphthalene	112 %	115 %	107 %
	Acenaphthene	136 %	2027 %	100 %		Acenaphthene	140 %	1339 %	100 %		Acenaphthene	144 %	832 %	100 %		Acenaphthene	152 %	495 %	104 %		Acenaphthene	147 %	258 %	107 %
	Fluorene	112 %	42617 %	100 %		Fluorene	114 %	26154 %	100 %		Fluorene	117 %	14589 %	100 %		Fluorene	126 %	7349 %	104 %		Fluorene	136 %	2872 %	107 %
	Phenanthrene	106 %	396536 %	100 %		Phenanthrene	107 %	239439 %	100 %		Phenanthrene	108 %	130466 %	100 %		Phenanthrene	114 %	63339 %	104 %		Phenanthrene	121 %	23157 %	107 %
	sum	143 %	439 %	100 %		sum	142 %	327 %	100 %		sum	137 %	237 %	100 %		sum	132 %	174 %	104 %		sum	114 %	119 %	107 %
	T 17	ExhIn	ExhOut	Aqout		T 17	ExhIn	ExhOut	Aqout		T 17	ExhIn	ExhOut	Aqout		T 17	ExhIn	gas	aq		T 17	ExhIn	ExhOut	aq
	Naphthalene	179 %	501 %	100 %		Naphthalene	146 %	267 %	100 %		Naphthalene	138 %	200 %	100 %		Naphthalene	123 %	145 %	100 %		Naphthalene	101 %	101 %	100 %
	Acenaphthene	159 %	2216 %	100 %		Acenaphthene	143 %	1012 %	100 %		Acenaphthene	147 %	643 %	100 %		Acenaphthene	147 %	380 %	100 %		Acenaphthene	134 %	203 %	100 %
	Fluorene	121 %	43650 %	100 %		Fluorene	116 %	17862 %	100 %		Fluorene	119 %	10043 %	100 %		Fluorene	124 %	4918 %	100 %		Fluorene	131 %	1917 %	100 %
	Phenanthrene	110 %	398763 %	100 %		Phenanthrene	108 %	158058 %	100 %		Phenanthrene	109 %	86503 %	100 %		Phenanthrene	111 %	40592 %	100 %		Phenanthrene	115 %	14646 %	100 %
	sum	169 %	521 %	100 %		sum	141 %	277 %	100 %		sum	135 %	207 %	100 %		sum	123 %	150 %	100 %		sum	103 %	104 %	100 %
	T 20	ExhIn	ExhOut	Aqout		T 20	ExhIn	ExhOut	Aqout		T 20	ExhIn	ExhOut	Aqout		T 20	ExhIn	gas	aq		T 20	ExhIn	ExhOut	aq
	Naphthalene	147 %	274 %	100 %		Naphthalene	141 %	216 %	100 %		Naphthalene	131 %	168 %	100 %		Naphthalene	116 %	128 %	100 %		Naphthalene	112 %	93 %	100 %
	Acenaphthene	144 %	994 %	100 %		Acenaphthene	148 %	687 %	100 %		Acenaphthene	149 %	454 %	100 %		Acenaphthene	145 %	283 %	100 %		Acenaphthene	148 %	163 %	100 %
	Fluorene	117 %	16448 %	100 %		Fluorene	120 %	10249 %	100 %		Fluorene	124 %	5843 %	100 %		Fluorene	129 %	2924 %	100 %		Fluorene	138 %	1185 %	100 %
	Phenanthrene	108 %	140943 %	100 %		Phenanthrene	109 %	85838 %	100 %		Phenanthrene	111 %	47334 %	100 %		Phenanthrene	114 %	22461 %	100 %		Phenanthrene	119 %	8265 %	100 %
	sum	142 %	284 %	100 %		sum	138 %	224 %	100 %		sum	130 %	174 %	100 %		sum	117 %	132 %	100 %		sum	114 %	96 %	100 %
	T 25	ExhIn	ExhOut	Aqout		T 25	ExhIn	ExhOut	Aqout		T 25	ExhIn	ExhOut	Aqout		T 25	ExhIn	gas	aq		T 25	ExhIn	ExhOut	aq
	Naphthalene	139 %	197 %	100 %		Naphthalene	131 %	164 %	100 %		Naphthalene	120 %	135 %	100 %		Naphthalene	106 %	109 %	100 %		Naphthalene	89 %	85 %	100 %
	Acenaphthene	150 %	541 %	100 %		Acenaphthene	150 %	395 %	100 %		Acenaphthene	147 %	281 %	100 %		Acenaphthene	136 %	192 %	100 %		Acenaphthene	114 %	125 %	100 %
	Fluorene	123 %	6698 %	100 %		Fluorene	127 %	4263 %	100 %		Fluorene	132 %	2507 %	100 %		Fluorene	137 %	1317 %	100 %		Fluorene	142 %	581 %	100 %
	Phenanthrene	111 %	52162 %	100 %		Phenanthrene	113 %	32126 %	100 %		Phenanthrene	116 %	17997 %	100 %		Phenanthrene	120 %	8747 %	100 %		Phenanthrene	125 %	3345 %	100 %
	sum	136 %	204 %	100 %		sum	130 %	170 %	100 %		sum	121 %	140 %	100 %		sum	108 %	113 %	100 %		sum	91 %	88 %	100 %
	T 27	ExhIn	ExhOut	Aqout		T 27	ExhIn	ExhOut	Aqout		T 27	ExhIn	ExhOut	Aqout		T 27	ExhIn	gas	aq		T 27	ExhIn	ExhOut	aq
	Naphthalene	135 %	177 %	100 %		Naphthalene	127 %	150 %	100 %		Naphthalene	116 %	126 %	100 %		Naphthalene	103 %	104 %	100 %		Naphthalene	87 %	83 %	100 %
	Acenaphthene	151 %	438 %	100 %		Acenaphthene	150 %	328 %	100 %		Acenaphthene	144 %	240 %	100 %		Acenaphthene	131 %	171 %	100 %		Acenaphthene	110 %	116 %	100 %
	Fluorene	126 %	4756 %	100 %		Fluorene	130 %	3060 %	100 %		Fluorene	135 %	1828 %	100 %		Fluorene	141 %	984 %	100 %		Fluorene	143 %	453 %	100 %
	Phenanthrene	113 %	35463 %	100 %		Phenanthrene	115 %	21960 %	100 %		Phenanthrene	118 %	12401 %	100 %		Phenanthrene	122 %	6102 %	100 %		Phenanthrene	129 %	2383 %	100 %
	sum	133 %	184 %	100 %		sum	126 %	156 %	100 %		sum	117 %	131 %	100 %		sum	105 %	108 %	100 %		sum	89 %	86 %	100 %

Appendix O. Case III

PSU	Case III LG14	Liq				LG12				LG10				LG8				8.001068				LG6			
	20 T 15	ExhIn	ExhOut	Aqout		T 15	ExhIn	ExhOut	Aqout		T 15	ExhIn	ExhOut	Aqout		T 15	ExhIn	ExhOut	Aqout		T 15	ExhIn	ExhOut	Aqout	
	Naphthalene	149 %	308 %	100 %		Naphthalene	147 %	244 %	102 %		Naphthalene	135 %	182 %	100 %		Naphthalene	119 %	135 %	100 %		Naphthalene	97 %	96 %	100 %	
	Acenaphthene	142 %	1312 %	100 %		Acenaphthene	149 %	906 %	102 %		Acenaphthene	149 %	570 %	100 %		Acenaphthene	147 %	342 %	100 %		Acenaphthene	132 %	186 %	100 %	
	Fluorene	115 %	23734 %	100 %		Fluorene	120 %	14964 %	102 %		Fluorene	121 %	8258 %	100 %		Fluorene	126 %	4057 %	100 %		Fluorene	133 %	1593 %	100 %	
	Phenanthrene	108 %	170334 %	100 %		Phenanthrene	111 %	105377 %	102 %		Phenanthrene	111 %	56568 %	100 %		Phenanthrene	113 %	26601 %	100 %		Phenanthrene	118 %	9647 %	100 %	
	sum	144 %	320 %	100 %		sum	143 %	253 %	102 %		sum	133 %	188 %	100 %		sum	120 %	139 %	100 %		sum	99 %	99 %	100 %	
	T 17	ExhIn	ExhOut	Aqout		T 17	ExhIn	ExhOut	Aqout		T 17	ExhIn	ExhOut	Aqout		T 17	ExhIn	ExhOut	Aqout		T 17	ExhIn	ExhOut	Aqout	
	Naphthalene	158 %	344 %	100 %		Naphthalene	156 %	272 %	102 %		Naphthalene	144 %	203 %	100 %		Naphthalene	128 %	150 %	100 %		Naphthalene	105 %	107 %	100 %	
	Acenaphthene	148 %	1485 %	100 %		Acenaphthene	156 %	1025 %	102 %		Acenaphthene	156 %	644 %	100 %		Acenaphthene	156 %	386 %	100 %		Acenaphthene	141 %	211 %	100 %	
	Fluorene	118 %	27200 %	100 %		Fluorene	123 %	17149 %	102 %		Fluorene	124 %	9464 %	100 %		Fluorene	130 %	4650 %	100 %		Fluorene	138 %	1826 %	100 %	
	Phenanthrene	109 %	196547 %	100 %		Phenanthrene	113 %	121593 %	102 %		Phenanthrene	112 %	65273 %	100 %		Phenanthrene	116 %	30695 %	100 %		Phenanthrene	121 %	11131 %	100 %	
	sum	151 %	358 %	100 %		sum	151 %	282 %	102 %		sum	141 %	210 %	100 %		sum	128 %	156 %	100 %		sum	107 %	110 %	100 %	
	T 20	ExhIn	ExhOut	Aqout		T 20	ExhIn	ExhOut	Aqout		T 20	ExhIn	ExhOut	Aqout		T 20	ExhIn	gas	aq		T 20	ExhIn	ExhOut	aq	
	Naphthalene	142 %	214 %	100 %		Naphthalene	134 %	175 %	100 %		Naphthalene	123 %	142 %	100 %		Naphthalene	108 %	113 %	100 %		Naphthalene	89 %	86 %	100 %	
	Acenaphthene	150 %	677 %	100 %		Acenaphthene	151 %	483 %	100 %		Acenaphthene	149 %	332 %	100 %		Acenaphthene	140 %	219 %	100 %		Acenaphthene	118 %	135 %	100 %	
	Fluorene	121 %	9314 %	100 %		Fluorene	125 %	5863 %	100 %		Fluorene	129 %	3394 %	100 %		Fluorene	135 %	1740 %	100 %		Fluorene	141 %	736 %	100 %	
	Phenanthrene	111 %	61158 %	100 %		Phenanthrene	113 %	37465 %	100 %		Phenanthrene	115 %	20836 %	100 %		Phenanthrene	119 %	10021 %	100 %		Phenanthrene	125 %	3774 %	100 %	
	sum	139 %	223 %	100 %		sum	133 %	182 %	100 %		sum	123 %	147 %	100 %		sum	110 %	117 %	100 %		sum	92 %	89 %	100 %	
	T 25	ExhIn	ExhOut	Aqout		T 25	ExhIn	ExhOut	Aqout		T 25	ExhIn	ExhOut	Aqout		T 25	ExhIn	gas	aq		T 25	ExhIn	ExhOut	aq	
	Naphthalene	132 %	164 %	100 %		Naphthalene	124 %	141 %	100 %		Naphthalene	113 %	120 %	100 %		Naphthalene	100 %	100 %	100 %		Naphthalene	84 %	81 %	100 %	
	Acenaphthene	152 %	393 %	100 %		Acenaphthene	150 %	297 %	100 %		Acenaphthene	142 %	221 %	100 %		Acenaphthene	129 %	159 %	100 %		Acenaphthene	107 %	110 %	100 %	
	Fluorene	129 %	3888 %	100 %		Fluorene	133 %	2514 %	100 %		Fluorene	138 %	1513 %	100 %		Fluorene	143 %	824 %	100 %		Fluorene	144 %	386 %	100 %	
	Phenanthrene	115 %	22978 %	100 %		Phenanthrene	118 %	14279 %	100 %		Phenanthrene	121 %	8105 %	100 %		Phenanthrene	126 %	4023 %	100 %		Phenanthrene	133 %	1602 %	100 %	
	sum	131 %	171 %	100 %		sum	124 %	146 %	100 %		sum	115 %	124 %	100 %		sum	103 %	104 %	100 %		sum	87 %	83 %	100 %	
	T 27	ExhIn	ExhOut	Aqout		T 27	ExhIn	ExhOut	Aqout		T 27	ExhIn	ExhOut	Aqout		T 27	ExhIn	gas	aq		T 27	ExhIn	ExhOut	aq	
	Naphthalene	128 %	151 %	100 %		Naphthalene	120 %	132 %	100 %		Naphthalene	110 %	114 %	100 %		Naphthalene	98 %	97 %	100 %		Naphthalene	83 %	80 %	100 %	
	Acenaphthene	152 %	327 %	100 %		Acenaphthene	147 %	254 %	100 %		Acenaphthene	138 %	194 %	100 %		Acenaphthene	124 %	145 %	100 %		Acenaphthene	103 %	104 %	100 %	
	Fluorene	132 %	2797 %	100 %		Fluorene	137 %	1834 %	100 %		Fluorene	141 %	1125 %	100 %		Fluorene	146 %	631 %	100 %		Fluorene	143 %	311 %	100 %	
	Phenanthrene	118 %	15748 %	100 %		Phenanthrene	120 %	9856 %	100 %		Phenanthrene	124 %	5653 %	100 %		Phenanthrene	129 %	2848 %	100 %		Phenanthrene	136 %	1169 %	100 %	
	sum	128 %	157 %	100 %		sum	121 %	137 %	100 %		sum	112 %	118 %	100 %		sum	100 %	100 %	100 %		sum	85 %	82 %	100 %	

PSU	Case III LG14	Liq																	
		LG12				LG10				LG8				LG6					
35	T 15	ExhIn	ExhOut	Aqout		T 15	ExhIn	ExhOut	Aqout		T 15	ExhIn	ExhOut	Aqout		T 15	ExhIn	ExhOut	Aqout
	Naphthalene	147 %	252 %	100 %		Naphthalene	140 %	201 %	100 %		Naphthalene	129 %	158 %	100 %		Naphthalene	92 %	89 %	100 %
	Acenaphlene	146 %	965 %	100 %		Acenaphlene	149 %	666 %	100 %		Acenaphlene	150 %	440 %	100 %		Acenaphlene	126 %	158 %	100 %
	Fluorene	118 %	15401 %	100 %		Fluorene	121 %	9573 %	100 %		Fluorene	125 %	5442 %	100 %		Fluorene	137 %	1094 %	100 %
	Phenanthrene	110 %	90882 %	100 %		Phenanthrene	111 %	55299 %	100 %		Phenanthrene	114 %	30468 %	100 %		Phenanthrene	122 %	5326 %	100 %
	sum	142 %	262 %	100 %		sum	137 %	208 %	100 %		sum	128 %	163 %	100 %		sum	94 %	92 %	100 %
	T 17	ExhIn	ExhOut	Aqout		T 17	ExhIn	ExhOut	Aqout		T 17	ExhIn	ExhOut	Aqout		T 17	ExhIn	ExhOut	Aqout
	Naphthalene	44 %	120 %			Naphthalene	149 %	179 %	100 %		Naphthalene	124 %	144 %	100 %		Naphthalene	89 %	86 %	100 %
	Acenaphlene	149 %	743 %	100 %		Acenaphlene	157 %	525 %	100 %		Acenaphlene	150 %	356 %	100 %		Acenaphlene	120 %	139 %	100 %
	Fluorene	121 %	10581 %	100 %		Fluorene	124 %	6639 %	100 %		Fluorene	128 %	3812 %	100 %		Fluorene	140 %	806 %	100 %
	Phenanthrene	111 %	60235 %	100 %		Phenanthrene	113 %	36827 %	100 %		Phenanthrene	116 %	20421 %	100 %		Phenanthrene	125 %	3664 %	100 %
	sum	140 %	228 %	100 %		sum	146 %	186 %	100 %		sum	124 %	149 %	100 %		sum	92 %	88 %	100 %
		100 %	100 %	100 %															
	T 20	ExhIn	ExhOut	Aqout		T 20	ExhIn	ExhOut	Aqout		T 20	ExhIn	gas	aq		T 20	ExhIn	ExhOut	aq
	Naphthalene	138 %	184 %	100 %		Naphthalene	165 %	155 %	100 %		Naphthalene	118 %	129 %	100 %		Naphthalene	86 %	82 %	100 %
	Acenaphlene	152 %	521 %	100 %		Acenaphlene	170 %	381 %	100 %		Acenaphlene	147 %	271 %	100 %		Acenaphlene	112 %	120 %	100 %
	Fluorene	125 %	6140 %	100 %		Fluorene	130 %	3903 %	100 %		Fluorene	134 %	2291 %	100 %		Fluorene	143 %	529 %	100 %
	Phenanthrene	114 %	32970 %	100 %		Phenanthrene	116 %	20330 %	100 %		Phenanthrene	119 %	11398 %	100 %		Phenanthrene	130 %	2148 %	100 %
	sum	136 %	191 %	100 %		sum	160 %	160 %	100 %		sum	119 %	133 %	100 %		sum	88 %	85 %	100 %
	T 25	ExhIn	ExhOut	Aqout		T 25	ExhIn	ExhOut	Aqout		T 25	ExhIn	gas	aq		T 25	ExhIn	ExhOut	aq
	Naphthalene	162 %	147 %	100 %		Naphthalene	118 %	129 %	100 %		Naphthalene	97 %	96 %	100 %		Naphthalene	82 %	79 %	100 %
	Acenaphlene	175 %	318 %	100 %		Acenaphlene	147 %	247 %	100 %		Acenaphlene	123 %	142 %	100 %		Acenaphlene	101 %	102 %	100 %
	Fluorene	135 %	2625 %	100 %		Fluorene	138 %	1722 %	100 %		Fluorene	147 %	596 %	100 %		Fluorene	143 %	295 %	100 %
	Phenanthrene	119 %	12594 %	100 %		Phenanthrene	122 %	7890 %	100 %		Phenanthrene	127 %	2304 %	100 %		Phenanthrene	139 %	955 %	100 %

PSU	Case III	Liq																						
	LG14					LG12				LG10				LG8				LG6						
40	T 15	ExhIn	ExhOut	Aqout		T 15	ExhIn	ExhOut	Aqout		T 15	ExhIn	ExhOut	Aqout		T 15	ExhIn	ExhOut	Aqout		T 15	ExhIn	ExhOut	Aqout
	Naphthalene	146 %	237 %	100 %		Naphthalene	141 %	195 %	102 %		Naphthalene	127 %	151 %	100 %		Naphthalene	111 %	117 %	100 %		Naphthalene	79 %	87 %	100 %
	Acenaphthene	148 %	875 %	100 %		Acenaphthene	154 %	621 %	102 %		Acenaphthene	151 %	406 %	100 %		Acenaphthene	144 %	256 %	100 %		Acenaphthene	100 %	150 %	100 %
	Fluorene	119 %	13535 %	100 %		Fluorene	125 %	8492 %	102 %		Fluorene	126 %	4746 %	100 %		Fluorene	132 %	2380 %	100 %		Fluorene	129 %	969 %	100 %
	Phenanthrene	110 %	73807 %	100 %		Phenanthrene	115 %	45906 %	102 %		Phenanthrene	115 %	24836 %	100 %		Phenanthrene	118 %	11824 %	100 %		Phenanthrene	122 %	4386 %	100 %
	sum	142 %	246 %	100 %		sum	139 %	202 %	102 %		sum	127 %	157 %	100 %		sum	113 %	122 %	100 %		sum	82 %	90 %	100 %
	T 17	ExhIn	ExhOut	Aqout		T 17	ExhIn	ExhOut	Aqout		T 17	ExhIn	ExhOut	Aqout		T 17	ExhIn	ExhOut	Aqout		T 17	ExhIn	ExhOut	Aqout
	Naphthalene	142 %	208 %	100 %		Naphthalene	134 %	171 %	100 %		Naphthalene	122 %	139 %	100 %		Naphthalene	107 %	110 %	100 %		Naphthalene	93 %	90 %	107 %
	Acenaphthene	151 %	678 %	100 %		Acenaphthene	152 %	482 %	100 %		Acenaphthene	150 %	331 %	100 %		Acenaphthene	140 %	217 %	100 %		Acenaphthene	126 %	142 %	107 %
	Fluorene	122 %	9193 %	100 %		Fluorene	125 %	5777 %	100 %		Fluorene	130 %	3336 %	100 %		Fluorene	136 %	1705 %	100 %		Fluorene	151 %	766 %	107 %
	Phenanthrene	112 %	48989 %	100 %		Phenanthrene	114 %	30002 %	100 %		Phenanthrene	117 %	16682 %	100 %		Phenanthrene	121 %	8028 %	100 %		Phenanthrene	136 %	3233 %	107 %
	sum	139 %	216 %	100 %		sum	132 %	177 %	100 %		sum	123 %	144 %	100 %		sum	109 %	114 %	100 %		sum	96 %	93 %	107 %
	T 20	ExhIn	ExhOut	Aqout		T 20	ExhIn	ExhOut	Aqout		T 20	ExhIn	ExhOut	Aqout		T 20	ExhIn	gas	aq		T 20	ExhIn	ExhOut	aq
	Naphthalene	136 %	176 %	100 %		Naphthalene	127 %	149 %	100 %		Naphthalene	136 %	125 %	100 %		Naphthalene	102 %	103 %	100 %		Naphthalene	84 %	81 %	100 %
	Acenaphthene	153 %	480 %	100 %		Acenaphthene	152 %	354 %	100 %		Acenaphthene	164 %	254 %	100 %		Acenaphthene	133 %	177 %	100 %		Acenaphthene	110 %	116 %	100 %
	Fluorene	126 %	5355 %	100 %		Fluorene	130 %	3417 %	100 %		Fluorene	137 %	2017 %	100 %		Fluorene	141 %	1067 %	100 %		Fluorene	144 %	477 %	100 %
	Phenanthrene	115 %	26885 %	100 %		Phenanthrene	117 %	16608 %	100 %		Phenanthrene	121 %	9361 %	100 %		Phenanthrene	125 %	4585 %	100 %		Phenanthrene	132 %	1790 %	100 %
	sum	134 %	183 %	100 %		sum	127 %	155 %	100 %		sum	136 %	129 %	100 %		sum	104 %	106 %	100 %		sum	87 %	83 %	100 %
	T 25	ExhIn	ExhOut	Aqout		T 25	ExhIn	ExhOut	Aqout		T 25	ExhIn	ExhOut	Aqout										

Appendix R. Case I

PSU	Case I				LG12				LG10				LG8				LG6			
	O T 15	ExhIn	ExhOut	Aqout	T 15	ExhIn	ExhOut	Aqout	T 15	ExhIn	ExhOut	Aqout	T 15	ExhIn	gas	aq	T 15	ExhIn	ExhOut	aq
	Naphthalene	152 %	460 %	100 %	Naphthalene	150 %	335 %	100 %	Naphthalene	143 %	236 %	100 %	Naphthalene	128 %	160 %	100 %	Naphthalene	101 %	101 %	100 %
	Acenaphlene	136 %	2273 %	100 %	Acenaphlene	140 %	1473 %	100 %	Acenaphlene	145 %	890 %	100 %	Acenaphlene	147 %	488 %	100 %	Acenaphlene	137 %	232 %	100 %
	Fluorene	112 %	48466 %	100 %	Fluorene	114 %	29258 %	100 %	Fluorene	117 %	15943 %	100 %	Fluorene	121 %	7439 %	100 %	Fluorene	127 %	2663 %	100 %
	Phenanthrene	106 %	450896 %	100 %	Phenanthrene	107 %	267854 %	100 %	Phenanthrene	108 %	142609 %	100 %	Phenanthrene	110 %	64152 %	100 %	Phenanthrene	113 %	21501 %	100 %
	sum	135 %	506 %	100 %	sum	135 %	368 %	100 %	sum	132 %	259 %	100 %	sum	124 %	175 %	100 %	sum	105 %	110 %	100 %
	T 17	ExhIn	ExhOut	Aqout	T 17	ExhIn	ExhOut	Aqout	T 17	ExhIn	ExhOut	Aqout	T 17	ExhIn	gas	aq	T 17	ExhIn	ExhOut	aq
	Naphthalene	152 %	379 %	100 %	Naphthalene	148 %	282 %	100 %	Naphthalene	139 %	205 %	100 %	Naphthalene	122 %	143 %	100 %	Naphthalene	96 %	94 %	100 %
	Acenaphlene	140 %	1683 %	100 %	Acenaphlene	144 %	1107 %	100 %	Acenaphlene	148 %	684 %	100 %	Acenaphlene	147 %	388 %	100 %	Acenaphlene	132 %	193 %	100 %
	Fluorene	114 %	32893 %	100 %	Fluorene	116 %	19961 %	100 %	Fluorene	120 %	10959 %	100 %	Fluorene	124 %	5171 %	100 %	Fluorene	131 %	1888 %	100 %
	Phenanthrene	107 %	296702 %	100 %	Phenanthrene	108 %	176803 %	100 %	Phenanthrene	109 %	94529 %	100 %	Phenanthrene	111 %	42781 %	100 %	Phenanthrene	115 %	14470 %	100 %
	sum	136 %	417 %	100 %	sum	135 %	310 %	100 %	sum	131 %	225 %	100 %	sum	121 %	157 %	100 %	sum	101 %	103 %	100 %
	T 20	ExhIn	ExhOut	Aqout	T 20	ExhIn	ExhOut	Aqout	T 20	ExhIn	ExhOut	Aqout	T 20	ExhIn	gas	aq	T 20	ExhIn	ExhOut	aq
	Naphthalene	150 %	292 %	100 %	Naphthalene	143 %	226 %	100 %	Naphthalene	132 %	170 %	100 %	Naphthalene	115 %	125 %	100 %	Naphthalene	90 %	87 %	100 %
	Acenaphlene	145 %	1102 %	100 %	Acenaphlene	149 %	745 %	100 %	Acenaphlene	150 %	477 %	100 %	Acenaphlene	145 %	285 %	100 %	Acenaphlene	124 %	154 %	100 %
	Fluorene	117 %	18658 %	100 %	Fluorene	120 %	11427 %	100 %	Fluorene	124 %	6356 %	100 %	Fluorene	129 %	3061 %	100 %	Fluorene	135 %	1157 %	100 %
	Phenanthrene	108 %	160221 %	100 %	Phenanthrene	109 %	95969 %	100 %	Phenanthrene	111 %	51676 %	100 %	Phenanthrene	114 %	23628 %	100 %	Phenanthrene	119 %	8121 %	100 %
	sum	136 %	322 %	100 %	sum	134 %	248 %	100 %	sum	128 %	187 %	100 %	sum	116 %	137 %	100 %	sum	97 %	94 %	100 %
	T 25	ExhIn	ExhOut	Aqout	T 25	ExhIn	ExhOut	Aqout	T 25	ExhIn	ExhOut	Aqout	T 25	ExhIn	gas	aq	T 25	ExhIn	ExhOut	aq
	Naphthalene	142 %	207 %	100 %	Naphthalene	133 %	168 %	100 %	Naphthalene	120 %	135 %	100 %	Naphthalene	104 %	106 %	100 %	Naphthalene	83 %	79 %	100 %
	Acenaphlene	152 %	590 %	100 %	Acenaphlene	152 %	421 %	100 %	Acenaphlene	148 %	290 %	100 %	Acenaphlene	135 %	190 %	100 %	Acenaphlene	109 %	116 %	100 %
	Fluorene	123 %	7560 %	100 %	Fluorene	127 %	4724 %	100 %	Fluorene	132 %	2704 %	100 %	Fluorene	138 %	1362 %	100 %	Fluorene	142 %	557 %	100 %
	Phenanthrene	111 %	59196 %	100 %	Phenanthrene	113 %	35833 %	100 %	Phenanthrene	116 %	19580 %	100 %	Phenanthrene	120 %	9149 %	100 %	Phenanthrene	126 %	3258 %	100 %
	sum	134 %	228 %	100 %	sum	129 %	185 %	100 %	sum	121 %	148 %	100 %	sum	109 %	116 %	100 %	sum	90 %	86 %	100 %
	T 27	ExhIn	ExhOut	Aqout	T 27	ExhIn	ExhOut	Aqout	T 27	ExhIn	ExhOut	Aqout	T 27	ExhIn	gas	aq	T 27	ExhIn	ExhOut	aq
	Naphthalene	137 %	185 %	100 %	Naphthalene	128 %	153 %	100 %	Naphthalene	116 %	126 %	100 %	Naphthalene	101 %	101 %	100 %	Naphthalene	81 %	77 %	100 %
	Acenaphlene	153 %	474 %	100 %	Acenaphlene	151 %	346 %	100 %	Acenaphlene	145 %	246 %	100 %	Acenaphlene	130 %	167 %	100 %	Acenaphlene	104 %	107 %	100 %
	Fluorene	126 %	5352 %	100 %	Fluorene	130 %	3378 %	100 %	Fluorene	135 %	1963 %	100 %	Fluorene	141 %	1012 %	100 %	Fluorene	142 %	431 %	100 %
	Phenanthrene	113 %	40198 %	100 %	Phenanthrene	115 %	24459 %	100 %	Phenanthrene	118 %	13461 %	100 %	Phenanthrene	122 %	6359 %	100 %	Phenanthrene	129 %	2307 %	100 %
	sum	132 %	204 %	100 %	sum	127 %	169 %	100 %	sum	118 %	138 %	100 %	sum	106 %	110 %	100 %	sum	88 %	83 %	100 %

Appendix S. Case I

PSU	Case I																			
	LG14				LG12				LG10				LG8				LG6			
	20	T 15	ExhIn	ExhOut	Aqout															

Appendix T. Case I

PSU	Case I				LG12				LG10				LG8				LG6			
35	T 15	ExhIn	ExhOut	Aqout	T 15	ExhIn	ExhOut	Aqout	T 15	ExhIn	ExhOut	Aqout	T 15	ExhIn	ExhOut	Aqout	T 15	ExhIn	ExhOut	Aqout
	Naphthalene	150 %	268 %	100 %	Naphthalene	142 %	209 %	100 %	Naphthalene	130 %	159 %	100 %	Naphthalene	111 %	118 %	100 %	Naphthalene	87 %	83 %	100 %
	Acenaphlene	147 %	1067 %	100 %	Acenaphlene	150 %	721 %	100 %	Acenaphlene	151 %	462 %	100 %	Acenaphlene	145 %	276 %	100 %	Acenaphlene	122 %	148 %	100 %
	Fluorene	118 %	17448 %	100 %	Fluorene	121 %	10660 %	100 %	Fluorene	125 %	5912 %	100 %	Fluorene	130 %	2837 %	100 %	Fluorene	137 %	1070 %	100 %
	Phenanthrene	110 %	103118 %	100 %	Phenanthrene	111 %	61700 %	100 %	Phenanthrene	114 %	33193 %	100 %	Phenanthrene	117 %	15178 %	100 %	Phenanthrene	122 %	5239 %	100 %
	sum	137 %	295 %	100 %	sum	134 %	230 %	100 %	sum	127 %	175 %	100 %	sum	114 %	129 %	100 %	sum	94 %	90 %	100 %
	T 17	ExhIn	ExhOut	Aqout	T 17	ExhIn	ExhOut	Aqout	T 17	ExhIn	ExhOut	Aqout	T 17	ExhIn	ExhOut	Aqout	T 17	ExhIn	ExhOut	Aqout
	Naphthalene	46 %	132 %	0 %	Naphthalene	138 %	185 %	100 %	Naphthalene	125 %	145 %	100 %	Naphthalene	107 %	110 %	100 %	Naphthalene	84 %	79 %	100 %
	Acenaphlene	150 %	817 %	100 %	Acenaphlene	153 %	564 %	100 %	Acenaphlene	151 %	371 %	100 %	Acenaphlene	142 %	230 %	100 %	Acenaphlene	116 %	130 %	100 %
	Fluorene	121 %	11968 %	100 %	Fluorene	124 %	7367 %	100 %	Fluorene	128 %	4131 %	100 %	Fluorene	134 %	2016 %	100 %	Fluorene	140 %	783 %	100 %
	Phenanthrene	111 %	68315 %	100 %	Phenanthrene	113 %	41057 %	100 %	Phenanthrene	116 %	22225 %	100 %	Phenanthrene	119 %	10257 %	100 %	Phenanthrene	125 %	3595 %	100 %
	sum	136 %	256 %	100 %	sum	132 %	204 %	100 %	sum	124 %	159 %	100 %	sum	111 %	121 %	100 %	sum	91 %	86 %	100 %
		100 %	100 %	100 %																
	T 20	ExhIn	ExhOut	Aqout	T 20	ExhIn	ExhOut	Aqout	T 20	ExhIn	ExhOut	Aqout	T 20	ExhIn	gas	aq	T 20	ExhIn	ExhOut	aq
	Naphthalene	140 %	192 %	100 %	Naphthalene	130 %	158 %	100 %	Naphthalene	118 %	128 %	100 %	Naphthalene	101 %	101 %	100 %	Naphthalene	80 %	76 %	100 %
	Acenaphlene	154 %	566 %	100 %	Acenaphlene	154 %	405 %	100 %	Acenaphlene	148 %	279 %	100 %	Acenaphlene	134 %	183 %	100 %	Acenaphlene	107 %	112 %	100 %
	Fluorene	125 %	6923 %	100 %	Fluorene	129 %	4319 %	100 %	Fluorene	134 %	2469 %	100 %	Fluorene	140 %	1243 %	100 %	Fluorene	143 %	509 %	100 %
	Phenanthrene	114 %	37349 %	100 %	Phenanthrene	116 %	22620 %	100 %	Phenanthrene	119 %	12378 %	100 %	Phenanthrene	124 %	5806 %	100 %	Phenanthrene	130 %	2092 %	100 %
	sum	134 %	213 %	100 %	sum	128 %	175 %	100 %	sum	120 %	141 %	100 %	sum	106 %	111 %	100 %	sum	87 %	82 %	100 %
	T 25	ExhIn	ExhOut	Aqout	T 25	ExhIn	ExhOut	Aqout	T 25	ExhIn	ExhOut	Aqout	T 25	ExhIn	gas	aq	T 25	ExhIn	ExhOut	aq
	Naphthalene	129 %	152 %	100 %	Naphthalene	119 %	131 %	100 %	Naphthalene	108 %	111 %	100 %	Naphthalene	94 %	92 %	100 %	Naphthalene	76 %	72 %	100 %
	Acenaphlene	154 %	339 %	100 %	Acenaphlene	149 %	258 %	100 %	Acenaphlene	139 %	192 %	100 %	Acenaphlene	121 %	138 %	100 %	Acenaphlene	95 %	93 %	100 %
	Fluorene	134 %	2935 %	100 %	Fluorene	138 %	1887 %	100 %	Fluorene	143 %	1126 %	100 %	Fluorene	147 %	606 %	100 %	Fluorene	137 %	271 %	98 %
	Phenanthrene	119 %	14197 %	100 %	Phenanthrene	122 %	8742 %	100 %	Phenanthrene	127 %	4898 %	100 %	Phenanthrene	132 %	2383 %	100 %	Phenanthrene	139 %	915 %	100 %
	sum	128 %	168 %	100 %	sum	122 %	144 %	100 %	sum	113 %	122 %	100 %	sum	100 %	100 %	100 %	sum	83 %	78 %	100 %
	T 27	ExhIn	ExhOut	Aqout	T 27	ExhIn	ExhOut	Aqout	T 27	ExhIn	ExhOut	Aqout	T 27	ExhIn	gas	aq	T 27	ExhIn	ExhOut	aq
	Naphthalene	125 %	141 %	100 %	Naphthalene	115 %	123 %	100 %	Naphthalene	104 %	106 %	100 %	Naphthalene	91 %	89 %	100 %	Naphthalene	75 %	72 %	100 %
	Acenaphlene	152 %	286 %	100 %	Acenaphlene	145 %	223 %	100 %	Acenaphlene	134 %	170 %	100 %	Acenaphlene	116 %	127 %	100 %	Acenaphlene	92 %	89 %	100 %
	Fluorene	138 %	2128 %	100 %	Fluorene	142 %	1389 %	100 %	Fluorene	146 %	847 %	100 %	Fluorene	148 %	471 %	100 %	Fluorene	141 %	235 %	103 %
	Phenanthrene	122 %	9787 %	100 %	Phenanthrene	125 %	6077 %	100 %	Phenanthrene	130 %	3446 %	100 %	Phenanthrene	136 %	1709 %	100 %	Phenanthrene	141 %	679 %	100 %
	sum	126 %	156 %	100 %	sum	119 %	136 %	100 %	sum	110 %	116 %	100 %	sum	98 %	97 %	100 %	sum	82 %	77 %	100 %

Appendix U. Case I

PSU	Case I LG14				LG12				LG10				LG8				LG6			
	40 T 15	ExhIn	ExhOut	Aqout	T 15	ExhIn	ExhOut	Aqout	T 15	ExhIn	ExhOut	Aqout	T 15	ExhIn	ExhOut	Aqout	T 15	ExhIn	ExhOut	Aqout
	Naphthalene	149 %	251 %	100 %	Naphthalene	140 %	198 %	100 %	Naphthalene	127 %	153 %	100 %	Naphthalene	109 %	114 %	100 %	Naphthalene	85 %	81 %	100 %
	Acenaphthene	149 %	965 %	100 %	Acenaphthene	152 %	657 %	100 %	Acenaphthene	152 %	425 %	100 %	Acenaphthene	144 %	257 %	100 %	Acenaphthene	120 %	141 %	100 %
	Fluorene	119 %	15117 %	100 %	Fluorene	122 %	9256 %	100 %	Fluorene	126 %	5150 %	100 %	Fluorene	132 %	2485 %	100 %	Fluorene	138 %	946 %	100 %
	Phenanthrene	110 %	83709 %	100 %	Phenanthrene	112 %	50158 %	100 %	Phenanthrene	115 %	27040 %	100 %	Phenanthrene	118 %	12405 %	100 %	Phenanthrene	124 %	4308 %	100 %
	sum	137 %	277 %	100 %	sum	133 %	218 %	100 %	sum	126 %	168 %	100 %	sum	113 %	125 %	100 %	sum	92 %	88 %	100 %
	T 17	ExhIn	ExhOut	Aqout	T 17	ExhIn	ExhOut	Aqout	T 17	ExhIn	ExhOut	Aqout	T 17	ExhIn	ExhOut	Aqout	T 17	ExhIn	ExhOut	Aqout
	Naphthalene	145 %	219 %	100 %	Naphthalene	136 %	176 %	100 %	Naphthalene	122 %	139 %	100 %	Naphthalene	105 %	107 %	100 %	Naphthalene	82 %	78 %	100 %
	Acenaphthene	152 %	743 %	100 %	Acenaphthene	153 %	517 %	100 %	Acenaphthene	151 %	344 %	100 %	Acenaphthene	140 %	216 %	100 %	Acenaphthene	113 %	125 %	100 %
	Fluorene	122 %	10390 %	100 %	Fluorene	125 %	6413 %	100 %	Fluorene	130 %	3609 %	100 %	Fluorene	136 %	1773 %	100 %	Fluorene	141 %	697 %	100 %
	Phenanthrene	112 %	55531 %	100 %	Phenanthrene	114 %	33431 %	100 %	Phenanthrene	117 %	18142 %	100 %	Phenanthrene	121 %	8406 %	100 %	Phenanthrene	127 %	2968 %	100 %
	sum	136 %	242 %	100 %	sum	131 %	194 %	100 %	sum	123 %	153 %	100 %	sum	110 %	117 %	100 %	sum	89 %	85 %	100 %
	T 20	ExhIn	ExhOut	Aqout	T 20	ExhIn	ExhOut	Aqout	T 20	ExhIn	ExhOut	Aqout	T 20	ExhIn	gas	aq	T 20	ExhIn	ExhOut	aq
	Naphthalene	138 %	183 %	100 %	Naphthalene	128 %	152 %	100 %	Naphthalene	116 %	124 %	100 %	Naphthalene	99 %	99 %	100 %	Naphthalene	79 %	75 %	100 %
	Acenaphthene	155 %	520 %	100 %	Acenaphthene	154 %	375 %	100 %	Acenaphthene	147 %	261 %	100 %	Acenaphthene	132 %	174 %	100 %	Acenaphthene	105 %	108 %	100 %
	Fluorene	126 %	6032 %	100 %	Fluorene	130 %	3776 %	100 %	Fluorene	135 %	2170 %	100 %	Fluorene	141 %	1101 %	100 %	Fluorene	143 %	457 %	100 %
	Phenanthrene	115 %	30435 %	100 %	Phenanthrene	117 %	18473 %	100 %	Phenanthrene	121 %	10142 %	100 %	Phenanthrene	125 %	4783 %	100 %	Phenanthrene	132 %	1740 %	100 %
	sum	133 %	203 %	100 %	sum	127 %	168 %	100 %	sum	118 %	137 %	100 %	sum	105 %	108 %	100 %	sum	86 %	81 %	100 %
	T 25	ExhIn	ExhOut	Aqout	T 25	ExhIn	ExhOut	Aqout	T 25	ExhIn	ExhOut	Aqout	T 25	ExhIn	gas	aq	T 25	ExhIn	ExhOut	aq
	Naphthalene	127 %	147 %	100 %	Naphthalene	118 %	127 %	100 %	Naphthalene	106 %	108 %	100 %	Naphthalene	92 %	90 %	100 %	Naphthalene	75 %	72 %	100 %
	Acenaphthene	154 %	317 %	100 %	Acenaphthene	148 %	243 %	100 %	Acenaphthene	137 %	183 %	100 %	Acenaphthene	119 %	133 %	100 %	Acenaphthene	94 %	91 %	100 %
	Fluorene	135 %	2578 %	100 %	Fluorene	140 %	1666 %	100 %	Fluorene	145 %	1002 %	100 %	Fluorene	148 %	545 %	100 %	Fluorene	141 %	258 %	101 %
	Phenanthrene	121 %	11636 %	100 %	Phenanthrene	124 %	7189 %	100 %	Phenanthrene	129 %	4049 %	100 %	Phenanthrene	134 %	1986 %	100 %	Phenanthrene	140 %	775 %	100 %
	sum	127 %	162 %	100 %	sum	121 %	140 %	100 %	sum	112 %	119 %	100 %	sum	99 %	99 %	100 %	sum	82 %	77 %	100 %
	T 27	ExhIn	ExhOut	Aqout	T 27	ExhIn	ExhOut	Aqout	T 27	ExhIn	ExhOut	Aqout	T 27	ExhIn	gas	aq	T 27	ExhIn	ExhOut	aq
	Naphthalene	123 %	137 %	100 %	Naphthalene	114 %	120 %	100 %	Naphthalene	103 %	104 %	100 %	Naphthalene	90 %	88 %	100 %	Naphthalene	74 %	71 %	100 %
	Acenaphthene	151 %	269 %	100 %	Acenaphthene	144 %	212 %	100 %	Acenaphthene	132 %	163 %	100 %	Acenaphthene	114 %	123 %	100 %	Acenaphthene	90 %	87 %	100 %
	Fluorene	139 %	1877 %	100 %	Fluorene	144 %	1233 %	100 %	Fluorene	148 %	759 %	100 %	Fluorene	148 %	427 %	100 %	Fluorene	135 %	210 %	100 %
	Phenanthrene	124 %	8045 %	100 %	Phenanthrene	127 %	5016 %	100 %	Phenanthrene	132 %	2862 %	100 %	Phenanthrene	138 %	1433 %	100 %	Phenanthrene	142 %	580 %	100 %
	sum	125 %	151 %	100 %	sum	118 %	133 %	100 %	sum	109 %	114 %	100 %	sum	97 %	96 %	100 %	sum	81 %	77 %	100 %

Appendix W. Case Extrapolated

PSU	Extrapolated LG14				LG12				LG10				LG8				LG6			
	0 T 15	ExhIn	ExhOut	Aqout	T 15	ExhIn	ExhOut	Aqout	T 15	ExhIn	ExhOut	Aqout	T 15	ExhIn	gas	aq	T 15	ExhIn	ExhOut	aq
	Naphthalene	152 %	460 %	100 %	Naphthalene	150 %	335 %	100 %	Naphthalene	143 %	236 %	100 %	Naphthalene	128 %	160 %	100 %	Naphthalene	101 %	101 %	100 %
	Acenaphthene	136 %	2273 %	100 %	Acenaphthene	140 %	1473 %	100 %	Acenaphthene	145 %	890 %	100 %	Acenaphthene	147 %	488 %	100 %	Acenaphthene	137 %	232 %	100 %
	Fluorene	112 %	48466 %	100 %	Fluorene	114 %	29257 %	100 %	Fluorene	117 %	15943 %	100 %	Fluorene	121 %	7439 %	100 %	Fluorene	127 %	2663 %	100 %
	Phenanthrene	106 %	450903 %	100 %	Phenanthrene	107 %	267855 %	100 %	Phenanthrene	108 %	142609 %	100 %	Phenanthrene	110 %	64152 %	100 %	Phenanthrene	113 %	21501 %	100 %
	sum	134 %	508 %	100 %	sum	135 %	370 %	100 %	sum	132 %	260 %	100 %	sum	124 %	176 %	100 %	sum	105 %	111 %	100 %
	T 17	ExhIn	ExhOut	Aqout	T 17	ExhIn	ExhOut	Aqout	T 17	ExhIn	ExhOut	Aqout	T 17	ExhIn	gas	aq	T 17	ExhIn	ExhOut	aq
	Naphthalene	152 %	379 %	100 %	Naphthalene	148 %	282 %	100 %	Naphthalene	139 %	205 %	100 %	Naphthalene	122 %	143 %	100 %	Naphthalene	96 %	94 %	100 %
	Acenaphthene	140 %	1683 %	100 %	Acenaphthene	144 %	1107 %	100 %	Acenaphthene	148 %	684 %	100 %	Acenaphthene	147 %	388 %	100 %	Acenaphthene	132 %	193 %	100 %
	Fluorene	114 %	32893 %	100 %	Fluorene	116 %	19961 %	100 %	Fluorene	120 %	10959 %	100 %	Fluorene	124 %	5171 %	100 %	Fluorene	131 %	1888 %	100 %
	Phenanthrene	107 %	296704 %	100 %	Phenanthrene	108 %	176802 %	100 %	Phenanthrene	109 %	94529 %	100 %	Phenanthrene	111 %	42781 %	100 %	Phenanthrene	115 %	14470 %	100 %
	sum	135 %	419 %	100 %	sum	135 %	312 %	100 %	sum	131 %	226 %	100 %	sum	121 %	158 %	100 %	sum	102 %	103 %	100 %
	T 20	ExhIn	ExhOut	Aqout	T 20	ExhIn	ExhOut	Aqout	T 20	ExhIn	ExhOut	Aqout	T 20	ExhIn	gas	aq	T 20	ExhIn	ExhOut	aq
	Naphthalene	150 %	293 %	100 %	Naphthalene	143 %	226 %	100 %	Naphthalene	132 %	171 %	100 %	Naphthalene	115 %	125 %	100 %	Naphthalene	90 %	87 %	100 %
	Acenaphthene	145 %	1102 %	100 %	Acenaphthene	149 %	745 %	100 %	Acenaphthene	150 %	478 %	100 %	Acenaphthene	145 %	285 %	100 %	Acenaphthene	124 %	154 %	100 %
	Fluorene	117 %	18658 %	100 %	Fluorene	120 %	11427 %	100 %	Fluorene	124 %	6356 %	100 %	Fluorene	129 %	3061 %	100 %	Fluorene	135 %	1157 %	100 %
	Phenanthrene	108 %	160221 %	100 %	Phenanthrene	109 %	95969 %	100 %	Phenanthrene	111 %	51676 %	100 %	Phenanthrene	114 %	23628 %	100 %	Phenanthrene	119 %	8121 %	100 %
	sum	136 %	324 %	100 %	sum	133 %	250 %	100 %	sum	128 %	188 %	100 %	sum	116 %	137 %	100 %	sum	97 %	95 %	100 %
	T 25	ExhIn	ExhOut	Aqout	T 25	ExhIn	ExhOut	Aqout	T 25	ExhIn	ExhOut	Aqout	T 25	ExhIn	gas	aq	T 25	ExhIn	ExhOut	aq
	Naphthalene	142 %	207 %	100 %	Naphthalene	133 %	168 %	100 %	Naphthalene	120 %	135 %	100 %	Naphthalene	104 %	106 %	100 %	Naphthalene	83 %	79 %	100 %
	Acenaphthene	152 %	590 %	100 %	Acenaphthene	152 %	421 %	100 %	Acenaphthene	148 %	290 %	100 %	Acenaphthene	135 %	190 %	100 %	Acenaphthene	109 %	116 %	100 %
	Fluorene	123 %	7560 %	100 %	Fluorene	127 %	4724 %	100 %	Fluorene	132 %	2704 %	100 %	Fluorene	138 %	1362 %	100 %	Fluorene	142 %	557 %	100 %
	Phenanthrene	111 %	59196 %	100 %	Phenanthrene	113 %	35833 %	100 %	Phenanthrene	116 %	19580 %	100 %	Phenanthrene	120 %	9149 %	100 %	Phenanthrene	126 %	3258 %	100 %
	sum	134 %	229 %	100 %	sum	129 %	186 %	100 %	sum	121 %	149 %	100 %	sum	109 %	116 %	100 %	sum	90 %	86 %	100 %
	T 27	ExhIn	ExhOut	Aqout	T 27	ExhIn	ExhOut	Aqout	T 27	ExhIn	ExhOut	Aqout	T 27	ExhIn	gas	aq	T 27	ExhIn	ExhOut	aq
	Naphthalene	137 %	185 %	100 %	Naphthalene	128 %	153 %	100 %	Naphthalene	116 %	126 %	100 %	Naphthalene	101 %	101 %	100 %	Naphthalene	81 %	77 %	100 %
	Acenaphthene	153 %	474 %	100 %	Acenaphthene	151 %	346 %	100 %	Acenaphthene	145 %	246 %	100 %	Acenaphthene	130 %	167 %	100 %	Acenaphthene	104 %	107 %	100 %
	Fluorene	126 %	5352 %	100 %	Fluorene	130 %	3378 %	100 %	Fluorene	135 %	1963 %	100 %	Fluorene	141 %	1012 %	100 %	Fluorene	142 %	431 %	100 %
	Phenanthrene	113 %	40198 %	100 %	Phenanthrene	115 %	24459 %	100 %	Phenanthrene	118 %	13461 %	100 %	Phenanthrene	122 %	6359 %	100 %	Phenanthrene	129 %	2307 %	100 %
	sum	132 %	205 %	100 %	sum	127 %	170 %	100 %	sum	118 %	139 %	100 %	sum	106 %	111 %	100 %	sum	88 %	84 %	100 %

Appendix V. Case Extrapolated

PSU	Extrapolated															
	LG14				LG12				LG10				LG8			
20	T 15	ExhIn	ExhOut	Aqout	T 15	ExhIn	ExhOut	Aqout	T 15	ExhIn	ExhOut	Aqout	T 15	ExhIn	ExhOut	Aqout
	Naphthalene	151 %	319 %	100 %	Naphthalene	145 %	242 %	100 %	Naphthalene	134 %	180 %	100 %	Naphthalene	116 %	129 %	100 %
	Acenaphthene	142 %	1394 %	100 %	Acenaphthene	146 %	925 %	100 %	Acenaphthene	149 %	578 %	100 %	Acenaphthene	146 %	333 %	100 %
	Fluorene	115 %	25540 %	100 %	Fluorene	118 %	15520 %	100 %	Fluorene	121 %	8540 %	100 %	Fluorene	126 %	4047 %	100 %
	Phenanthrene	108 %	183195 %	100 %	Phenanthrene	109 %	109240 %	100 %	Phenanthrene	111 %	58479 %	100 %	Phenanthrene	113 %	26532 %	100 %
	sum	136 %	353 %	100 %	sum	134 %	268 %	100 %	sum	129 %	198 %	100 %	sum	117 %	142 %	100 %
	T 17	ExhIn	ExhOut	Aqout	T 17	ExhIn	ExhOut	Aqout	T 17	ExhIn	ExhOut	Aqout	T 17	ExhIn	ExhOut	Aqout
	Naphthalene	148 %	271 %	100 %	Naphthalene	141 %	211 %	100 %	Naphthalene	129 %	160 %	100 %	Naphthalene	111 %	119 %	100 %
	Acenaphthene	146 %	1052 %	100 %	Acenaphthene	149 %	711 %	100 %	Acenaphthene	150 %	456 %	100 %	Acenaphthene	144 %	273 %	100 %
	Fluorene	118 %	17436 %	100 %	Fluorene	120 %	10665 %	100 %	Fluorene	124 %	5923 %	100 %	Fluorene	129 %	2848 %	100 %
	Phenanthrene	109 %	120977 %	100 %	Phenanthrene	110 %	72413 %	100 %	Phenanthrene	112 %	38968 %	100 %	Phenanthrene	115 %	17816 %	100 %
	sum	136 %	300 %	100 %	sum	133 %	233 %	100 %	sum	126 %	177 %	100 %	sum	114 %	130 %	100 %
	T 20	ExhIn	ExhOut	Aqout	T 20	ExhIn	ExhOut	Aqout	T 20	ExhIn	ExhOut	Aqout	T 20	ExhIn	gas	aq
	Naphthalene	143 %	219 %	100 %	Naphthalene	135 %	176 %	100 %	Naphthalene	122 %	139 %	100 %	Naphthalene	105 %	107 %	100 %
	Acenaphthene	150 %	712 %	100 %	Acenaphthene	152 %	497 %	100 %	Acenaphthene	149 %	333 %	100 %	Acenaphthene	138 %	211 %	100 %
	Fluorene	121 %	9998 %	100 %	Fluorene	125 %	6186 %	100 %	Fluorene	129 %	3493 %	100 %	Fluorene	135 %	1724 %	100 %
	Phenanthrene	111 %	65753 %	100 %	Phenanthrene	113 %	39613 %	100 %	Phenanthrene	115 %	21510 %	100 %	Phenanthrene	119 %	9967 %	100 %
	sum	134 %	243 %	100 %	sum	130 %	195 %	100 %	sum	122 %	154 %	100 %	sum	109 %	118 %	100 %
	T 25	ExhIn	ExhOut	Aqout	T 25	ExhIn	ExhOut	Aqout	T 25	ExhIn	ExhOut	Aqout	T 25	ExhIn	gas	aq
	Naphthalene	133 %	166 %	100 %	Naphthalene	123 %	140 %	100 %	Naphthalene	111 %	117 %	100 %	Naphthalene	96 %	95 %	100 %
	Acenaphthene	153 %	407 %	100 %	Acenaphthene	150 %	302 %	100 %	Acenaphthene	142 %	218 %	100 %	Acenaphthene	126 %	151 %	100 %
	Fluorene	129 %	4153 %	100 %	Fluorene	133 %	2636 %	100 %	Fluorene	138 %	1545 %	100 %	Fluorene	143 %	807 %	100 %
	Phenanthrene	115 %	24657 %	100 %	Phenanthrene	118 %	15058 %	100 %	Phenanthrene	121 %	8336 %	100 %	Phenanthrene	126 %	3977 %	100 %
	sum	130 %	185 %	100 %	sum	124 %	155 %	100 %	sum	115 %	129 %	100 %	sum	103 %	104 %	100 %
	T 27	ExhIn	ExhOut	Aqout	T 27	ExhIn	ExhOut	Aqout	T 27	ExhIn	ExhOut	Aqout	T 27	ExhIn	gas	aq
	Naphthalene	128 %	152 %	100 %	Naphthalene	119 %	130 %	100 %	Naphthalene	107 %	111 %	100 %	Naphthalene	93 %	92 %	100 %
	Acenaphthene	153 %	337 %	100 %	Acenaphthene	147 %	256 %	100 %	Acenaphthene	137 %	190 %	100 %	Acenaphthene	120 %	137 %	100 %
	Fluorene	132 %	2979 %	100 %	Fluorene	137 %	1916 %	100 %	Fluorene	142 %	1144 %	100 %	Fluorene	145 %	615 %	100 %
	Phenanthrene	118 %	16875 %	100 %	Phenanthrene	120 %	10376 %	100 %	Phenanthrene	124 %	5800 %	100 %	Phenanthrene	130 %	2810 %	100 %
	sum	127 %	169 %	100 %	sum	121 %	145 %	100 %	sum	112 %	122 %	100 %	sum	100 %	100 %	100 %

PSU	Extrapolated																							
	LG14				LG12				LG10				LG8				LG6							
35	T 15	ExhIn	ExhOut	Aqout	T 15	ExhIn	ExhOut	Aqout	T 15	ExhIn	ExhOut	Aqout	T 15	ExhIn	ExhOut	Aqout	T 15	ExhIn	ExhOut	Aqout				
	Naphthalene	150 %	268 %	100 %	Naphthalene	142 %	209 %	100 %	Naphthalene	130 %	159 %	100 %	Naphthalene	112 %	118 %	100 %	Naphthalene	87 %	83 %	100 %				
	Acenaphthene	147 %	1067 %	100 %	Acenaphthene	150 %	721 %	100 %	Acenaphthene	151 %	462 %	100 %	Acenaphthene	145 %	276 %	100 %	Acenaphthene	122 %	148 %	100 %				
	Fluorene	118 %	17448 %	100 %	Fluorene	121 %	10660 %	100 %	Fluorene	125 %	5912 %	100 %	Fluorene	130 %	2837 %	100 %	Fluorene	137 %	1070 %	100 %				
	Phenanthrene	110 %	103118 %	100 %	Phenanthrene	111 %	61699 %	100 %	Phenanthrene	114 %	33193 %	100 %	Phenanthrene	117 %	15178 %	100 %	Phenanthrene	122 %	5239 %	100 %				
	sum	137 %	297 %	100 %	sum	134 %	231 %	100 %	sum	127 %	176 %	100 %	sum	115 %	130 %	100 %	sum	94 %	90 %	100 %				
	T 17	ExhIn	ExhOut	Aqout	T 17	ExhIn	ExhOut	Aqout	T 17	ExhIn	ExhOut	Aqout	T 17	ExhIn	ExhOut	Aqout	T 17	ExhIn	ExhOut	Aqout				
	Naphthalene	46 %	132 %	0 %	Naphthalene	138 %	185 %	100 %	Naphthalene	125 %	145 %	100 %	Naphthalene	107 %	110 %	100 %	Naphthalene	84 %	79 %	100 %				
	Acenaphthene	150 %	817 %	100 %	Acenaphthene	153 %	564 %	100 %	Acenaphthene	151 %	371 %	100 %	Acenaphthene	142 %	230 %	100 %	Acenaphthene	116 %	130 %	100 %				
	Fluorene	121 %	11968 %	100 %	Fluorene	124 %	7367 %	100 %	Fluorene	128 %	4131 %	100 %	Fluorene	134 %	2016 %	100 %	Fluorene	140 %	783 %	100 %				
	Phenanthrene	111 %	68315 %	100 %	Phenanthrene	113 %	41057 %	100 %	Phenanthrene	116 %	22225 %	100 %	Phenanthrene	119 %	10257 %	100 %	Phenanthrene	125 %	3595 %	100 %				
	sum	136 %	257 %	100 %	sum	132 %	205 %	100 %	sum	124 %	160 %	100 %	sum	111 %	121 %	100 %	sum	91 %	87 %	100 %				
		100 %	100 %	100 %																				
	T 20	ExhIn	ExhOut	Aqout	T 20	ExhIn	ExhOut	Aqout	T 20	ExhIn	ExhOut	Aqout	T 20	ExhIn	gas	aq	T 20	ExhIn	ExhOut	aq				
	Naphthalene	140 %	192 %	100 %	Naphthalene	130 %	158 %	100 %	Naphthalene	118 %	128 %	100 %	Naphthalene	101 %	101 %	100 %	Naphthalene	80 %	76 %	100 %				
	Acenaphthene	154 %	566 %	100 %	Acenaphthene	154 %	405 %	100 %	Acenaphthene	148 %	279 %	100 %	Acenaphthene	134 %	183 %	100 %	Acenaphthene	107 %	112 %	100 %				
	Fluorene	125 %	6923 %	100 %	Fluorene	129 %	4319 %	100 %	Fluorene	134 %	2469 %	100 %	Fluorene	140 %	1243 %	100 %	Fluorene	143 %	509 %	100 %				
	Phenanthrene	114 %	37349 %	100 %	Phenanthrene	116 %	22620 %	100 %	Phenanthrene	119 %	12378 %	100 %	Phenanthrene	124 %	5806 %	100 %	Phenanthrene	130 %	2092 %	100 %				
	sum	134 %	214 %	100 %	sum	128 %	176 %	100 %	sum	120 %	142 %	100 %	sum	107 %	111 %	100 %	sum	88 %	83 %	100 %				
	T 25	ExhIn	ExhOut	Aqout	T 25	ExhIn	ExhOut	Aqout	T 25	ExhIn	ExhOut	Aqout	T 25	ExhIn	gas	aq	T 25	ExhIn	ExhOut	aq				
	Naphthalene	129 %	152 %	100 %	Naphthalene	119 %	131 %	1																

Appendix Y. Case Extrapolated

PSU	Extrapolated															
	LG14				LG12				LG10				LG8			
40	T 15	ExhIn	ExhOut	Aqout	T 15	ExhIn	ExhOut	Aqout	T 15	ExhIn	ExhOut	Aqout	T 15	ExhIn	ExhOut	Aqout
	Naphthalene	148 %	249 %	100 %	Naphthalene	140 %	196 %	100 %	Naphthalene	127 %	151 %	100 %	Naphthalene	109 %	114 %	100 %
	Acenaphthene	148 %	954 %	100 %	Acenaphthene	151 %	650 %	100 %	Acenaphthene	151 %	421 %	100 %	Acenaphthene	144 %	255 %	100 %
	Fluorene	119 %	14915 %	100 %	Fluorene	122 %	9134 %	100 %	Fluorene	126 %	5083 %	100 %	Fluorene	132 %	2454 %	100 %
	Phenanthrene	110 %	82561 %	100 %	Phenanthrene	112 %	49474 %	100 %	Phenanthrene	115 %	26674 %	100 %	Phenanthrene	118 %	12239 %	100 %
	sum	136 %	276 %	100 %	sum	133 %	217 %	100 %	sum	125 %	167 %	100 %	sum	113 %	125 %	100 %
	T 17	ExhIn	ExhOut	Aqout	T 17	ExhIn	ExhOut	Aqout	T 17	ExhIn	ExhOut	Aqout	T 17	ExhIn	ExhOut	Aqout
	Naphthalene	144 %	217 %	100 %	Naphthalene	135 %	175 %	100 %	Naphthalene	122 %	138 %	100 %	Naphthalene	105 %	107 %	100 %
	Acenaphthene	152 %	735 %	100 %	Acenaphthene	153 %	511 %	100 %	Acenaphthene	151 %	341 %	100 %	Acenaphthene	140 %	214 %	100 %
	Fluorene	122 %	10253 %	100 %	Fluorene	125 %	6329 %	100 %	Fluorene	130 %	3563 %	100 %	Fluorene	136 %	1751 %	100 %
	Phenanthrene	112 %	54773 %	100 %	Phenanthrene	114 %	32977 %	100 %	Phenanthrene	117 %	17898 %	100 %	Phenanthrene	121 %	8294 %	100 %
	sum	135 %	241 %	100 %	sum	131 %	194 %	100 %	sum	123 %	153 %	100 %	sum	109 %	117 %	100 %
	T 20	ExhIn	ExhOut	Aqout	T 20	ExhIn	ExhOut	Aqout	T 20	ExhIn	ExhOut	Aqout	T 20	ExhIn	gas	aq
	Naphthalene	138 %	182 %	100 %	Naphthalene	128 %	151 %	100 %	Naphthalene	115 %	124 %	100 %	Naphthalene	99 %	99 %	100 %
	Acenaphthene	155 %	515 %	100 %	Acenaphthene	153 %	371 %	100 %	Acenaphthene	147 %	259 %	100 %	Acenaphthene	132 %	172 %	100 %
	Fluorene	126 %	5953 %	100 %	Fluorene	130 %	3728 %	100 %	Fluorene	135 %	2143 %	100 %	Fluorene	141 %	1088 %	100 %
	Phenanthrene	115 %	30023 %	100 %	Phenanthrene	117 %	18225 %	100 %	Phenanthrene	121 %	10007 %	100 %	Phenanthrene	125 %	4720 %	100 %
	sum	133 %	203 %	100 %	sum	127 %	168 %	100 %	sum	118 %	137 %	100 %	sum	105 %	108 %	100 %
	T 25	ExhIn	ExhOut	Aqout	T 25	ExhIn	ExhOut	Aqout	T 25	ExhIn	ExhOut	Aqout	T 25	ExhIn	gas	aq
	Naphthalene	127 %	146 %	100 %	Naphthalene	117 %	126 %	100 %	Naphthalene	106 %	108 %	100 %	Naphthalene	92 %	90 %	100 %
	Acenaphthene	154 %	314 %	100 %	Acenaphthene	147 %	241 %	100 %	Acenaphthene	136 %	181 %	100 %	Acenaphthene	119 %	132 %	100 %
	Fluorene	135 %	2546 %	100 %	Fluorene	140 %	1646 %	100 %	Fluorene	145 %	991 %	100 %	Fluorene	148 %	539 %	100 %
	Phenanthrene	121 %	11482 %	100 %	Phenanthrene	124 %	7095 %	100 %	Phenanthrene	129 %	3997 %	100 %	Phenanthrene	134 %	1962 %	100 %
	sum	127 %	162 %	100 %	sum	120 %	140 %	100 %	sum	111 %	119 %	100 %	sum	99 %	99 %	100 %
	T 27	ExhIn	ExhOut	Aqout	T 27	ExhIn	ExhOut	Aqout	T 27	ExhIn	ExhOut	Aqout	T 27	ExhIn	gas	aq
	Naphthalene	122 %	136 %	100 %	Naphthalene	113 %	120 %	100 %	Naphthalene	103 %	104 %	100 %	Naphthalene	90 %	88 %	100 %
	Acenaphthene	151 %	267 %	100 %	Acenaphthene	143 %	210 %	100 %	Acenaphthene	131 %	162 %	100 %	Acenaphthene	114 %	122 %	100 %
	Fluorene	139 %	1855 %	100 %	Fluorene	144 %	1219 %	100 %	Fluorene	148 %	750 %	100 %	Fluorene	148 %	423 %	100 %
	Phenanthrene	124 %	7940 %	100 %	Phenanthrene	127 %	4952 %	100 %	Phenanthrene	132 %	2827 %	100 %	Phenanthrene	138 %	1416 %	100 %
	sum	124 %	151 %	100 %	sum	118 %	132 %	100 %	sum	109 %	114 %	100 %	sum	97 %	96 %	100 %